NASA Technical Memorandum

NASA TM- 100393

COMPENDIUM OF FRACTURE MECHANICS PROBLEMS

By R. Stallworth, C. Wilson, and C. Meyers

Structures and Dynamics Laboratory
Science and Engineering Directorate

April 1990

National Aeronautics and
Space Administration

George C. Marshall Space Flight Center

NASA

Report Documentation Page

1. Report No.	2. Government Accession No.	3. Recipient's Catalog No.
NASA TM-100393		

4. Title and Subtitle	5. Report Date
Compendium of Fracture Mechanics Problems	April 1990
	6. Performing Organization Code: ED21
7. Author(s)	8. Performing Organization Report No.
R. Stallworth, C. Wilson, and C. Meyers	
	10. Work Unit No.
9. Performing Organization Name and Address	11. Contract or Grant No.
George C. Marshall Space Flight Center Marshall Space Flight Center, Alabama 35812	
	13. Type of Report and Period Covered
12. Sponsoring Agency Name and Address	Technical Memorandum
National Aeronautics and Space Administration Washington, D.C. 20546	14. Sponsoring Agency Code

15. Supplementary Notes

Prepared by Structures and Dynamics Laboratory, Science and Engineering Directorate.

16. Abstract

This report presents fracture mechanics analysis results from the following structures/components analyzed at Marshall Space Flight Center (MSFC) between 1982 and 1989: space shuttle main engine (SSME), Hubble Space Telescope (HST), external tank attach ring, B-1 stand LOX inner tank, and solid rocket booster (SRB). Results from the SSME high pressure fuel turbopump (HPFTP) second stage blade parametric analysis determined a critical flaw size for a wide variety of stress intensity values. The engine 0212 failure analysis was a time-dependent fracture life assessment. Results indicated that the disk ruptured due to an overspeed condition. Results also indicated that very small flaws in the curvic coupling area could propagate and lead to failure under normal operating conditions. It was strongly recommended that a nondestructive evaluation inspection schedule be implemented. The main ring of the HST, scheduled to launch in 1990, was analyzed by safe-life and fail-safe analyses. First safe-life inspection criteria curves for the ring inner and outer skins and the fore and aft channels were derived. Afterwards the skins and channels were determined to be fail-safe by analysis. A conservative safe-life analysis was done on the 270 redesign external tank attach ring. Results from the analysis were used to determine the nondestructive evaluation technique required. A leak before burst analysis of the B-1 stand LOX inner tank indicated that leakage would be detected well before burst conditions developed.

17. Key Words (Suggested by Author(s))	18. Distribution Statement
Critical stress intensity, modified Forman equation, leakage before burst, turbine blade, disk, safe life, fail-safe, fracture control, nondestructive evaluation	Unclassified – Unlimited

19. Security Classif. (of this report)	20. Security Classif. (of this page)	21. No. of pages	22. Price
Unclassified	Unclassified	175	NTIS

NASA FORM 1626 OCT 86

For sale by the National Technical Information Service, Springfield, VA 22161-2171

TABLE OF CONTENTS

		Page
I.	INTRODUCTION	1
II.	OBJECTIVE	1
III.	APPROACH	1
IV.	MSFC POLICY	2
V.	TECHNICAL BACKGROUND	4
VI.	ANALYSIS CODES	9
VII.	ANALYSIS PROBLEMS	11
	A. SSME HPFTP Turbine Blade	11
	B. Engine 0212 Failure Investigation	23
	C. Hubble Space Telescope/Optical Telescope Assembly	38
	D. Space Support Equipment Trunnion	47
	E. 270-Degree ET Attach Ring: Ring Cap and Web Segment	51
	F. B-1 Stand LOX Inner Tank	61
VIII.	SUMMARY	70
APPENDIX		75
	A. Main Ring HST	77
	B. SRB Aft Skirt	103
REFERENCES		166

LIST OF ILLUSTRATIONS

Figure	Title	Page
1.	Fracture control selection and disposition of parts	3
2.	Stress intensity factors for practical geometries	7
3.	Typical fatigue crack growth rate curve	8
4.	NASCRAC analysis types	10
5.	HPFTP section	13
6.	HPFTP first and second stage blade	14
7.	HPFTP blade with symmetrical rotor plot	15
8.	HPFTP blade and rotor model	16
9.	HPFTP second stage turbine blade cracks	17
10.	HPFTP two-dimensional firtree model	18
11.	HPFTP second stage blade, neck 3 stress versus distance along firtree	19
12.	NASCRAC through edge crack model	20
13.	HPFTP K versus a curve for σ_{max}	21
14.	HPFTP K versus a curve for σ_{avg}	22
15.	High pressure oxidizer turbopump (HPOTP) first stage disk after incident	28
16.	HPOTP disc sections analyzed	29
17.	HPOTP stress contour plot, 65-percent power level	30
18.	HPOTP stress contour plot, 100-percent power level	31
19.	HPOTP stress contour plot, 104-percent power level	32
20.	HPOTP stress contour plot, 109-percent power level	33
21.	HPOTP stress contour plot, overspeed condition	34

LIST OF ILLUSTRATIONS (Continued)

Figure	Title	Page
22.	HPOTP data from Aerospace Materials Handbook	35
23.	HPOTP NASCRAC geometry models	36
24.	HPOTP disk burst speed	37
25.	HST attach main ring forward surface	42
26.	HST primary mirror assembly	43
27.	HST main ring cross section	44
28.	HST NASA/FLAGRO center panel part-through crack geometry model	45
29.	HST NASA/FLAGRO center panel through crack geometry model	45
30.	HST inspection curve for fore and aft channels	46
31.	HST inspection curve for inner and outer skins	46
32.	SSE trunnion SPAR quarter model	49
33.	SSE trunnion SPAR quarter model side view	50
34.	SSE NASA/FLAGRO surface crack in solid cylinder geometry model	50
35.	ET 270-degree external attach ring	57
36.	ET 270-degree external attach ring cross section	58
37.	ET NASA/FLAGRO part-through crack at a hole	59
38.	ET external attach ring cap segment	59
39.	ET external attach ring web segment	60
40.	ET NASA/FLAGRO embedded flaw geometry	60
41.	B-1 LOX tank configuration	65
42.	B-1 schematic of tank	66

LIST OF ILLUSTRATIONS (Concluded)

Figure	Title	Page
43.	NASA/FLAGRO center crack panel	67
44.	B-1 critical through crack length versus stress level	67
45.	B-1 NASTRAN plot of lower head	68
46.	B-1 NASTRAN plot of LOX tank	69
47.	Fracture control sequence	71
48.	Fracture analysis sequence	72
49.	Sample fracture mechanics analysis reporting sheet	73

LIST OF TABLES

Table	Title	Page
1.	Engine 0212 material properties derivation	25
2.	Engine 0212 stress spectra	26
3.	Engine 0212 critical flaw size results	27
4.	OTA loading scenario	39
5.	OTA load spectra	40
6.	OTA stress spectrum	41
7.	SSE fatigue stress spectrum	48
8.	ET attach ring – ring cap spectrum loading	54
9.	ET attach ring stress spectra breakdown, step by step	55
10.	ET attach ring – web segment loading spectrum	56
11.	B-1 stand LOX tank wall results	64
12.	B-1 LOX tank fill penetration weld results	64
13.	B-1 LOX tank drain penetration weld results	64

TECHNICAL MEMORANDUM

COMPENDIUM OF FRACTURE MECHANICS PROBLEMS

I. INTRODUCTION

The structural analysis sector of Marshall Space Flight Center (MSFC) has been involved in solving a variety of fracture mechanics analysis problems throughout the years. This report highlights some of the interesting and challenging fracture mechanics problems analyzed by MSFC engineers and their contractors.

It has been the policy of NASA and MSFC to provide safe space flight structures. The structural integrity of space flight hardware is established by a combination of qualification tests and analyses which simulate actual operating conditions, including flight loads, temperatures, and corrosive environments.

It is required that if structural failure of a part in a space vehicle system would cause a catastrophic event, then that part must be subjected to fracture control. Fracture control is a process which eliminates or controls the conditions under which cracks are tolerated and is based on fracture mechanics. Fracture mechanics is an engineering discipline that quantifies the conditions under which a structure can fail due to growth of a crack contained in that body. It provides an analytical tool for assessing defect acceptability.

II. OBJECTIVE

The objective of this report is to provide the engineer working in the fracture mechanics discipline a guideline as well as a reference for working a variety of fracture mechanics problems. Often textbook and manual examples do not depict real-world situations or conditions. The problems highlighted in this report were analyzed from real-time conditions. Some of the problems are taken from fracture mechanics analyses of the Hubble Space Telescope (HST), space shuttle main engines (SSME), and solid rocket boosters (SRB).

III. APPROACH

The parts highlighted in this report have been classified as fracture sensitive. Fracture sensitive parts must be dispositioned by one of the following methods: low mass, contained/restrained, fail-safe, damage tolerant, or safe life. The major emphasis of this paper is on parts classified as fail-safe or safe life.

A. Fail-Safe

MSFC-HDBK-1453 defines a part as fail-safe if it can be shown by analysis or test that, due to structural redundancy, the structure remaining after failure of the one part can sustain the limit loads with an ultimate factor of safety equal to or greater than one, and the remaining structure has sufficient fatigue life to complete the mission [1].

B. Safe Life

A metallic or glass part is defined by MSFC-HDBK-1453 as safe life if it can be shown that the largest undetected flaw that could exist in the part will not grow to failure when subjected to the cyclic and sustained loads and environments encountered in four complete mission lifetimes.

All structures and parts classified as safe life require a fracture mechanics analysis and nondestructive evaluation (NDE) to ensure that no flaws (cracks) exist that will grow to critical size in four lifetimes [1].

The following computer codes were used for safe life analysis problems highlighted in this paper:

NASCRAC – NASA Crack Analysis Code developed by Failure Analysis Associates (FaAA) under contract to MSFC. NASCRAC uses influence functions to generate stress intensity solutions [2].

NASA/FLAGRO – Fatigue crack growth computer program that provides an automated procedure for calculating the fatigue life of cyclically loaded structures with initial crack-like defects [3].

FLAGRO4 – Developed by Rockwell International for fracture control analysis of the space shuttle [4].

IV. MSFC POLICY

All space flight structures and components shall be examined to determine their fracture control requirements. All parts shall undergo an evaluation as shown in Figure 1. The criteria for selecting parts for fracture control are based on safety rather than mission success. A determination must be made for all parts as to whether or not their structural failure will cause a catastrophic event. Any structural failure must be assumed to lead to a catastrophic event unless it can be shown otherwise. The exit "no" path (Fig. 1) may be chosen for those parts which are clearly low mass, contained/restrained, or fail-safe. The exit "yes" path must be chosen for all other parts. The parts in the "yes" path are termed fracture sensitive and they must be dispositioned by rigorous analyses and/or tests. At MSFC, fracture mechanics analysis is done in accordance with MSFC-HDBK-1453 "Fracture Control Program Requirements" and MSFC-STD-1249 "Standard NDE Guidelines and Requirements for Fracture Control Programs" [5].

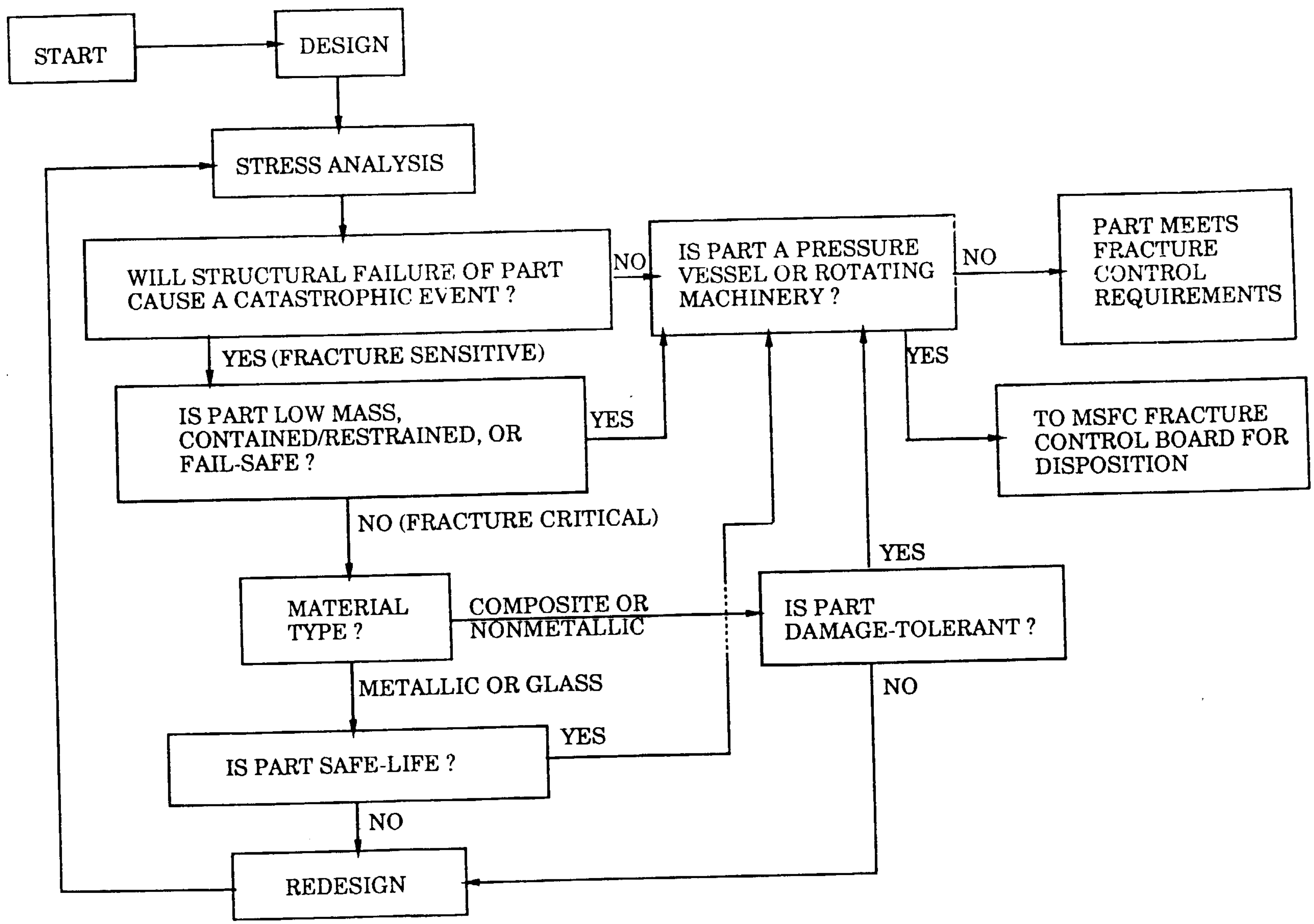

Figure 1. Fracture control selection and disposition of parts.

For safe-life analysis, a safety factor of four is required. The factor of four was selected to account for typical scatter in fatigue crack growth rate data. The factor was determined after a statistical study of several different materials. A single variable analysis of the growth rate constant C indicates that C multiplied by four was approximately equal to a 2σ variation and adequately bounded the growth rate data. Also, comparisons of life predictions with numerous cycles to failure tests have shown that the factor of four was conservative. If a part has less than a safety factor of four on life there are several options for disposition:

1. Conduct more precise load, stress, and spectrum analyses.

2. Monitor structural or system testing to obtain refined loads.

3. Verify safe life with fracture mechanics oriented component tests.

4. Apply specially designed inspection procedures to disclose smaller flaws.

5. Apply periodic reinspection or replacement.

6. Apply stress-intensity factor reduction methods.

7. Wave requirements, where specifically justified, such as improbability of certain flaw orientations based on a review of manufacturing processes.

8. Redesign part according to fracture mechanics recommendations [6].

At MSFC, the Fracture Control Board (FCB) is responsible for ensuring preparation, maintenance, review, and approval of all fracture control plans, procedures, and requirements. The FCB oversees all projects at MSFC. Within each project, the technical leads, chief engineers, and project offices are responsible for implementing fracture control as required by MSFC-HDBK-1453 and for carrying out FCB directives [1].

V. TECHNICAL BACKGROUND

What is the residual strength of a structure as a function of crack size? What is the maximum permissible crack size that a structure can tolerate? How long does it take for a crack to grow from its initial size to the maximum permissible size? What is the service life of a structure when a certain preexisting flaw size is assumed to exist? How often should a structure be inspected for cracks? Fracture mechanics can provide quantitative answers to questions involving crack-like flaws in structures. Fracture mechanics is the study of the failure of load-bearing structures by fracture before general yielding occurs in the net section due to the presence of a crack-like flaw. The use of high strength-to-weight ratios in the design of space structures has stimulated a keen interest in fracture mechanics [7].

In 1920, A.A. Griffith successfully analyzed the fracture-dominant problem of propagation of brittle cracks in glass. Griffith formulated an energy balance between the decrease in elastic strain energy of a body under stress as the crack extends and the energy needed to create the new crack surfaces. In the 1950's, G. Irwin determined that the Griffith energy balance must be between the stored strain energy of a stressed body and the surface energy plus the work done by plastic deformation on the body. For relatively ductile materials, Irwin stated that the energy required to form new crack surfaces is very small compared to the work of plastic deformation. Irwin defined a material property known as crack driving force or energy release rate, G, as the total energy absorbed during cracking per unit increase in crack length and per unit thickness. In 1957, Irwin postulated that fracture occurs when a critical stress distribution ahead of the crack tip is reached. Irwin equated his stress intensity approach to the energy approach of Griffith. The material property, G_c, the critical energy release rate, has an equivalent critical stress intensity factor, K_c. The ability to work in terms of stress intensity instead of energy release rate is the basis of Linear Elastic Fracture Mechanics (LEFM). The stress intensity factor K is the fundamental parameter used to characterize crack extension.

The stress intensity factor gives the magnitude of the elastic stress field in the region near the crack tip as:

$$K = \sigma \sqrt{\pi a}\, f\left(\frac{a}{W}\right)$$

where

σ = stress at a given location,

a = flaw size,

f(a/W) = parameter depending on geometry and crack orientation.

Dimensional analysis shows that K must be linearly related to stress and related to the square root of crack length. Irwin stated that the stresses in the vicinity of the crack tip are:

$$\sigma_{ij} = \frac{K}{\sqrt{2\pi r}} f_{ij}(\theta) + \ldots ,$$

where r and θ are the polar coordinates of a point with respect to the crack tip. As r tends to zero, the stresses become infinite; a stress singularity exists at the crack tip. In reality, structural materials deform plastically above the yield stress so that a plastic zone surrounds the crack tip. When the plastic zone is small compared to the flaw size, the stress field of the cracked body is closely approximated by the above equation. For subcritical crack growth, where crack extension takes place at stress intensities well below K_c, the stress intensity approach can provide correlations of data for fatigue crack growth.

Stress intensity solutions have been developed for various geometries. For the center cracked tension specimen in Figure 2, the mode I (opening mode) stress intensity factor K_I can be written:

$$K_I = \sigma \sqrt{\pi a} \sqrt{\sec (\pi a/W)} \quad .$$

This equation was developed as an approximation by Feddersen in 1966. Numerous other solutions for this geometry exist. Other practical geometries are shown in Figure 2, along with the corresponding stress intensity solution.

For a crack through the thickness of a wide plate subjected to remote loading that varies cyclically between a minimum and a maximum value, the stress range is $\Delta\sigma = \sigma_{max} - \sigma_{min}$, and the stress intensity range is $\Delta K = K_{max} - K_{min}$ or $\Delta K = \Delta\sigma \sqrt{\pi a}$.

The change in stress intensity is a controlling parameter in fatigue crack growth rate (FCGR). The FCGR is defined as crack extension during a small number of cycles and is written as the derivative da/dN. Experimentally, it has been found that for a given stress ratio, $R = \sigma_{min}/\sigma_{max}$, da/dN is a function of ΔK. The functional relationship between da/dN and stress intensity range and stress ratio exists for specimens tested with different stress ranges and crack lengths, as well as specimens of different geometry. This correlation can be shown graphically on a double logarithmic plot (Fig. 3). The crack growth rate curve usually has a sigmoidal trend.

The sigmoidal trend of a da/dN-ΔK curve divides the curve into three regions according to curve shape, crack growth mechanisms, and other influences. In region I, a threshold value of ΔK occurs. The crack will not grow after ΔK drops below this threshold. Just above ΔK_o, the crack propagation rate increases rapidly with increasing ΔK. Crack growth rate in this region is influenced by microstructure, mean stress, and environment. Region II is characterized by a near-linear log-log relationship between da/dN and ΔK; this region is influenced largely by certain combinations of environment, mean stress, and frequency. Microstructure and thickness have little influence on the crack growth of region II. In region III, the crack growth rate rises to an infinite slope caused when the maximum stress intensity factor, K_{max}, becomes equal to the critical stress intensity factor, K_c. For mode I loading, K_c is denoted as K_{Ic} (or as K_{1c}) and is known as the fracture toughness. Microstructure, mean stress, and thickness are large influences on the crack growth rate in this region.

Since no known physical law governs FCGR, attempts to describe the crack growth rate curve using empirical formulas fitted to a set of data have been widespread. In 1962, Paris used crack growth rate data obtained from specimens with different stress ratios and developed an empirical crack growth law:

$$da/dN = C (\Delta K)^n \quad .$$

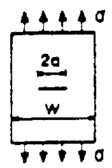

$$K_I = \sigma\sqrt{\pi a}\left(\sec\frac{\pi a}{W}\right)^{1/2}$$

$$K_{II} = \tau\sqrt{\pi a}\left(\text{small}\ \frac{a}{W}\right)$$

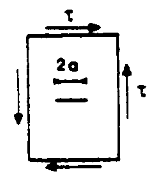

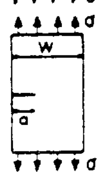

$$K_I = 1.12\sigma\sqrt{\pi a}\left(\text{small}\ \frac{a}{W}\right)$$

or $K_I = Y\sigma\sqrt{a}$

with $Y = 1.99 - 0.41\frac{a}{W} + 18.7\left(\frac{a}{W}\right)^2 - 38.48\left(\frac{a}{W}\right)^3 + 53.85\left(\frac{a}{W}\right)^4$

$(1.99 = 1.12\sqrt{\pi})$

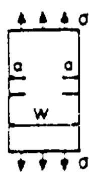

$$K_I = 1.12\sigma\sqrt{\pi a}\left(\text{small}\ \frac{a}{W}\right)$$

or $K_I = Y\sigma\sqrt{a}$

with $Y = 1.99 + 0.76\frac{a}{W} - 8.48\left(\frac{a}{W}\right)^2 + 27.36\left(\frac{a}{W}\right)^3$

$(1.99 = 1.12\sqrt{\pi})$

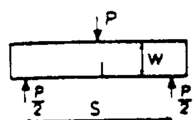

Thickness **B**

$$K_I = \frac{PS}{BW^{3/2}}\left[2.9\left(\frac{a}{W}\right)^{1/2} - 4.6\left(\frac{a}{W}\right)^{3/2} + 21.8\left(\frac{a}{W}\right)^{5/2} - 37.6\left(\frac{a}{W}\right)^{7/2} + 38.7\left(\frac{a}{W}\right)^{9/2}\right]$$

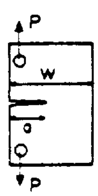

Thickness B

$$K_I = \frac{P}{BW^{1/2}}\left[29.6\left(\frac{a}{W}\right)^{1/2} - 185.5\left(\frac{a}{W}\right)^{3/2} + 655.7\left(\frac{a}{W}\right)^{5/2} - 1017\left(\frac{a}{W}\right)^{7/2} + 63.9\left(\frac{a}{W}\right)^{9/2}\right]$$

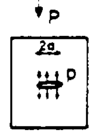

p per unit thickness

$$K_I = p\sqrt{\pi a}$$

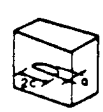

$$K_{I_{max}} = 1.12\frac{\sigma}{\Phi}\sqrt{\pi a}$$

$$K_{I_{min}} = 1.12\frac{\sigma}{\Phi}\sqrt{\pi a^2/c}$$

$$\Phi = \int_0^{\pi/2}\left[1 - \frac{c^2 - a^2}{c^2}\sin^2\varphi\right]d\varphi$$

$$\phi \cong \frac{3\pi}{8} + \frac{\pi a^2}{8c^2}$$

Figure 2. Stress intensity factors for practical geometries.

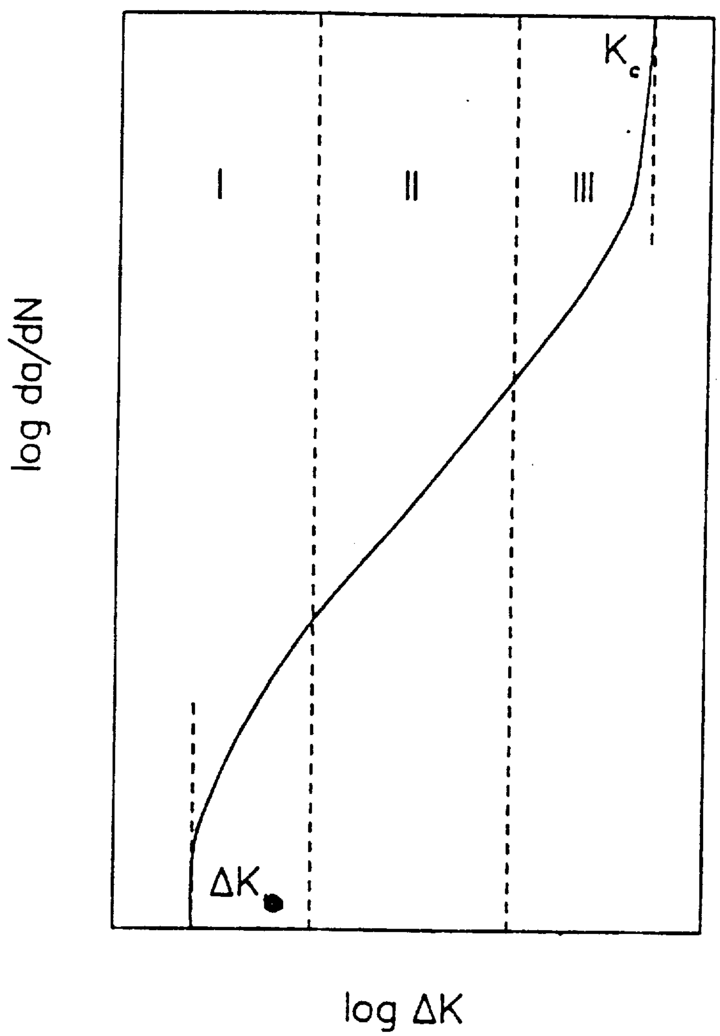

Figure 3. Typical fatigue crack growth rate curve.

C and n are empirical coefficients which are constants for a given material. This simple power function describes only the linear region of the crack propagation curve. In 1967, Forman argued that the value of da/dN approaches infinity as the crack approaches its critical length; in terms of the stress intensity factor, as K_{max} approaches K_{Ic}. This behavior can be described as follows:

$$\frac{da}{dN} = C\ (\Delta K)^n \frac{K_{max}}{K_{Ic}-K_{max}} \quad .$$

By taking K_{max} into account, Forman's equation describes regions II and III. The significance of these equations is limited, but they can provide estimates of crack growth behavior, especially if region II linearity exists over a wide range of crack growth rates.

The Paris equation directly accounts for the effects of ΔK on da/dN for a given R. In addition to ΔK and R, the Forman equation accounts for the effect of K_{Ic} on fatigue crack growth rate. However, many other factors which influence fatigue crack growth are accounted for in the empirical coefficients used in the previously stated equations for crack growth rate. Other equations, such as the modified Forman equation, the hyberbolic sine equation, and the Collipriest equation exist. Fatigue crack growth is affected by a countless number of parameters and many of these factors interact with each other. Engineering judgment must decide what effects are dominant influences on the crack growth rate for each individual problem [8,9].

VI. ANALYSIS CODES

Currently two types of computer codes for solving fracture mechanics analysis problems, NASA/FLAGRO and NASCRAC, are being used by fracture analysts at MSFC.

NASA/FLAGRO (commonly known as NASGRO) became available in 1986 from the NASA Johnson Space Center. The program was developed under the guidance of the NASA Fracture Control Analytical Methodology Panel and contains stress intensity factor solutions to a number of commonly used crack geometries. Service life calculations are performed with the modified Forman equation which reduces to the Walker or Paris equation depending on material constants used.

NASA/FLAGRO is menu driven and prompts the user for information in a serial manner. After selecting the type of analysis desired, such as safe life, the user answers a series of questions and enters data depending on the particular path taken. Generally, the program operates serially, requiring the user to follow the same path and answer a number of basic questions before each execution.

NASCRAC was developed by Failure Analysis Associates under contract to MSFC. NASCRAC can perform time and/or cycle dependent analysis of subcritical crack growth and evaluate J integrals from previous published results.

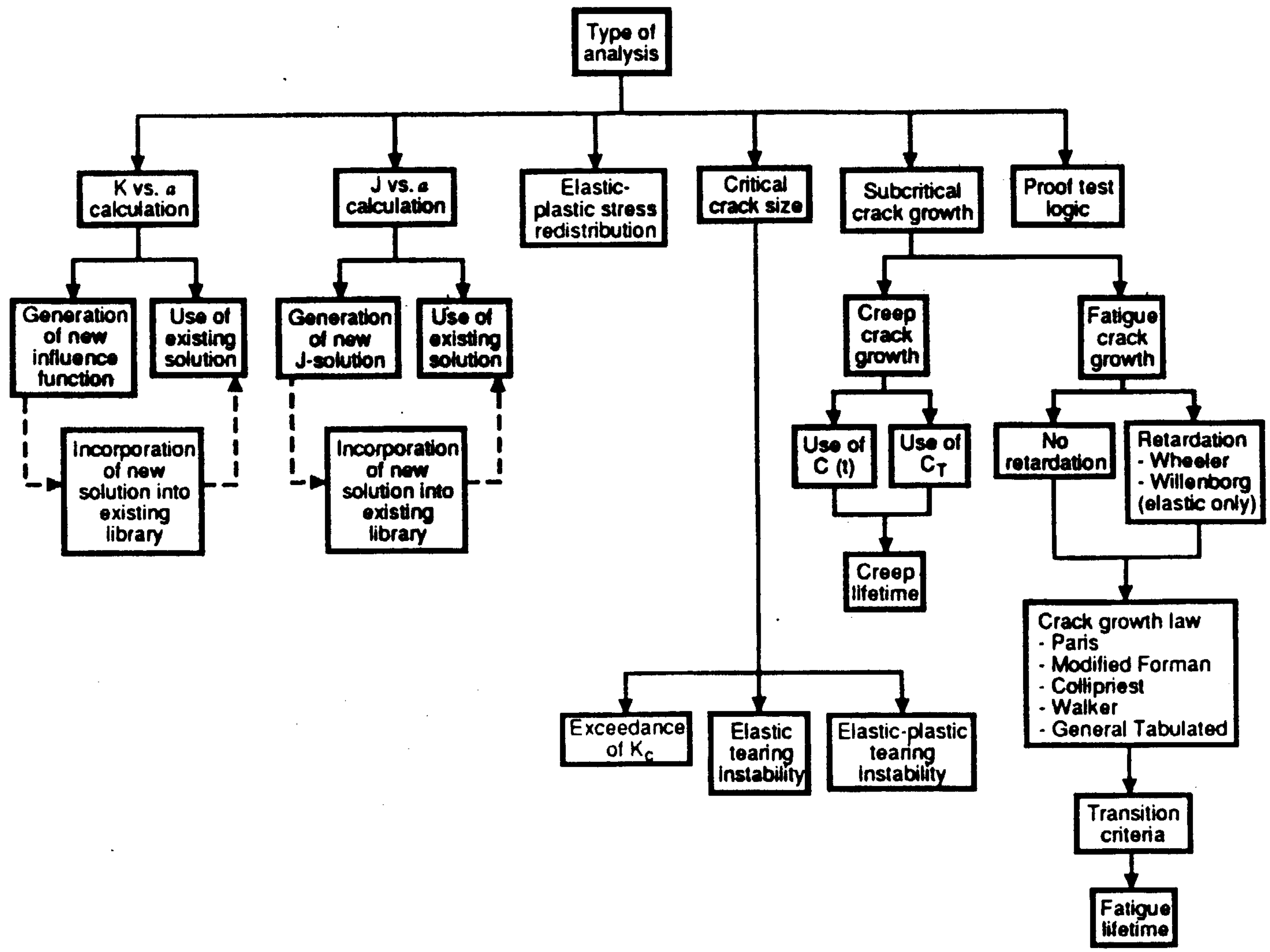

Figure 4. NASCRAC analysis types.

NASCRAC is menu-driven which makes it very easy for the analyst to input data and obtain results. The code contains a wide variety of stress intensity factor solutions. Many of the stress intensity factor solutions in NASCRAC are based on influence functions. The subcritical crack growth analysis portion of the code is tailored primarily for fatigue crack growth although time-dependencies, such as introduced by hold times and various cyclic loading frequencies, can also be analyzed. Several fatigue crack growth laws such as Paris, Forman, Walker, Collipriest, etc., are included in the code. Load interactions are accounted for by a variety of user-selected models, including the Wheeler and Willenborg treatments. Final crack instability is treated by exceedance of a critical value of the stress intensity factor. Figure 4 diagrams the types of analysis contained in the code [2].

VII. ANALYSIS PROBLEMS

The following problems are from fracture mechanics analysis problems solved in the past 8 years (1982–1989) by the fracture mechanics sector at MSFC. The problems are from SSME, HST, SSE, SRB, and the B-1 LOX stand. The problems highlighted are intended to be used as a guide so that the reader may acquire a working knowledge of how to solve real-time fracture mechanics analysis problems.

A. SSME High Pressure Fuel Turbopump Turbine Engine Cracking

The SSME high pressure fuel turbopump (HPFTP) turbine is a two-stage reaction turbine with curvic-coupled rotors powered with 5,500 psi hydrogen-rich steam generated by a fuel preburner producing hot gas temperatures near 2,000 R (1,540 °F). Gaseous hydrogen flows as coolant beneath the platform, passing between the blades and disk in the firtree area at 140 R (-320 °F) on the first stage and 1,400 R (940 °F) on the second stage. Figure 5 shows a cross section of the turbine.

At full power level (FPL) (109 percent of rated power level), the machine produces some 74,000 horsepower while rotating at 36,595 rpm. With 63 blades on the first stage rotor and 59 blades on the second stage rotor, this translates to over 600 hp per blade. The SSME HPFTP first and second stage blades (Fig. 6) have historically experienced a large variation in types and locations of cracks [11].

Figures 7 and 8 show the blade with symmetrical rotor plot and blade/rotor model, respectively. Figure 9 shows a variety of second stage blade cracks.

A fracture mechanics analysis was done on the crack at the transverse downstream firtree face (Fig. 9f) of the second stage blade.

1. Stress Information

A crack in the area of neck 3 (Fig. 10) was analyzed. The stresses were obtained from an ANSYS three-dimensional finite element model (row of 30 equally spaced elements along the firtree longitudinal axis, i.e., into paper in Figure 10). The top curve of Figure 11 depicts the maximum stress at any given station along the firtree axis. The bottom curve depicts the average stresses at any given station along the firtree axis.

NOTE: In order to accurately analyze this problem, the analyst should pick the stresses from the curves in Figure 11 corresponding to x distances from center to center of the 30 equally spaced elements from 0 to 1.06 in.

2. Material Properties

The blades are made of MAR-M246. An "a versus K" solution was initiated to determine a critical crack size for the second stage blade, therefore crack growth constants were not required. The critical stress intensity factor K is needed in this type of analysis. At the time of the analysis, the K value had not been determined, therefore a curve was drawn (one curve using the maximum stresses across the section and the other using the average stress across the section), and a critical crack size for the blade could be determined for any range of K values.

3. Solution Model

The crack was assumed to have propagated all the way across the face shown in Figures 12, 13, and 14 and is growing from the trailing edge to the leading edge. The NASCRAC computer code was used in this analysis. A conservative analysis was done using the through edge crack model in Figure 12. The width (W) = 1.06 in.

4. Results

As stated above, the curves in Figures 13 and 14 were used to determine the critical flaw size for the second stage blade [12].

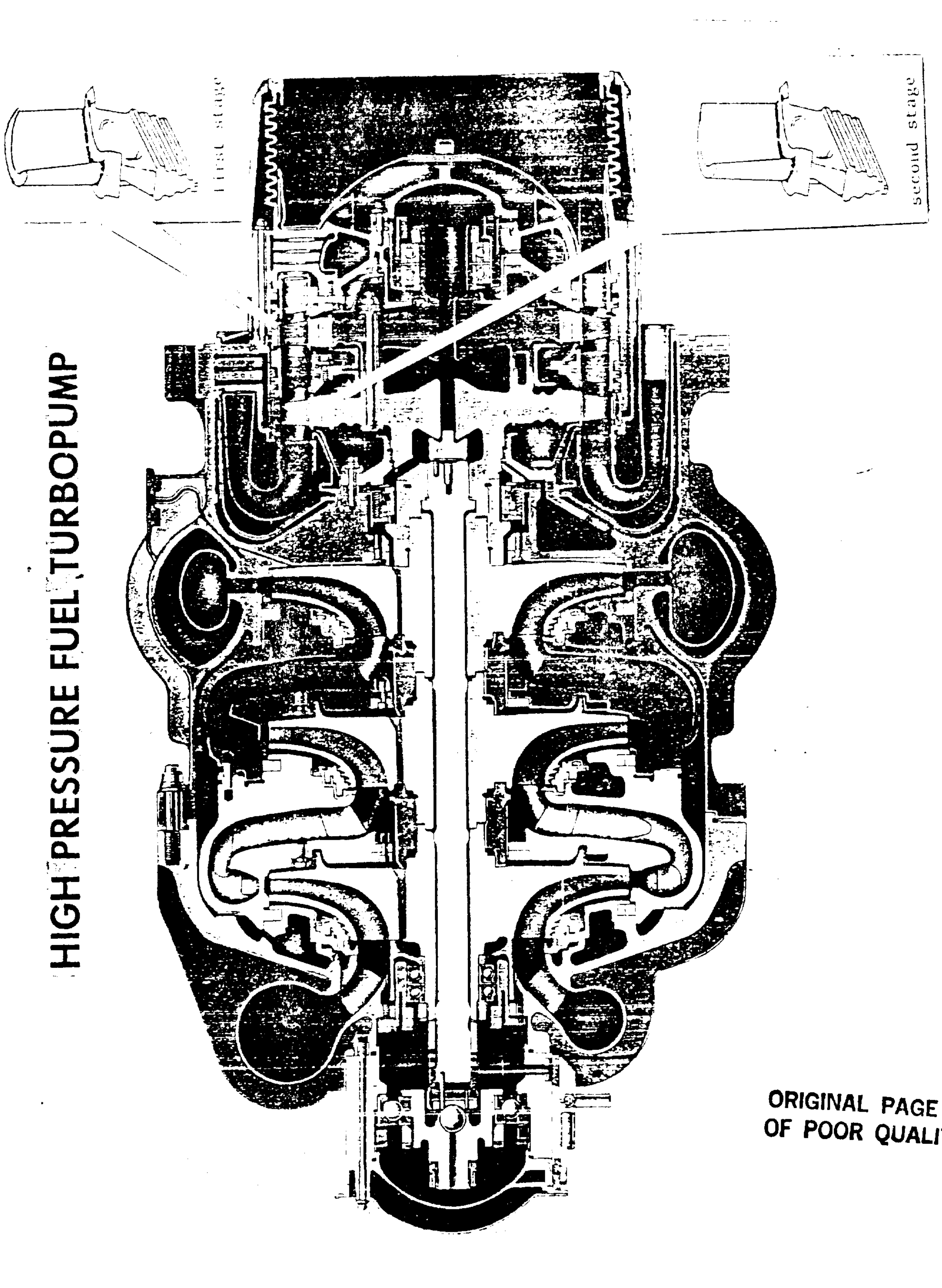

Figure 5. HPFTP section.

ORIGINAL PAGE IS
OF POOR QUALITY

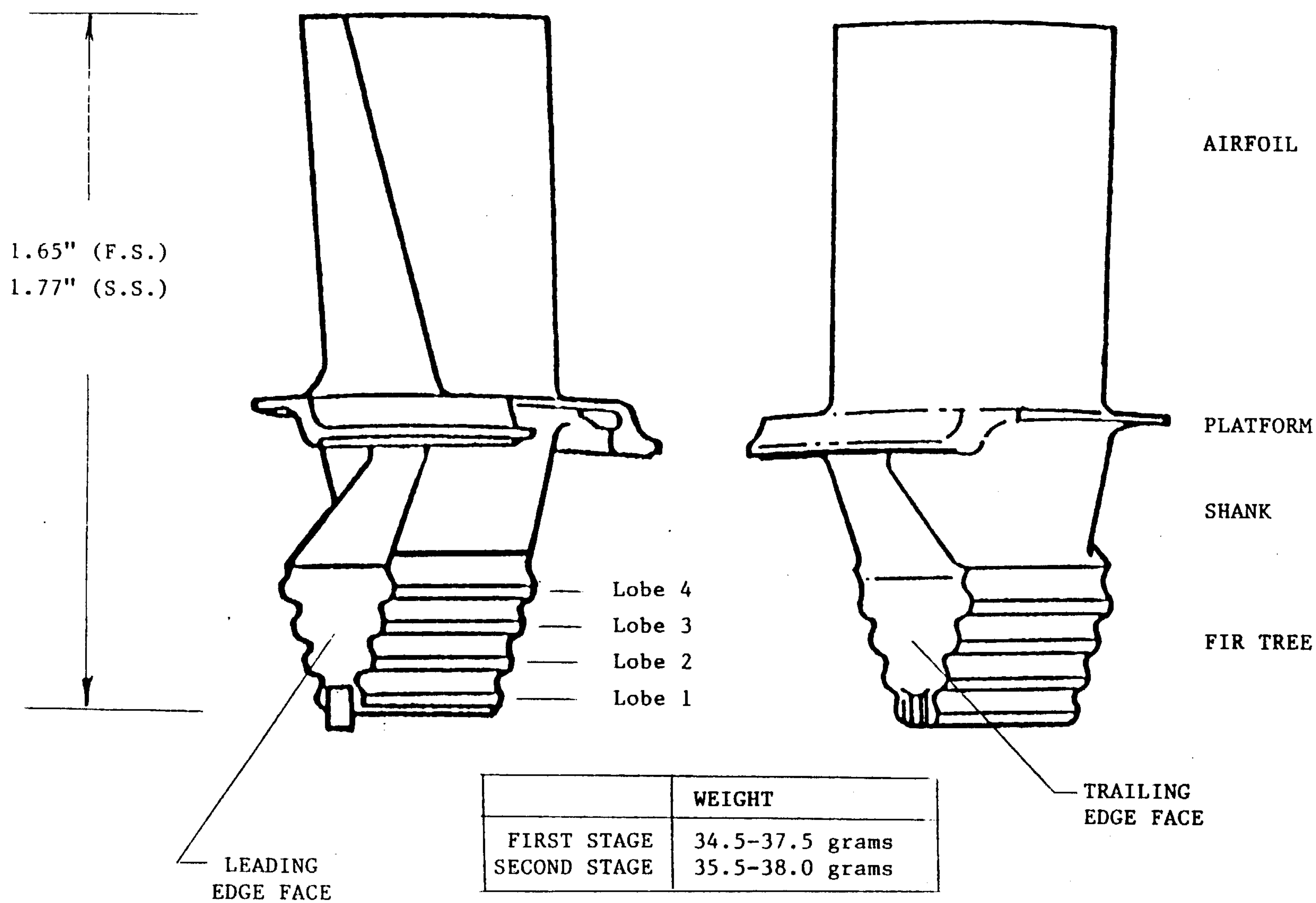

	WEIGHT
FIRST STAGE	34.5-37.5 grams
SECOND STAGE	35.5-38.0 grams

Figure 6. HPFTP first and second stage blade.

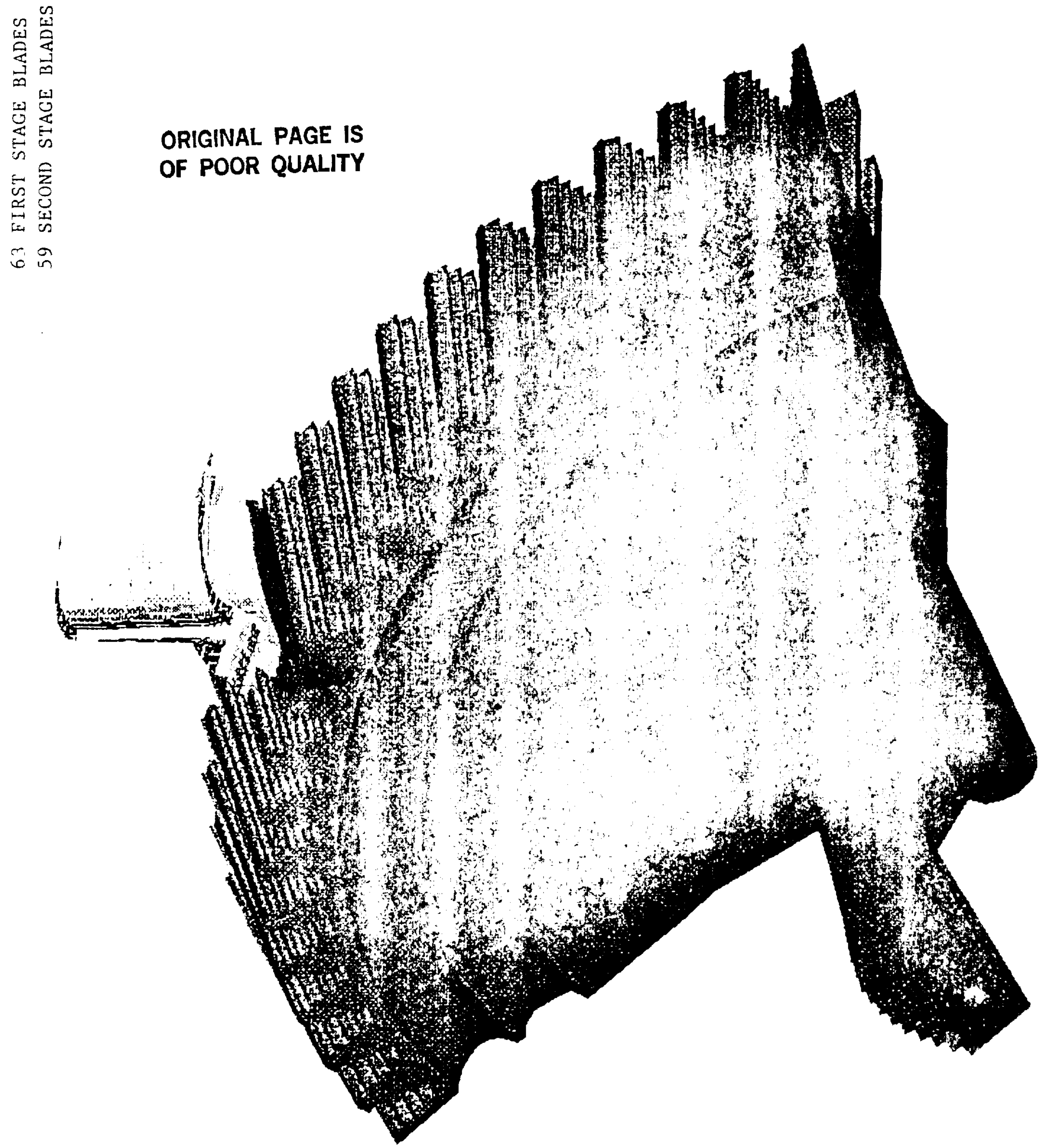

Figure 7. HPFTP blade with symmetrical rotor plot.

ORIGINAL PAGE IS
OF POOR QUALITY

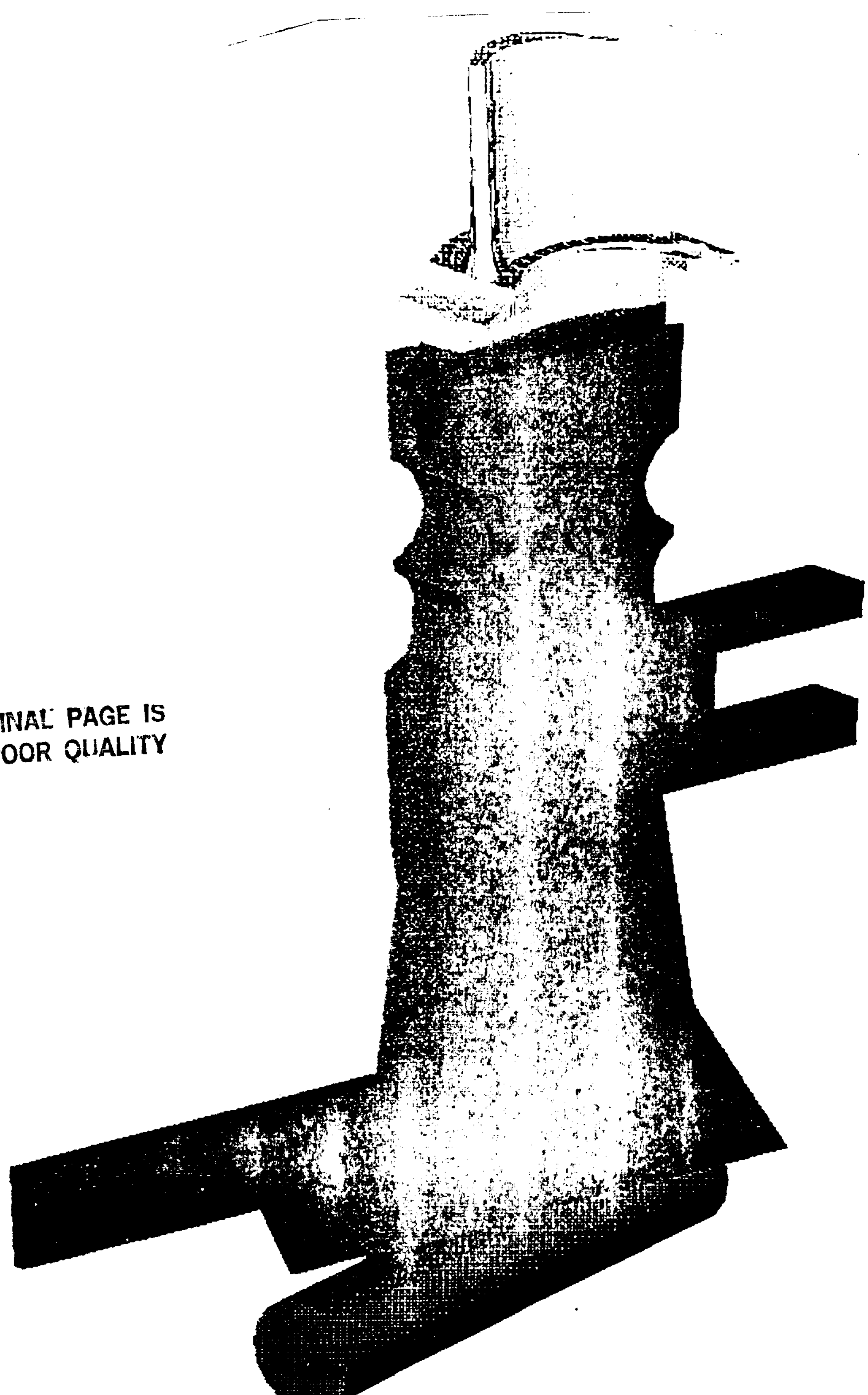

Figure 8. HPFTP blade and rotor model.

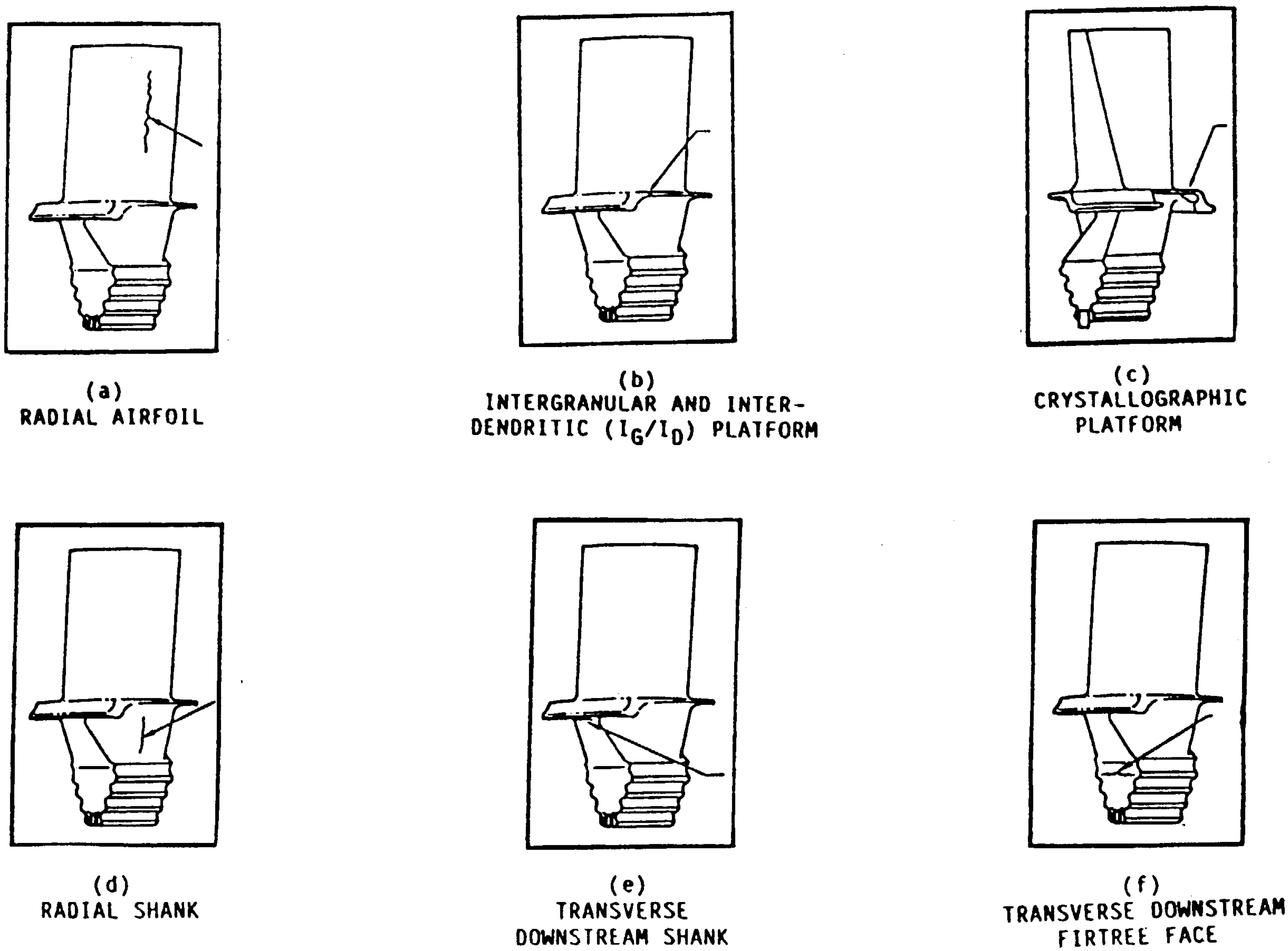

Figure 9. HPFTP second stage turbine blade cracks.

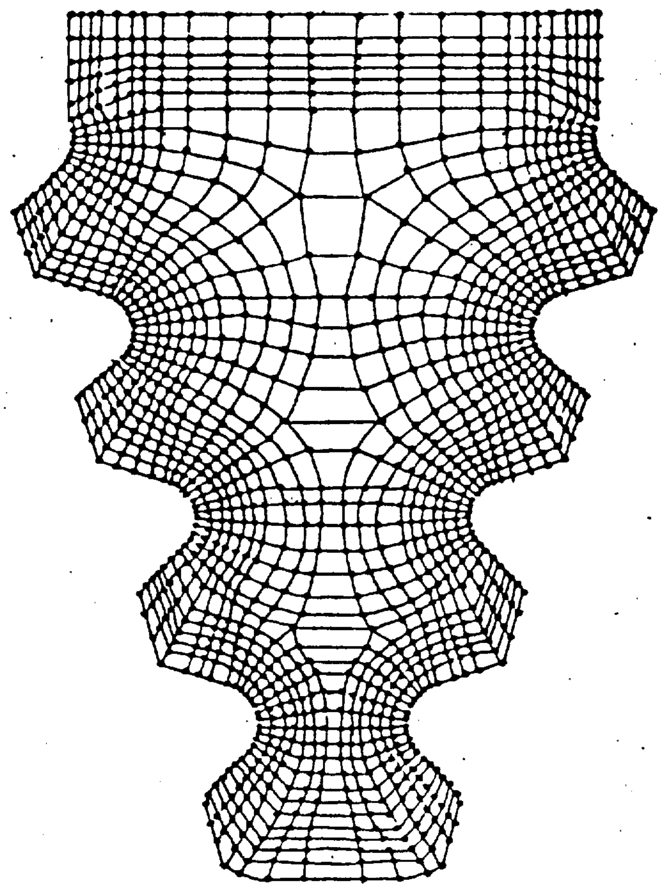

Figure 10. HPFTP two-dimensional firtree model.

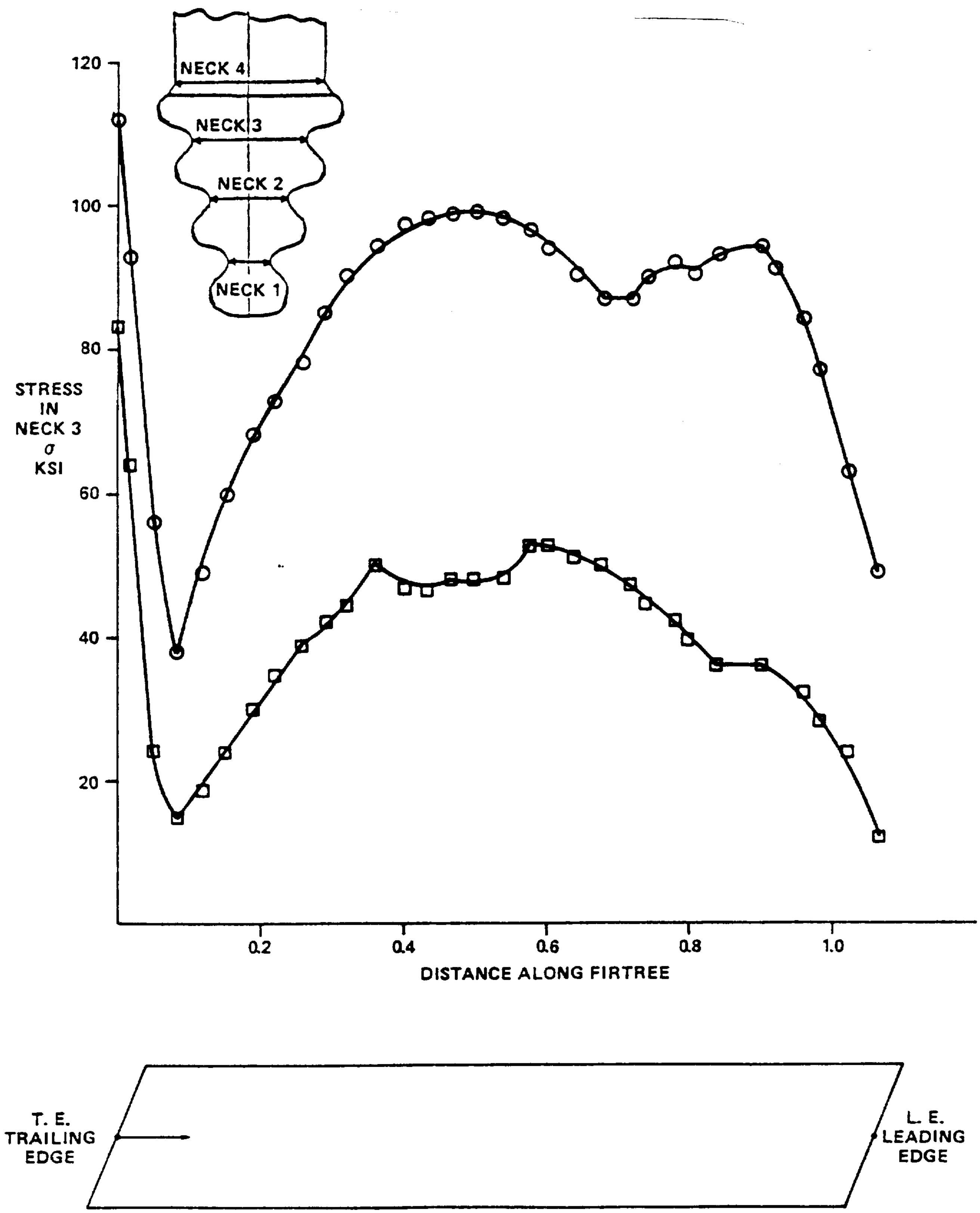

Figure 11. HPFTP second stage blade, neck 3 stress versus distance along firtree.

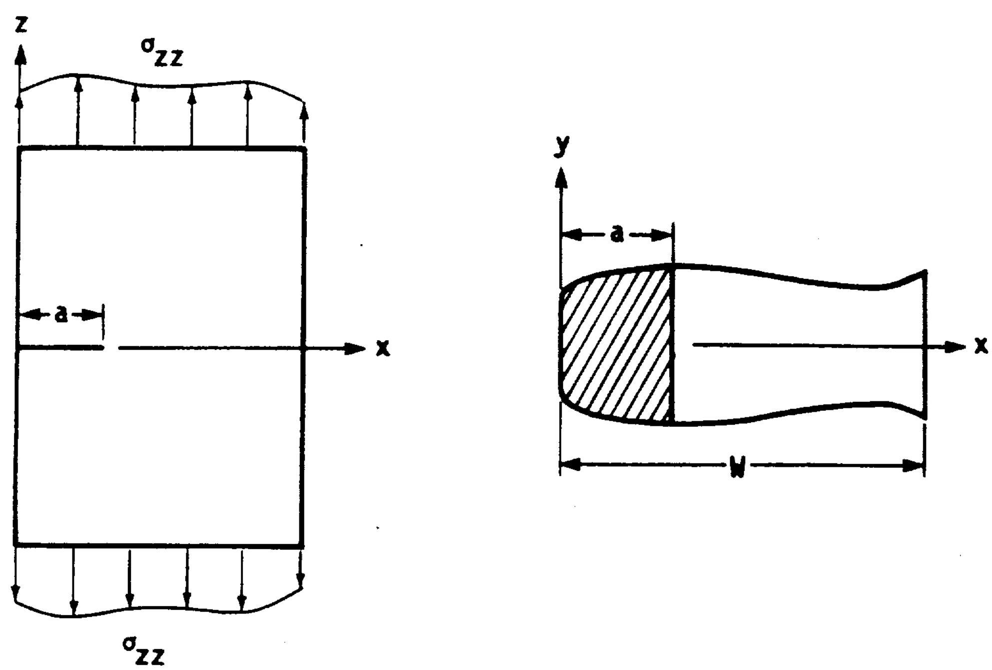

Figure 12. NASCRAC through edge crack model.

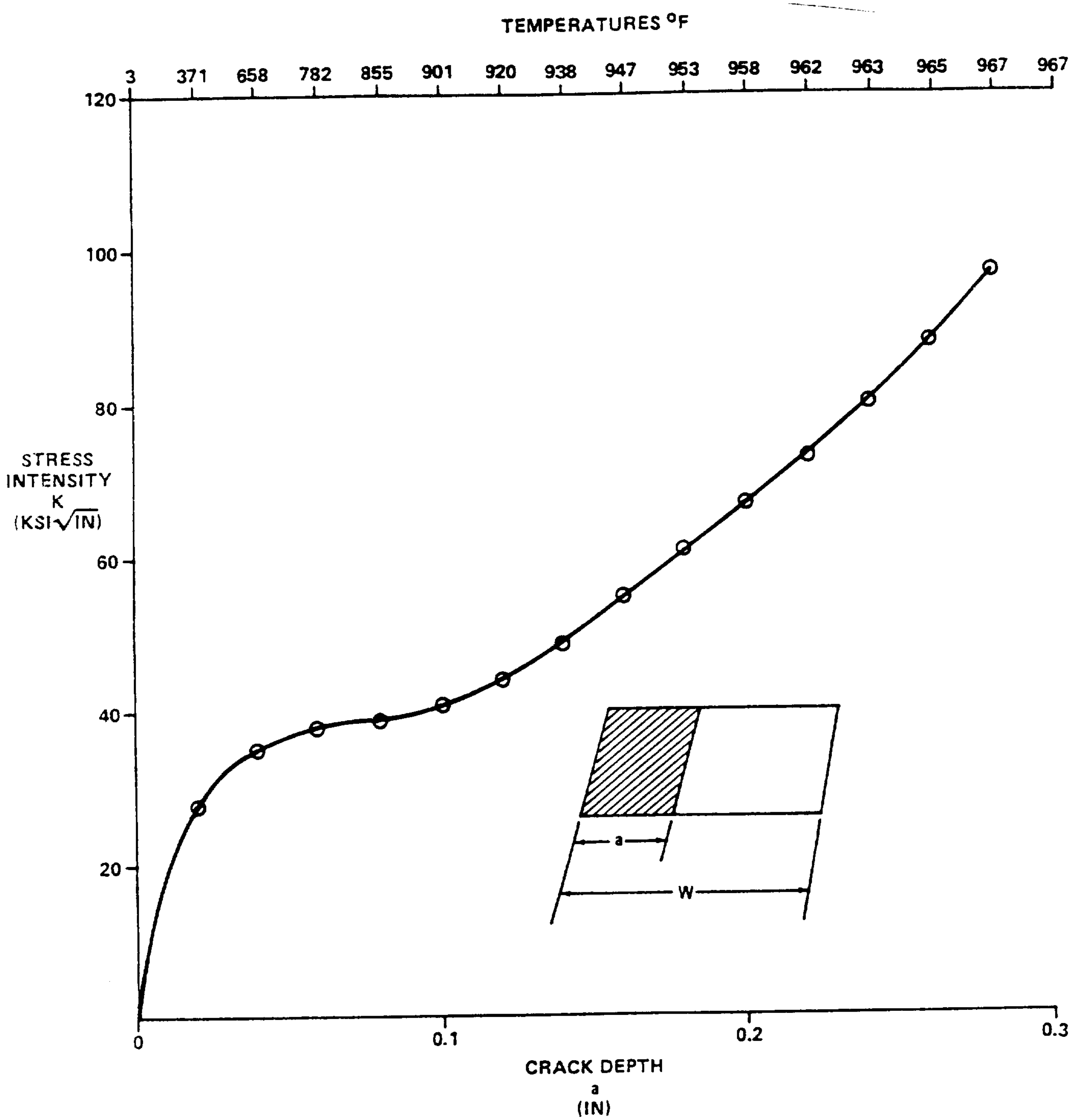

Figure 13. HPFTP K versus a curve for σ_{max}.

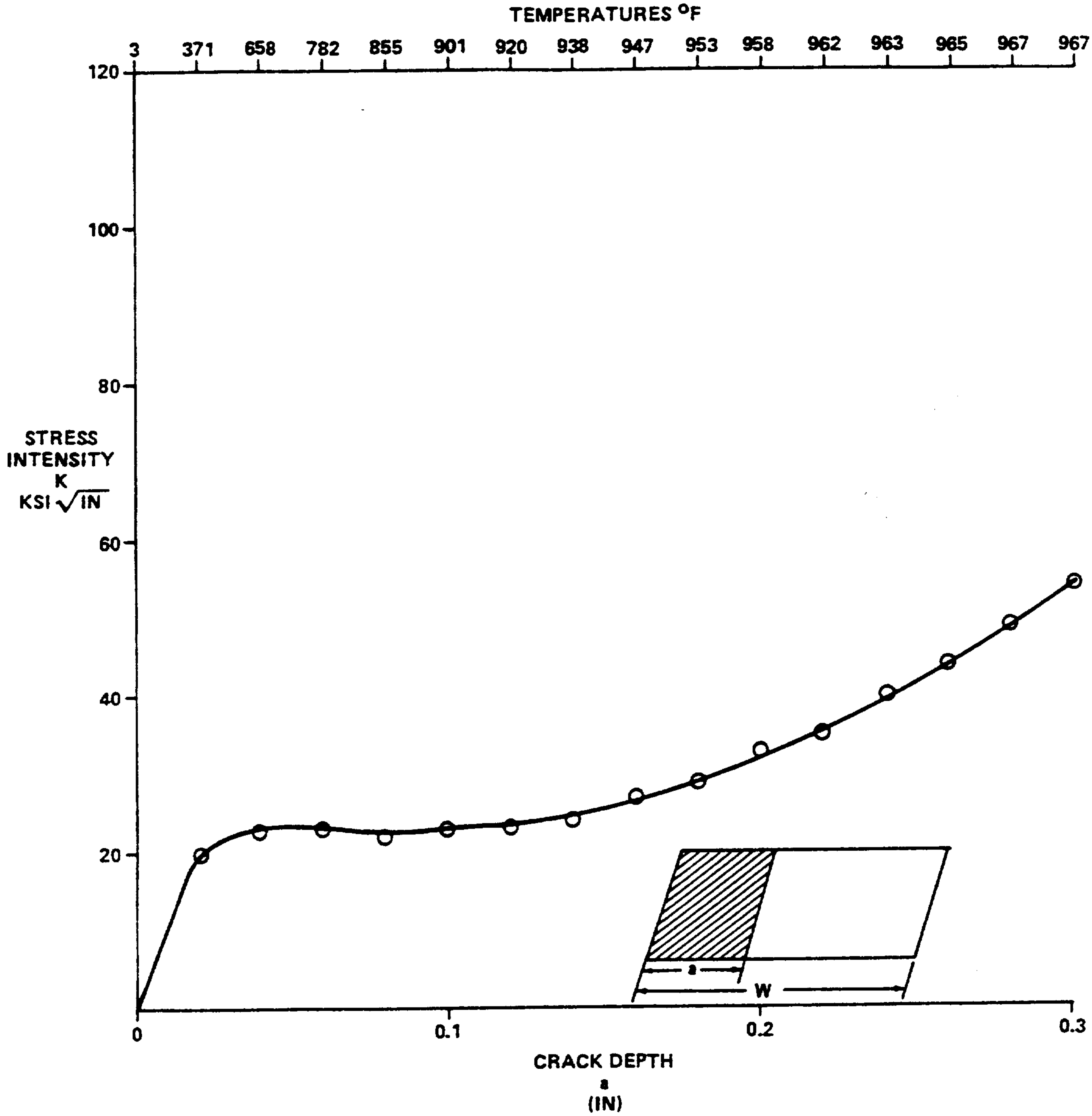

Figure 14. HPFTP K versus a curve for σ_{avg}.

B. Engine 0212 Failure Investigation
High Pressure Oxygen Turbopump (HPOTP) First Stage Disk
Fracture Mechanics Analysis

Test 904-044 was prematurely shutdown at 1,270.7 seconds into a planned 1,338-second test. The first-stage disk was found atop components of the second-stage disk. The first-stage disk failed in three pieces (Fig. 15). A fracture mechanics analysis of the first-stage disk was undertaken at two locations on the disk: (1) crack at base of firtree and (2) crack at curvic bolt hole. Both areas are shown in Figure 16.

1. Stress Information

The fracture mechanics analysis of the first-stage disk was performed using data derived from engine test history. Four cases were examined:

a. Twenty-two tests prior to incident

b. Last test only (with no overspeed condition)

c. Overspeed condition

d. All 23 tests (with no overspeed condition).

The stresses used for the test history in cases a through d were obtained from an axisymmetric ANSYS finite element model. For cases a, b, and d the stresses were obtained for power levels of 65, 100, 104, and 109 percent, respectively. For case c, the stresses were obtained for the power level corresponding to the overspeed condition (42,200 rpm). The stress contour plots for the disk at power levels of 65 to 109 percent and at the overspeed condition are shown in Figures 17 through 21 [13].

2. Material Properties

The first stage disk is made of Waspaloy. Operating conditions for the disk were 550 °F, 4,400 psi in hydrogen gas. The disk was subjected to stresses for a time period exceeding 20 minutes. A literature search revealed crack growth rate data (da/dN-ΔK) for Waspaloy at room temperature, 5,000 psi in hydrogen gas. The reference data were taken for a typical SSME duty cycle of 9 minutes. Approximately 8.2 minutes of hold time at maximum load occurred in the test data.

To approximate the fatigue crack propagation properties of Waspaloy at 550 °F and 4,400 psi hydrogen, data taken at room temperature and 5,000 psi hydrogen were used (Fig. 22a). A hold time of approximately 490 seconds (8.2 minutes) was used to convert da/dN-ΔK data into da/dt-ΔK by considering the cyclic effect to be small. Crack growth with respect to time (da/dt) was calculated by dividing the cyclic crack growth rate (da/dN) by the hold time (1 cycle = 490 seconds). For hold times from 8 to 16 minutes, da/dt values were increased by a factor of 5, and for hold times greater than 16 minutes, a factor of 10 was used. These factors are needed to account for the increase in da/dt for larger hold times.

The estimated increases in da/dt are conjectural, i.e., there are no hold time data in hydrogen to verify these estimates. However, da/dN data taken at 1,200 °F for hold times ranging from 2 to 15 minutes indicate an increase in da/dN of close to a factor of 10 (Fig. 22b). If the hydrogen effect with hold times behaves similarly, then the estimated increases in da/dt are plausible. At the current time, no better scheme for hold times greater than 8 minutes has been developed [14].

Table 1 shows the time in seconds at each power level. For tests greater than 8 minutes, higher growth rates were used for analysis, as previously described.

3. Solution Model

The NASCRAC was used in this investigation to perform life analyses and to calculate critical initial flaw sizes (CIFS). Two areas of interest were examined: (1) a through crack growing radially inward from the base of the firtree, and (2) a part-through crack growing from a bolt hole near the curvic coupling of the disk. The geometry models are shown in Figure 23. It should be noted that the analyses were conducted on a per unit time basis (seconds) and not on a per cycle basis. Therefore, when NASCRAC refers to a load cycle, it should be interpreted to mean 1 second.

4. Results

Tables 2 and 3 show the results of the failure investigation. The flaws in the curvic bolt hole area are much smaller than the flaws at the firtree root. Therefore, the CIFS's calculated for the curvic bolt area are the dominating flaws. Figure 24 contains a plot of disk burst speed versus critical flaw size. It can be seen from the figure that flaw size has a significant effect on burst speed. The shaded portion of the figure is the area of yielding due to the stresses near the bolt hole. The curve was estimated in this area with the end points determined by the burst speed predicted when no flaw exists and the limits of linear elastic fracture mechanics.

TABLE 1. ENGINE 0212 MATERIAL PROPERTIES DERIVATION

A) All 23 tests (8372 seconds)

Totals	Power Levels				Data Used
	65%	100%	104%	109%	
Time under 8 minutes	157	408	4105	1367	da/dt
8-16 minutes	69	147	1247	581	5 * da/dt
Over 16 minutes	9	55	166	61	10 * da/dt
Time at each power level	235	610	5518	2009	

B) Last test only (1271 seconds)

Totals	Power Levels				Data Used
	65%	100%	104%	109%	
Time under 8 minutes	15	93	279	103	da/dt
8-16 minutes	15	93	279	103	5 * da/dt
Over 16 minutes	9	55	166	61	10 * da/dt
Time at each power level	39	241	724	267	

C) First 22 tests (7101 seconds)

Totals	Power Levels				Data Used
	65%	100%	104%	109%	
Time under 8 minutes	142	315	3826	1264	da/dt
8-16 minutes	54	54	968	478	5 * da/dt
Over 16 minutes	0	0	0	0	10 * da/dt
Time at each power level	196	369	4794	1742	

TABLE 2. ENGINE 0212 STRESS SPECTRA

A) Base of Firtree

Description (Power Level)	σ_{hoop} (ksi)	Time Duration (sec)
65%	23.0	235
100%	47.0	610
104%	51.0	5518
109%	55.0	2009
Overspeed (42,200 RPM)	110.0	1

B) Curvic Bolt Hole Area

Description (Power Level)	σ_{hoop} (ksi)	Time Duration (sec)
65%	28.3	235
100%	58.1	610
104%	62.3	5518
109%	67.4	2009
Overspeed (42,200 RPM)	122.0	1

TABLE 3. ENGINE 0212 CRITICAL FLAW SIZE RESULTS

A) Base of Firtree

Condition	Critical Initial Flaw Size	Time Duration
22 test prior to incident	0.2083	7100
Last Test Only (no overspeed condition)	0.7310	1272
Last test only (overspeed condition)	0.2369	1
All 23 test (no overspeed condition)	0.1961	8372

B) Curvic Bolt Hole Area

Condition	Critical Initial Flaw Size	Time Duration
22 tests prior to incident	0.0366 x 0.0366	7100
Last test only (no overspeed condition)	0.0535 x 0.053	1272
Last test only (overspeed condition)	0.0180 x 0.018	1
All 23 tests (no overspeed condition)	0.0322 x 0.0322	8372

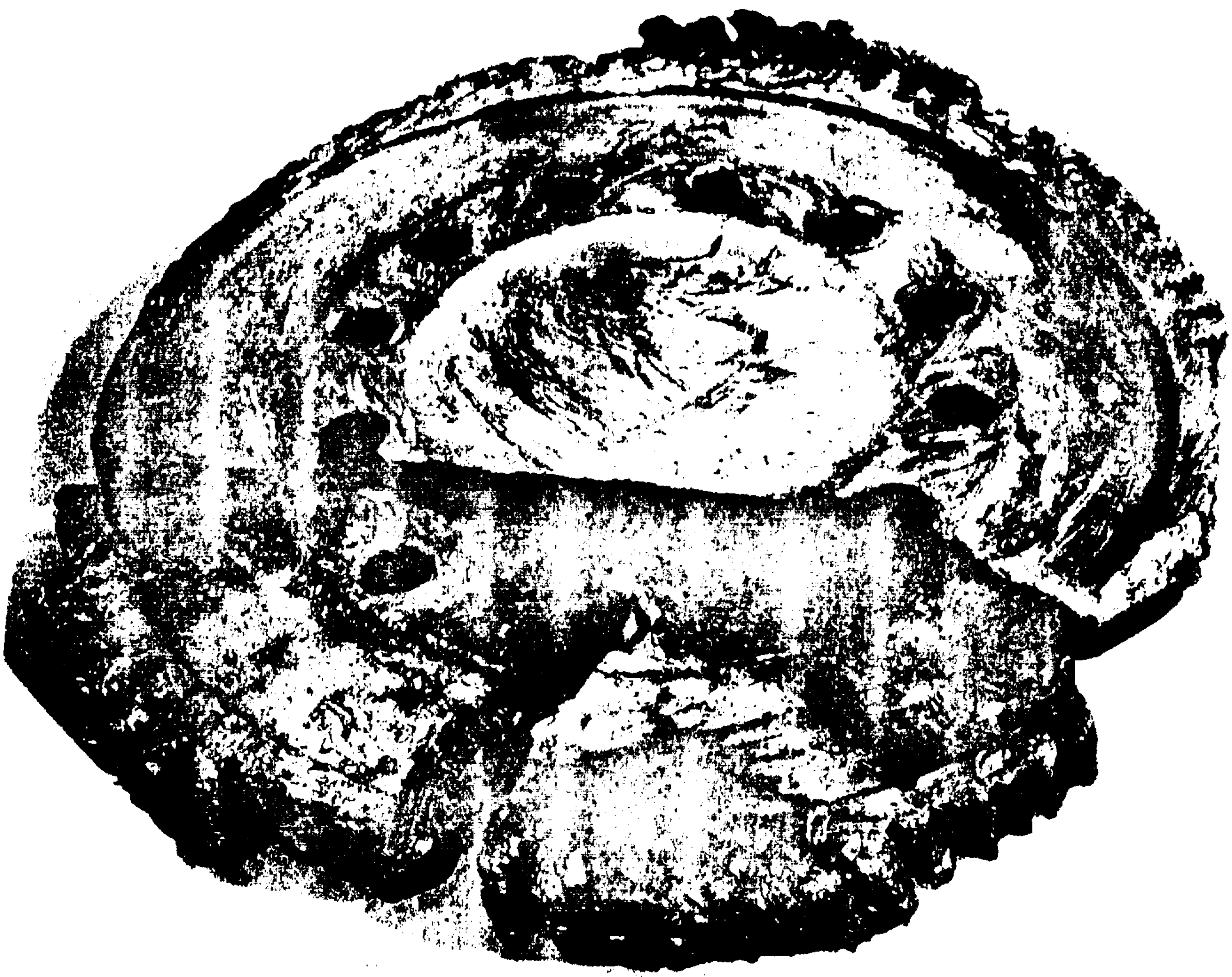

Figure 15. HPOTP first stage disk after incident.

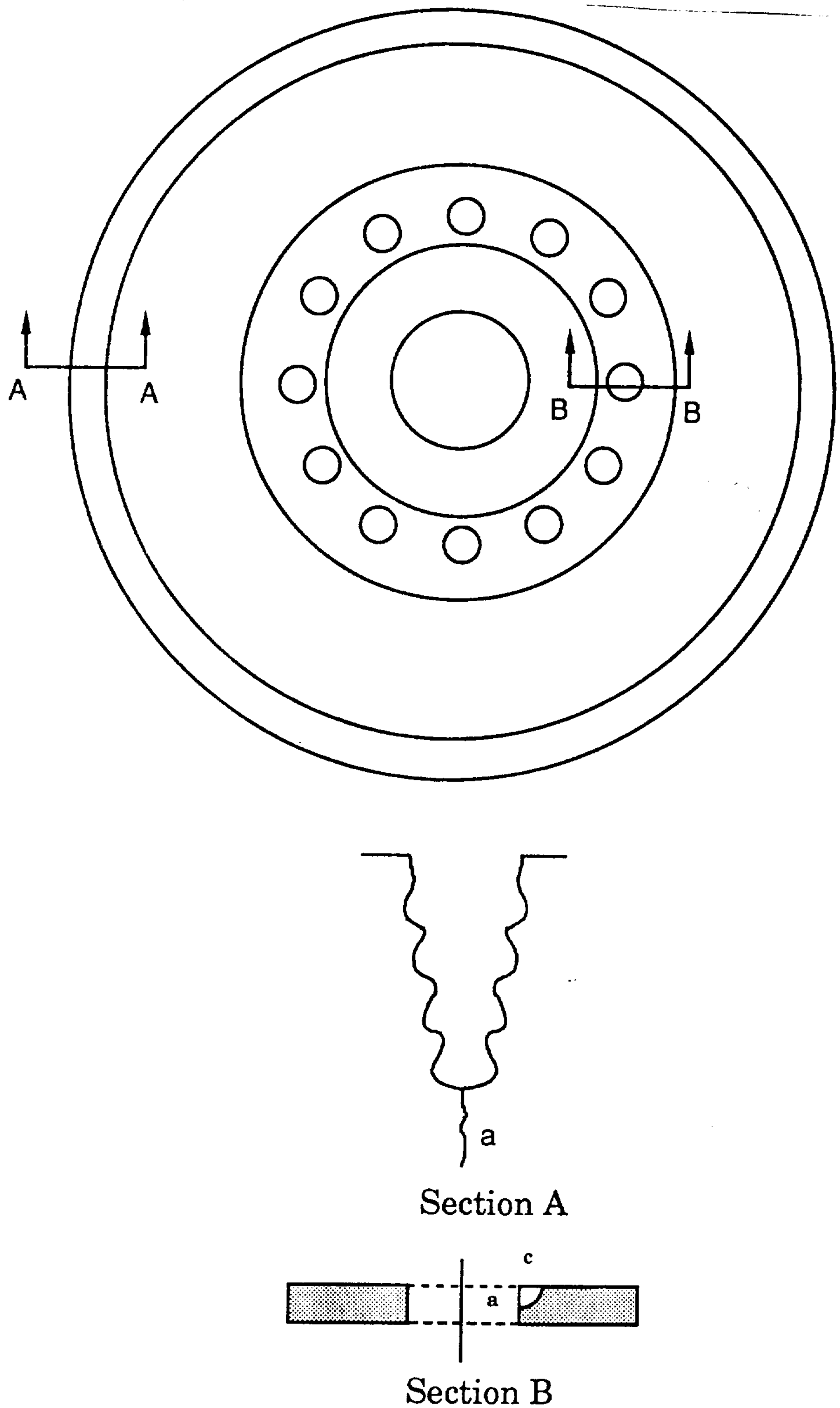

Figure 16. HPOTP disk sections analyzed.

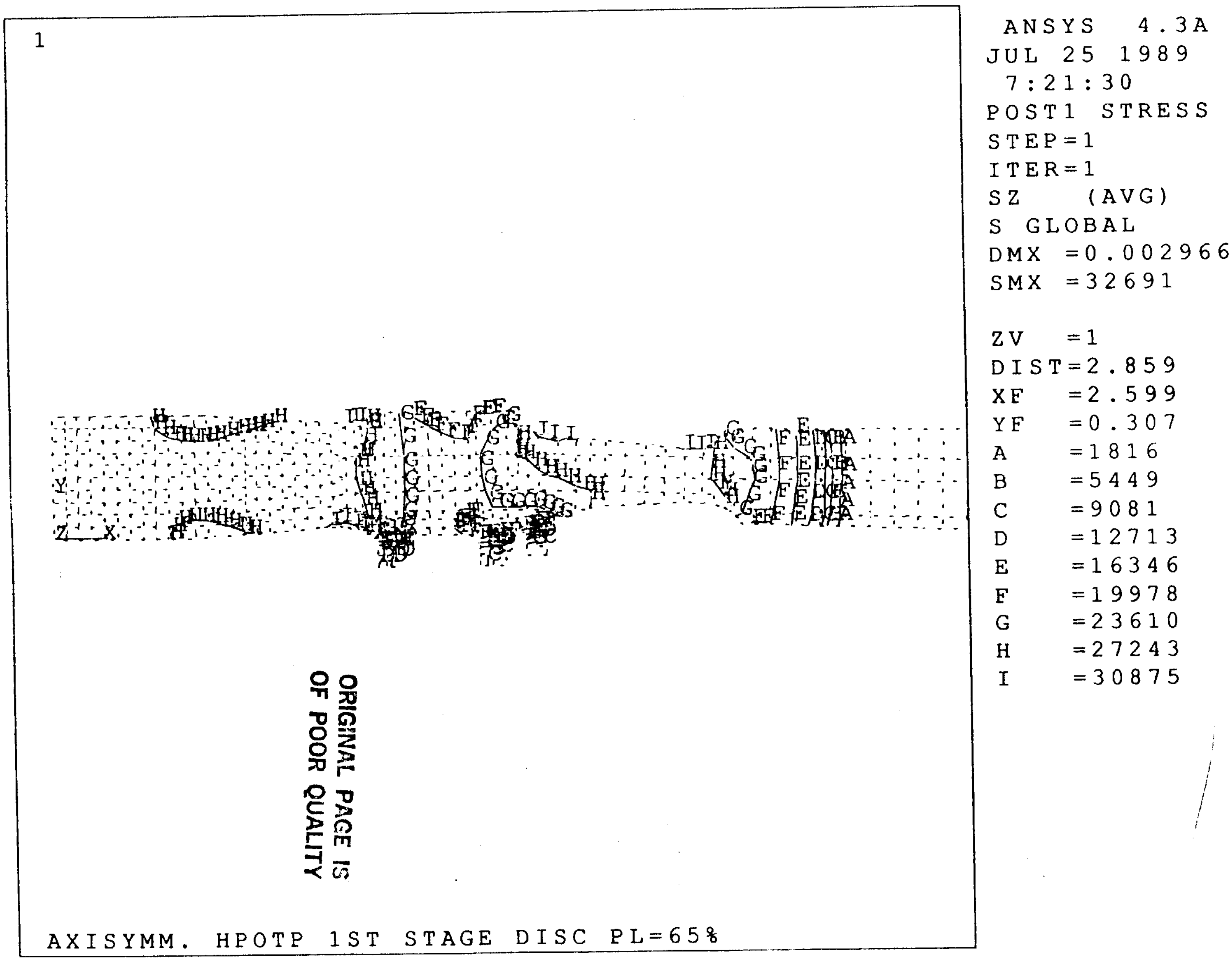

Figure 17. HPOTP stress contour plot. 65-percent power level.

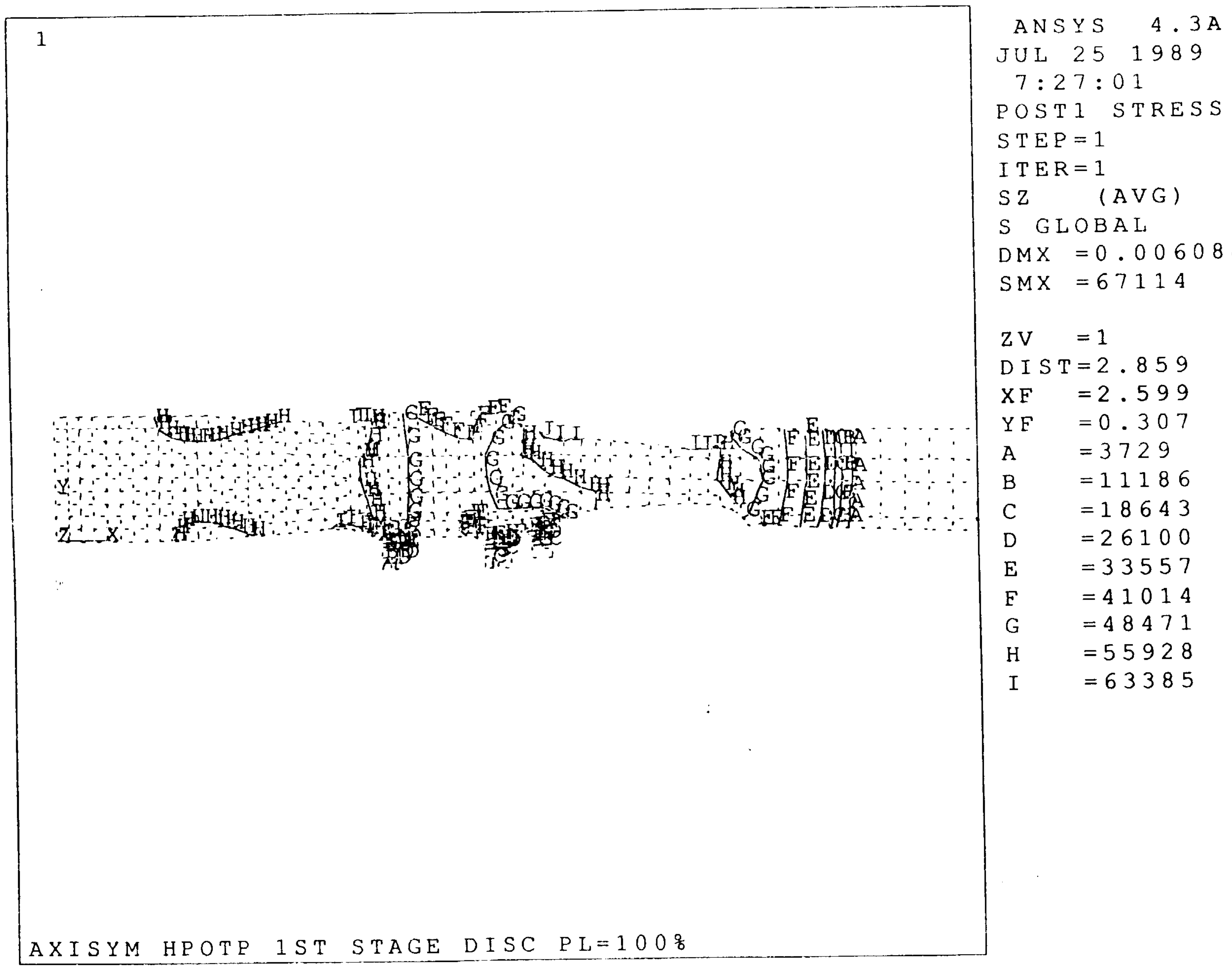

Figure 18. HPOTP stress contour plot, 100-percent power level.

ORIGINAL PAGE IS
OF POOR QUALITY

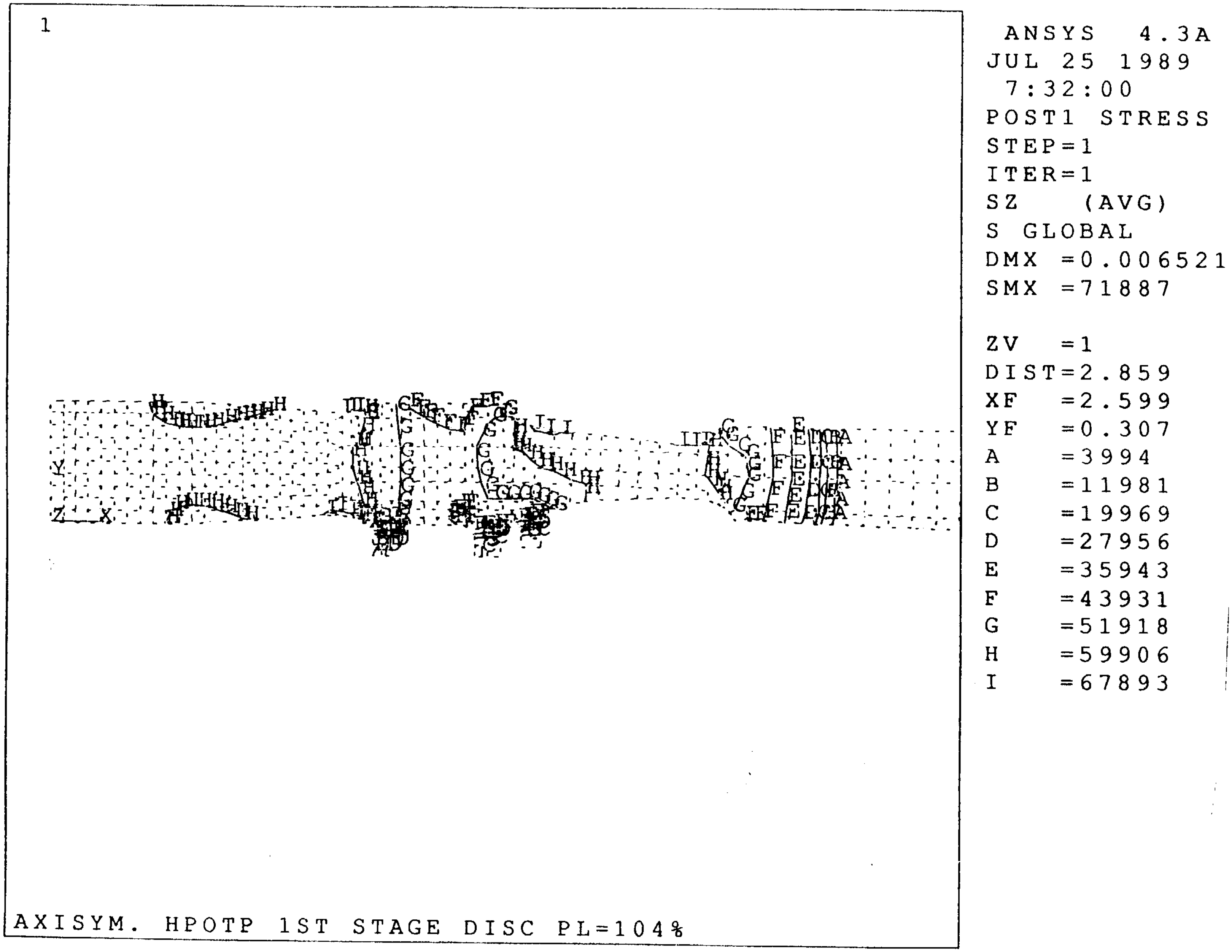

Figure 19. HPOTP stress contour plot, 104-percent power level.

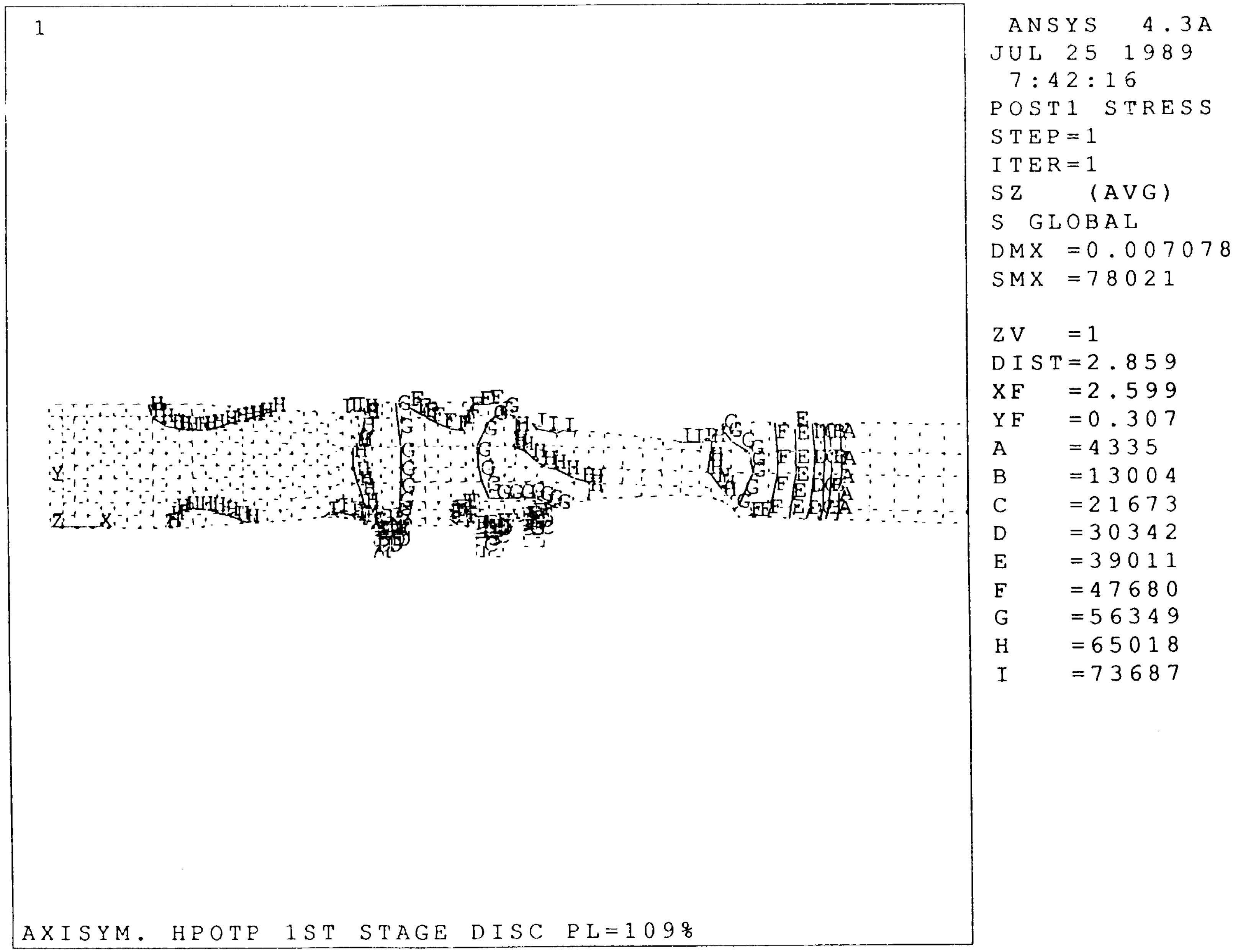

Figure 20. HPOTP stress contour plot, 109-percent power level.

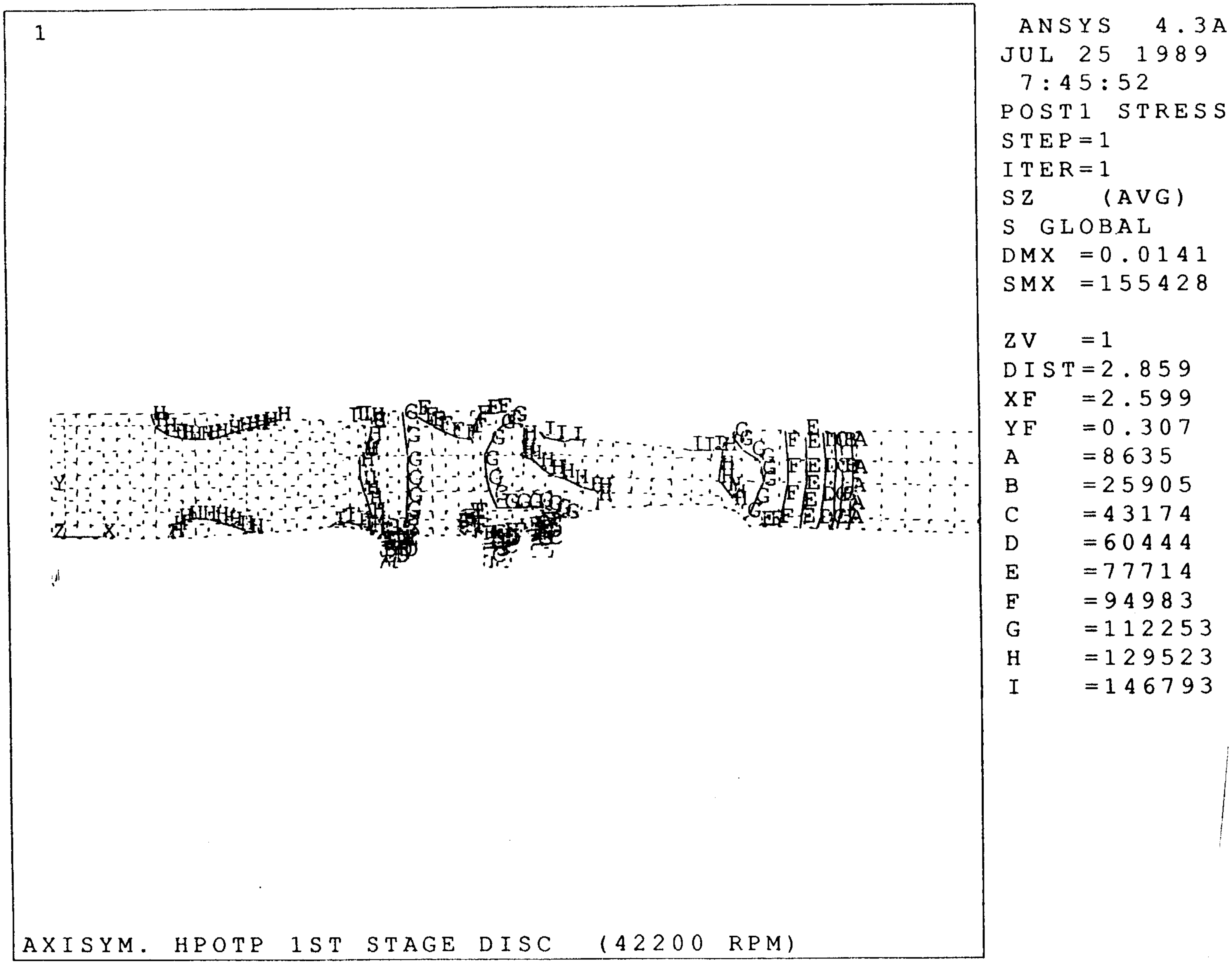

Figure 21. HPOTP stress contour plot, overspeed condition.

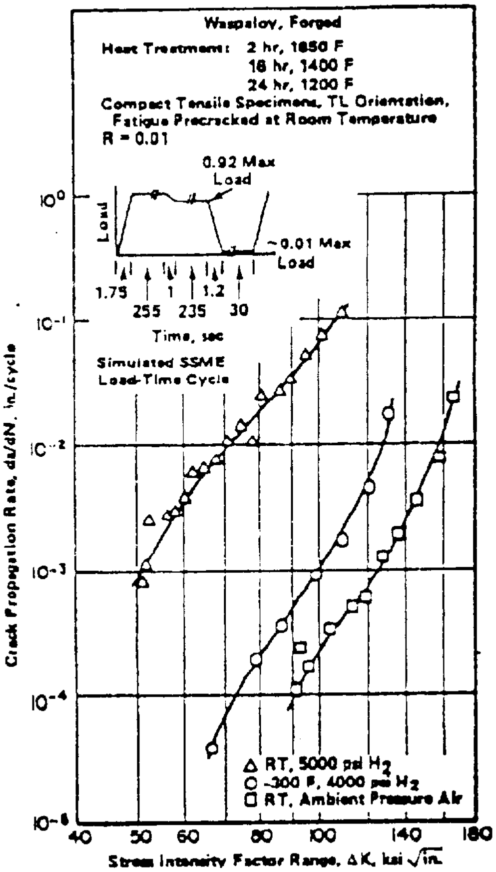

FIGURE 3.06122. EFFECTS OF HYDROGEN ON SIMULATED SPACE SHUTTLE MAIN ENGINE (SSME) CYCLE CRACK PROPAGATION RATE OF WASPALOY AT ROOM TEMPERATURE AND -300 F (68)

(A)

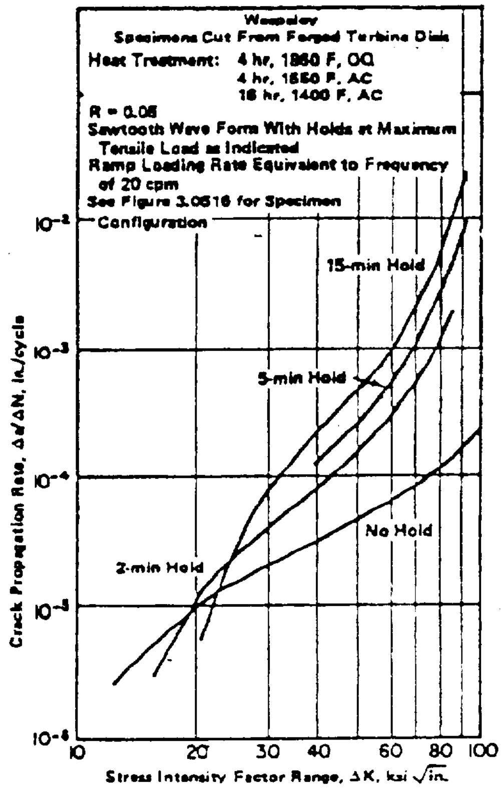

FIGURE 3.05115. EFFECT OF HOLD TIME ON CRACK PROPAGATION RATES FOR WASPALOY AT 1200 F (60)

(B)

Figure 22. HPOTP data from "Aerospace Materials Handbook."

ORIGINAL PAGE IS
OF POOR QUALITY

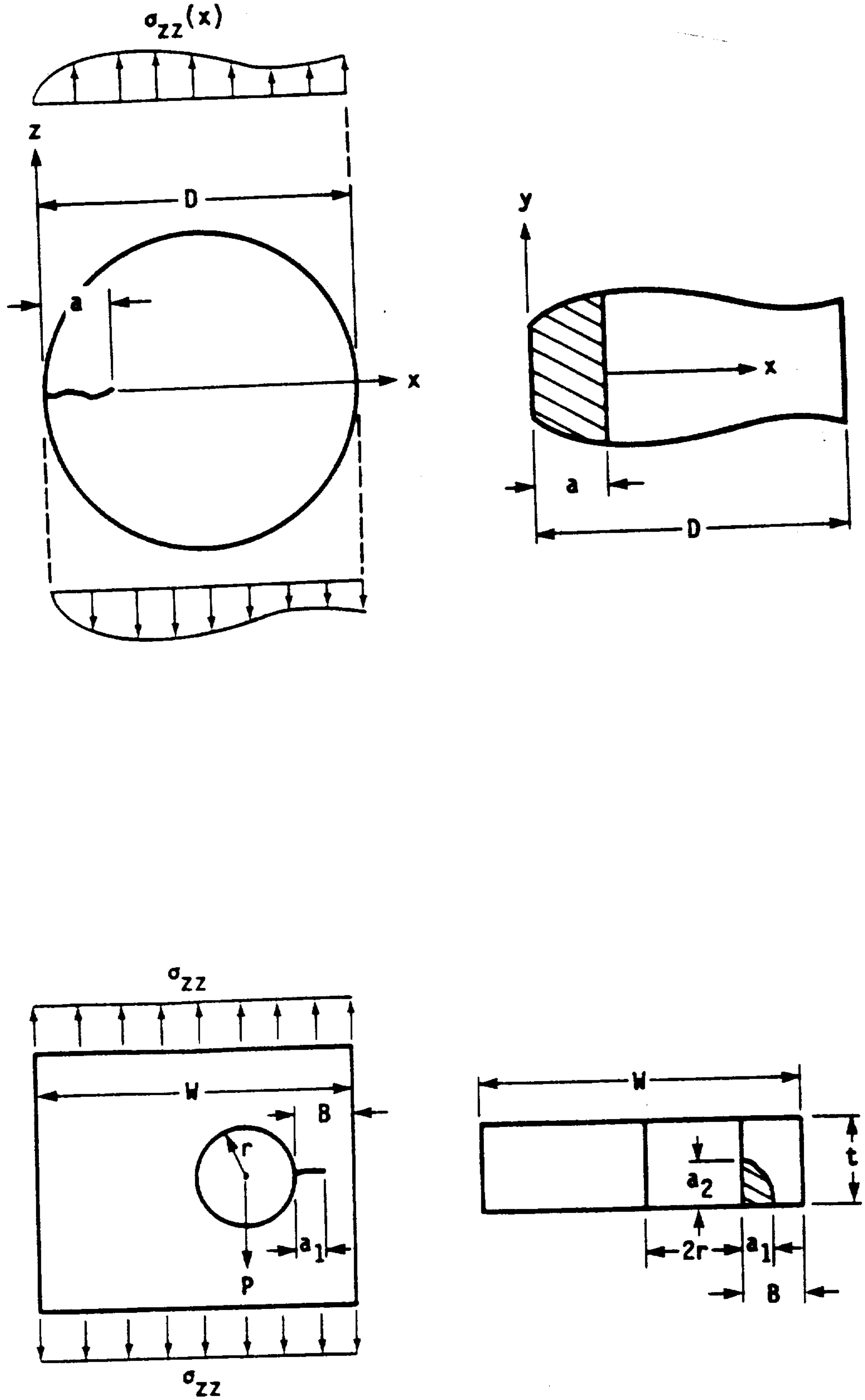

Figure 23. HPOTP NASCRAC geometry models.

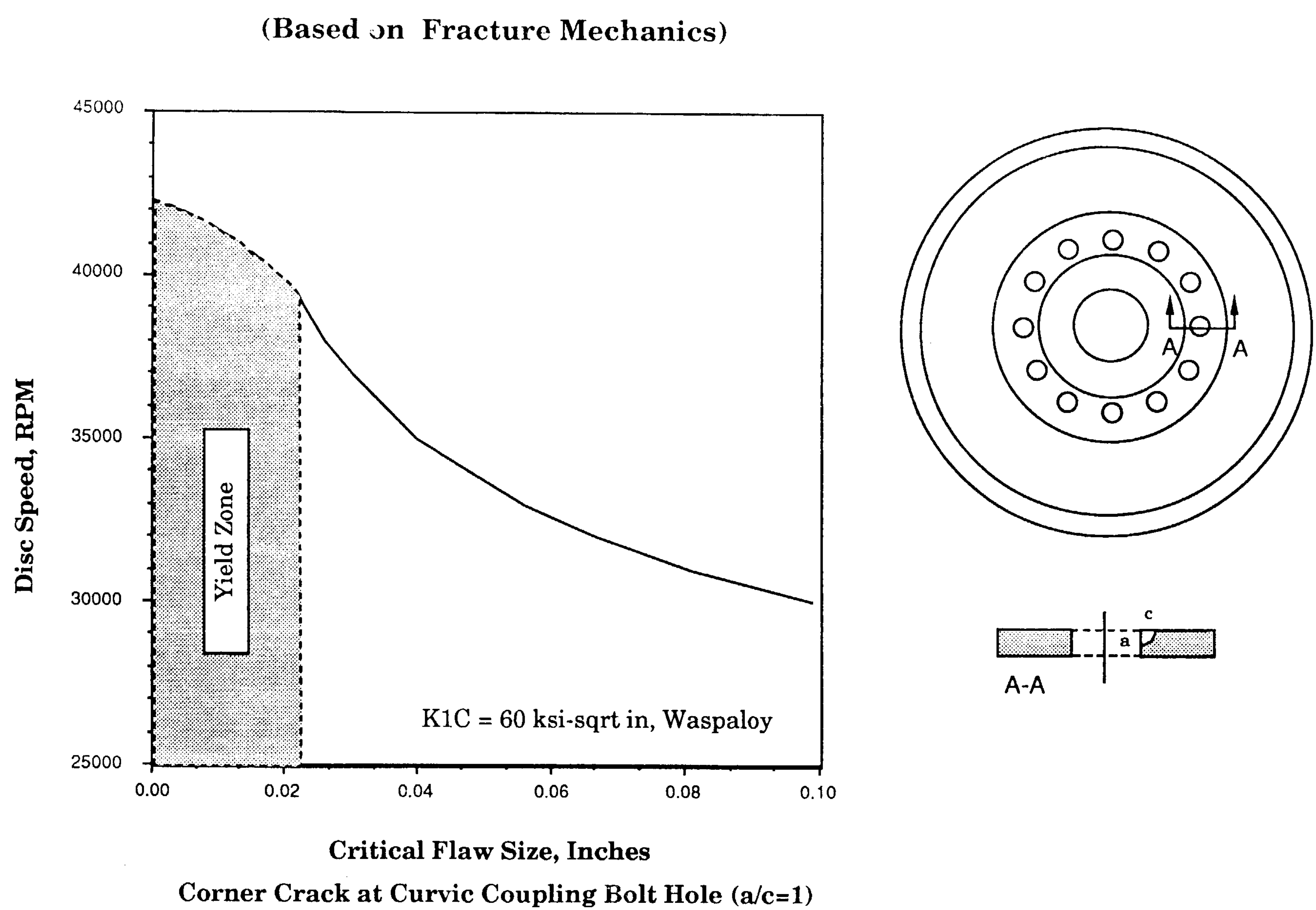

Figure 24. HPOTP disk burst speed.

C. Hubble Space Telescope

The HST will allow scientists and engineers to see seven times farther than ever before. The telescope consists of two mirrors – a primary and a secondary. The telescope weighs approximately 25,000 lb and is 43 ft long.

The fracture mechanics analysis results [15] of this section are from problems analyzed in 1982 and 1983. Portions of the following analyses have since been updated to account for new load conditions, improved inspection criteria, etc. The fracture mechanics analysis was originally done for a five launch, four landing scenario. Based on a memo from the chief engineer's office [16], the fracture mechanics analysis was done for the scenario listed in Table 4, steps 1 through 12. This criteria was for three launches and two returns. The analysis highlighted in this section is for steps 1 through 7 in Table 4, and was based on instructions per engineering management (two launches and two returns).

The HST fracture mechanics analyses highlighted are for the following fracture sensitive parts of the optical telescope assembly (OTA) main ring: inner and outer skins and fore and aft channel.

The main ring (Fig. 25) is an annular shell with rectangular cross sections. The main ring is the main structural component of the OTA. All OTA loads are transmitted through the ring. Figure 26 shows a view of the ring as part of the primary mirror assembly. The rectangular section of the ring consists of channels and skins (Fig. 27).

1. Stress Information

Table 5 shows the OTA loads spectra [17,18] and Table 6 shows the stresses used in the fracture analysis based on Lockheed's stress analysis (liftoff combination No. 17).

2. Material Properties

Ti-6Al 4V

$c = 5.7 \times 10^{-10}$

$n = 3.18$

$K_{Ic} = 84.0$ ksi-$\sqrt{in}$

$\Delta K_{th} = 6.0$ ksi-$\sqrt{in}$

$\sigma ys = 126.0$ ksi

3. Solution Model

The FLAGRO4 computer code was used in the analysis. Two types of crack models were analyzed:

1) Part through center crack (Fig. 28)

2) Through center crack (Fig. 29)

Channel section – W = 9.0 in, t = 0.195 in

Skin section – W = 15.0 in, t = 0.25 in.

4. Results

The analysis results are shown in Figures 30 and 31 in the form of inspection criteria curves. The curves were to be used as guidelines in the nondestructive evaluation of the ring.

NOTE: After the safe-life analysis had been completed and inspection curves derived, it was determined by analysis that the ring skins and channels were fail-safe. A very thorough and complete fail-safe analysis is contained in the appendix.

TABLE 4. OTA LOADING SCENARIO

THE FOLLOWING SCENARIO IS BEING USED TO DEFINE THE LIFETIME FOR THE OTA. TO MEET SERVICE LIFE REQUIREMENTS THE OTA MUST SURVIVE FOUR LIFETIMES.

1. OTA AND SI'S TO LMSC VIA C-5A AND AIR RIDE VAN
2. ALL UP ST ACOUSTIC TEST
3. ST TO KSC VIA BARGE
4. LAUNCH
5. LAND (RETURN FOR SIX MONTHS AFTER FIVE YEARS IN ORBIT)
6. LAUNCH
7. LAND (RETURN FOR 30 MONTHS AFTER 10 YEARS TOTAL IN ORBIT)

---

8. ST TO LMSC VIA BARGE
9. OTA AND SI'S TO RESPECTIVE ASSEMBLY SITES VIA C-5A AND AIR RIDE VAN
10. OTA AND SI TO LMSC VIA C-5A AND AIR RIDE VAN
11. ST TO KSC VIA BARGE
12. LAUNCH

TABLE 5. OTA LOAD SPECTRA

Event	"Load" Amplitude (Zero to Peak)	Number of Cycles (3)			
		Range 100%→75%	Range 75%→50%	Range 50%→25%	Range 25%→0%
Shuttle Launch (Duration = 7 sec.)	±100% CLC Liftoff	4	7	13	30
Shuttle Landing (Duration = 3 sec.)	±100% CLC Landing	4	5	10	4
Air Transportation (1) (15-Hour Guppy Flight)	±53% CLC Landing	$6.1x10^3$	$40.3x10^3$	$109.4x10^3$	$218x10^3$
Barge (2) (Duration = 1 Month)	±14% CLC Landing	$400x10^3$	$2500x10^3$	$7400x10^3$	$13400x10^3$

(1) Assumes shipping system with 7 Hz isolation system and Q=5.0

(2) Assumes shipping system with 5 Hz isolation system and Q=3.0

(3) One cycle = full reversal of load

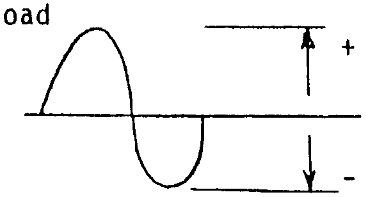

1 cycle

TABLE 6. OTA STRESS SPECTRUM

MODE	STRESS MAX	STRESS MIN	CYCLES	BENDING FACTOR (see note below)
GUPPY	20.71	-20.71	6100	1
	15.53	-15.53	40300	1
	10.35	-10.35	109400	1
	5.18	-5.18	218000	1
BARGE	16.02	5.1	400000	1
	12.01	3.81	2500000	1
	8.01	2.54	7400000	1
	4	1.3	13400000	1
LAUNCH	39.07	-39.07	4	1
	29.3	-29.3	7	1
	19.54	-19.54	13	1
	9.77	-9.77	30	1
LANDING	39.07	-39.07	4	1
	29.3	-29.3	5	1
	19.54	-19.54	10	1
	9.77	-9.77	4	1

NOTE : BENDING FACTOR OF 1 -INDICATES PURE BENDING

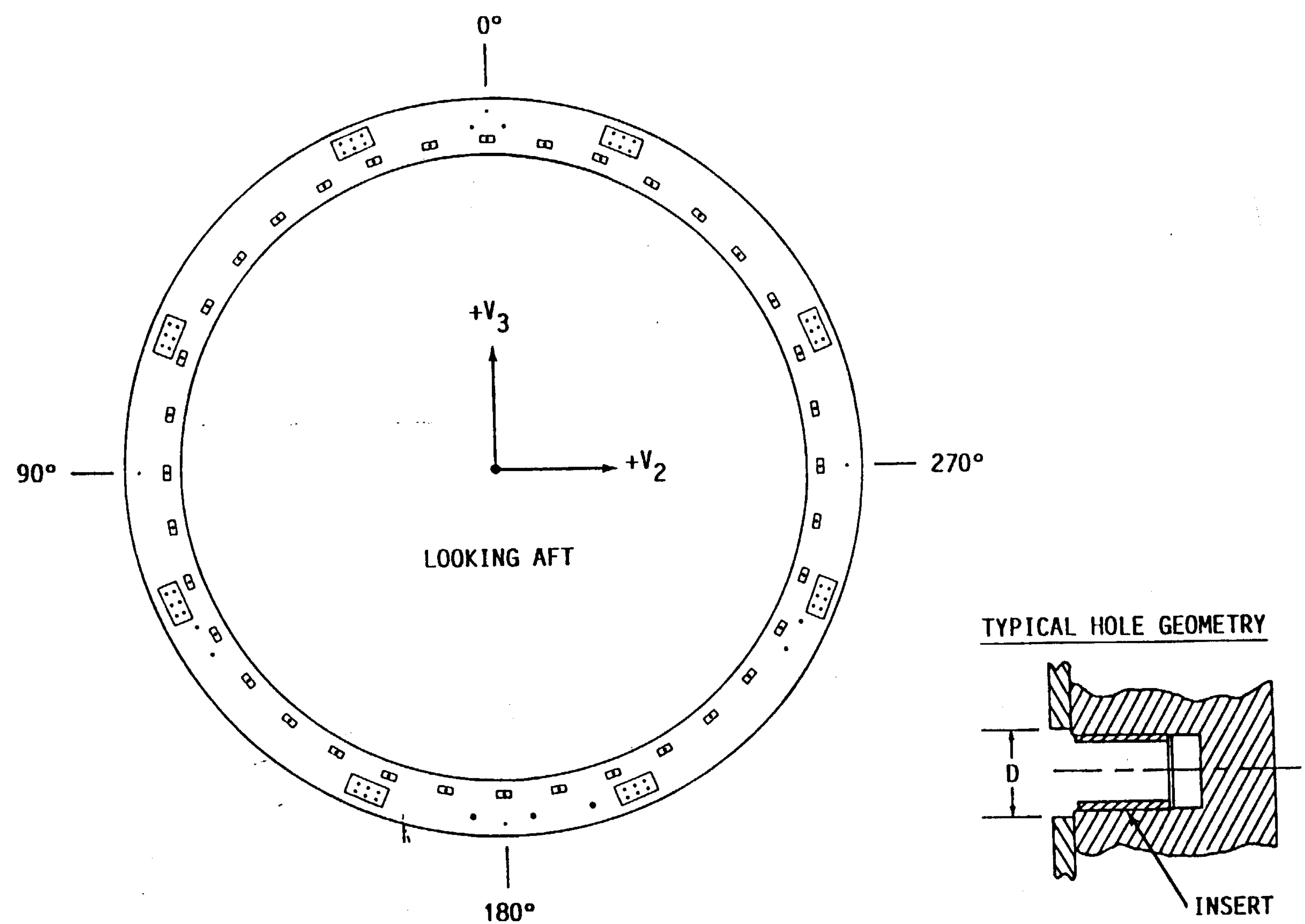

Figure 25. HST attach main ring forward surface.

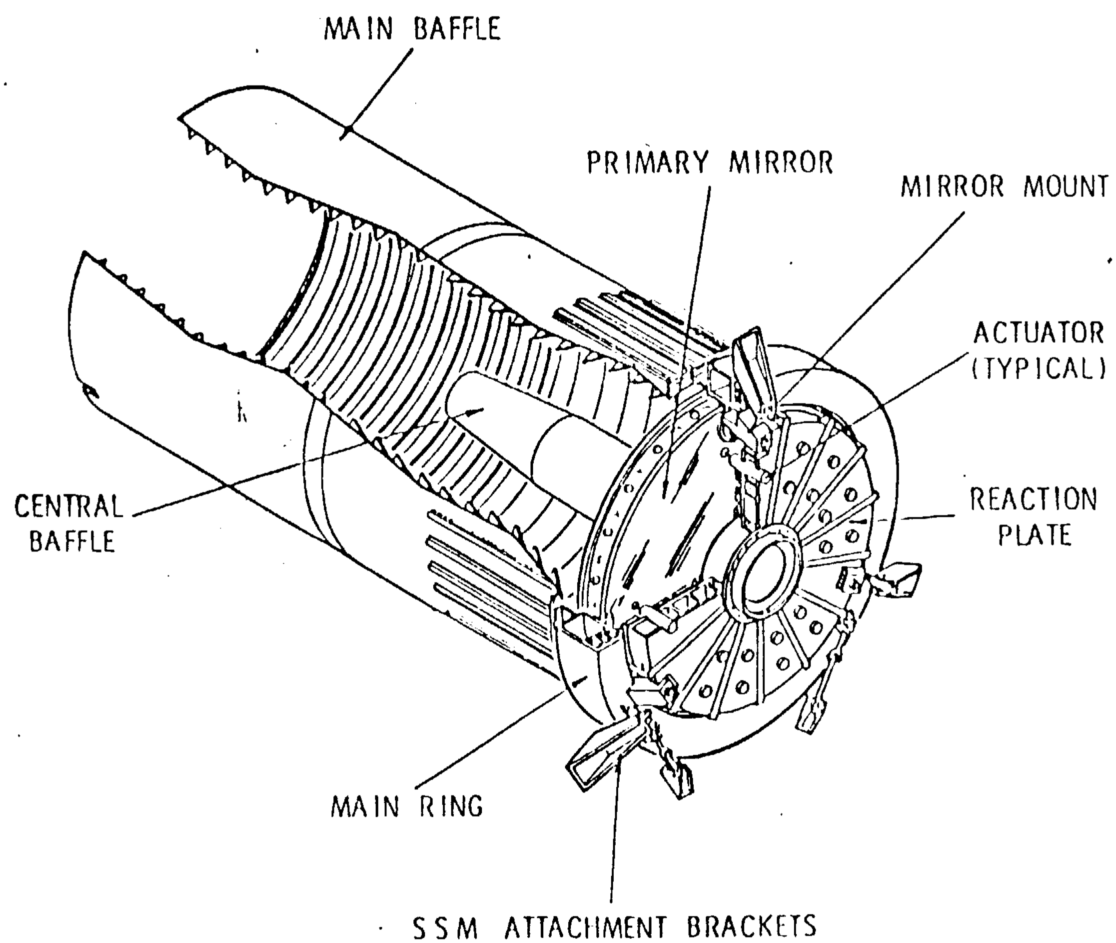

Figure 26. HST primary mirror assembly.

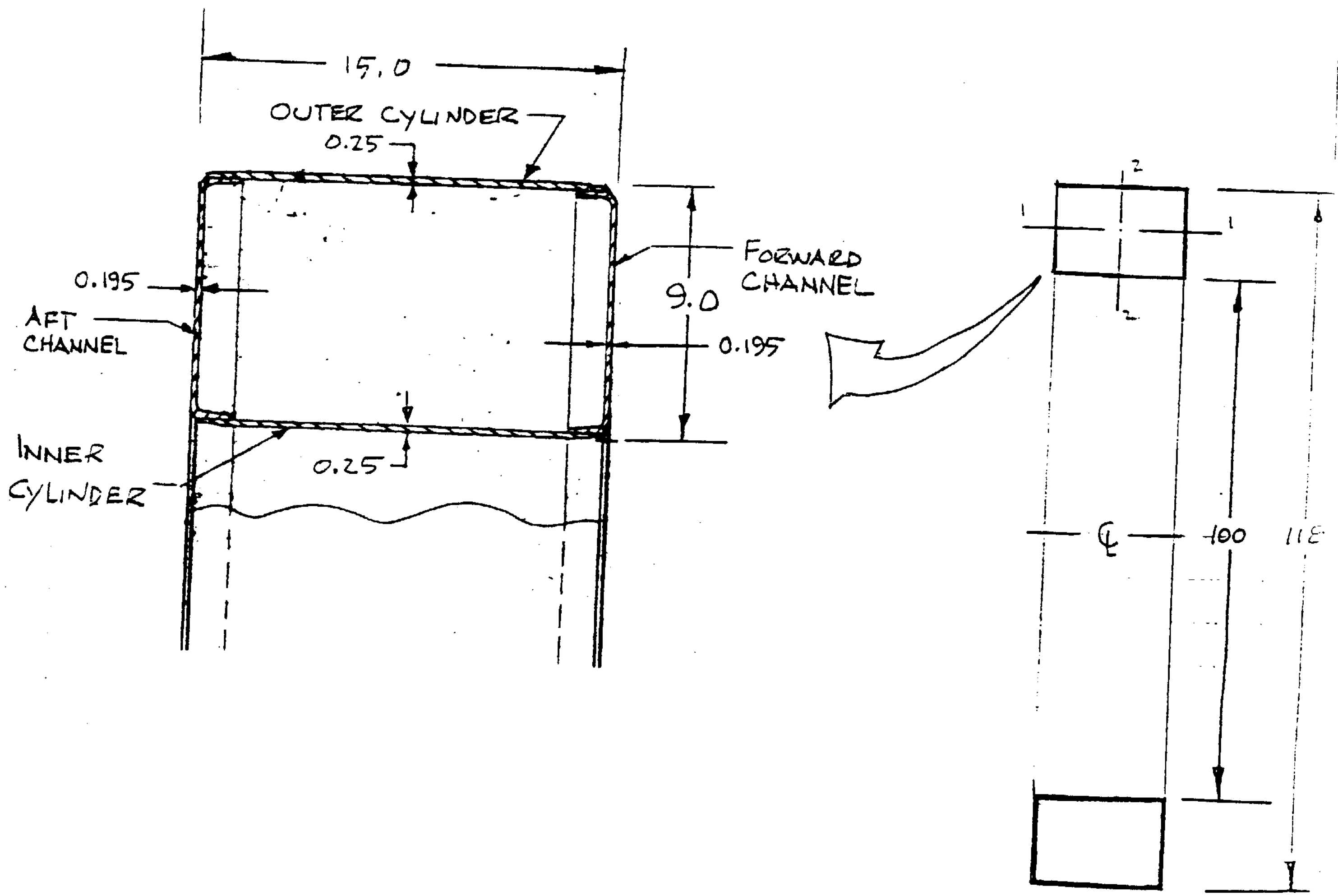

Figure 27. HST main ring cross section.

Description	Stress Adjustment Factors		Variable Correction Factors
	(1)	(2)	
Case 1 Center Panel Part Through Crack 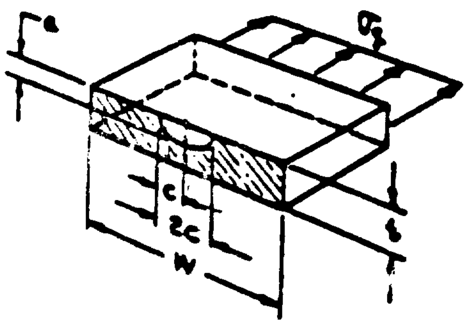	α_{max} for bending	α_{min} for bending	VAF = f(a) VCF = f(c)

Figure 28. HST NASA/FLAGRO center panel part-through crack geometry model.

Description	Stress Adjustment Factors		Variable Correction Factors
	(1)	(2)	
Case 1 Center Through Crack 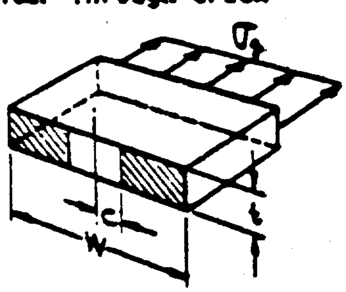	Not Available	Not Available	VCF = f(c)

Figure 29. HST NASA/FLAGRO center panel through crack geometry model.

ORIGINAL PAGE IS
OF POOR QUALITY

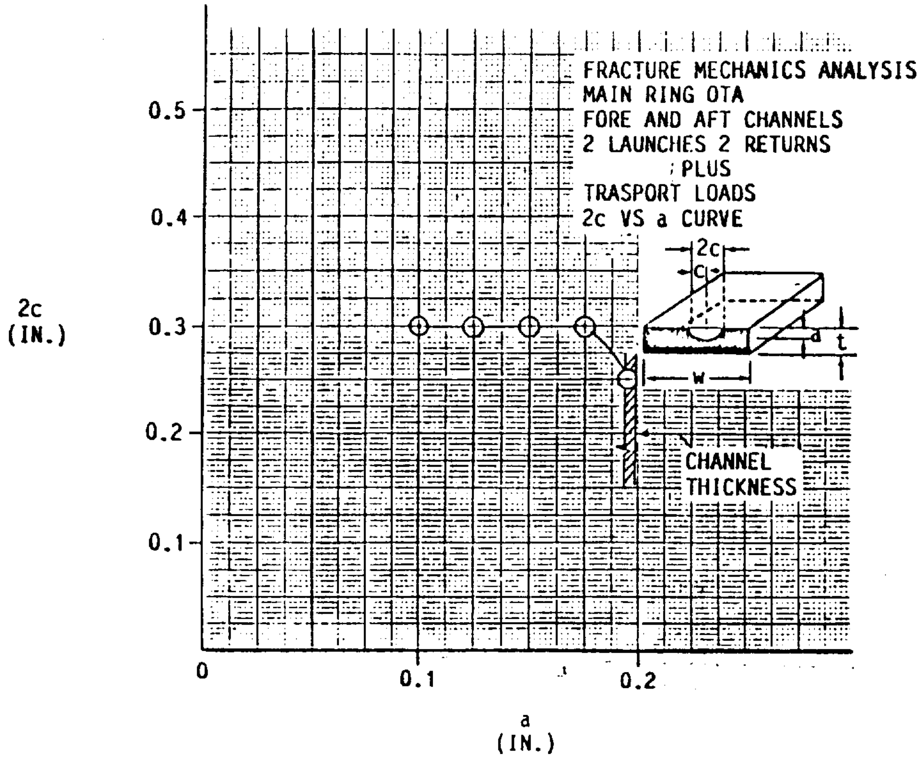

Figure 30. HST inspection curve for fore and aft channels.

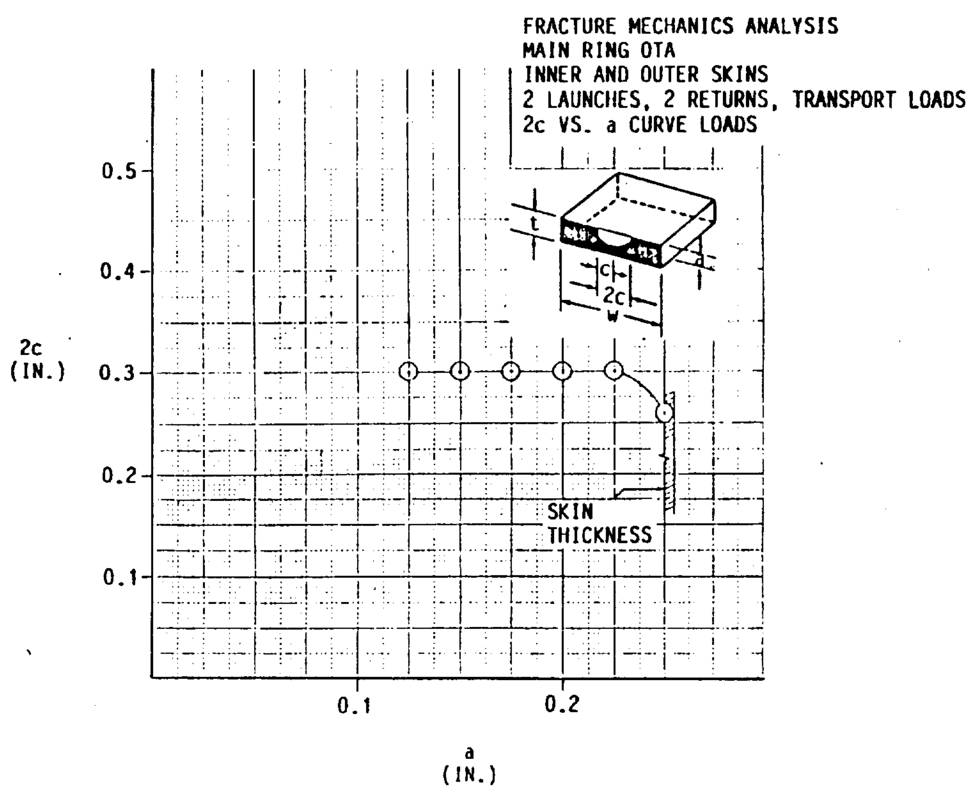

Figure 31. HST inspection curve for inner and outer skins.

D. Space Support Equipment (SSE) Scientific Instrument Protective Enclosure (SIPE) Trunnion

The SSE consists of those hardware items mounted, stowed on, and transported by the Space Transportation System (STS) to provide scheduled maintenance of the HST equipment and scientific instruments. The SSE will provide environmental protection for orbital replaceable units (ORU's) during prelaunch, launch, and orbit transfer. Once orbital altitude is attained, the SSE will provide a maintenance platform to berth the HST in the cargo bay of the orbiter. This platform will tilt and rotate the HST to aid in maintenance activities. The SSE will aid the crew in removal, temporary storage, translation, installation, and activation activities associated with replacing failed or degraded HST components (ORU's). It will also provide for storage for the failed component during return to Earth in the orbiter [19].

The trunnion, composed of Inconel 718 material (Figs. 32 and 33) [19], is designed to support the SIPE to the load isolation system (LIS). Two trunnions are required for the flight assembly, one each on the port and starboard sides. The trunnion is shaped as a hollow cone approximately 11-in long and is fastened to the SIPE with eight bolts at the base and connected to the LIS through a moonball at the apex. The trunnion is loaded transversely by translational forces parallel to the orbiter X and Z coordinate axes [17].

1. Stress Information [20,21]

Maximum stress: Bending stress = 132,338 psi at 100 percent load at 6,598 lb combined X and Z load (CDR landing case 36). Maximum liftoff load = 58,881 lb X load (CDR liftoff case 105). Maximum stress = 118,097 psi. Load spectra cycles for load alleviation system:

Liftoff: 9 cycles at 100% load
17 cycles at 75%
28 cycles at 50%
138 cycles at 25%

Landing: 16 cycles at 100%
25 cycles at 75%
30 cycles at 50%
47 cycles at 25%

Table 7 contains the entire spectrum as used in the analysis.

2. Material Properties

Inconel 718

$K_{Ic} = 90$ ksi-$\sqrt{in}$

$c = 0.103 \times 10^{-8}$

$n = 2.63$

$p = q = 0.50$

$\Delta K_o = 6.50$

$Co = 0.70$

$d = 1.00$

$\Delta K_1 = 19.67$

$Alpha = 2.00$

3. Solution Model

The NASA/FLAGRO surface crack in a solid cylinder model in Figure 34 was used in the analysis. The cylinder diameter was D = 0.7489 in. The initial surface flaw length was 0.100 (standard level eddy current).

4. Results

A 0.100-in flaw in the circumferential direction of 0.7489-in solid cyclinder was analyzed. Critical area was in a 0.12-in radius where 0.7489/0.7492-in diameter becomes 1.090-in diameter. The analysis results proved conservative by using the smaller diameter. The NASA/FLAGRO results indicated that this part survived the required 52 missions (13 x scatter of 4) for the above flaw size. In addition, no unstable crack growth occurred until halfway through mission 60.

TABLE 7. SSE FATIGUE STRESS SPECTRUM

STEP NO.		STRESS	(KSI)		CYCLES	BENDING
		MAX	MIN			FACTOR
1		118.1	-118.1		9	1
2		88.57	-88.57		17	
3		59.05	-59.05		28	
4		29.52	-29.52		138	
5		132.34	-132.34		16	
6		99.25	-99.25		25	
7		66.17	-66.17		30	
8		33.08	-33.08		47	
	NOTE: BENDING FACTOR OF 1-INDICATES PURE BENDING					

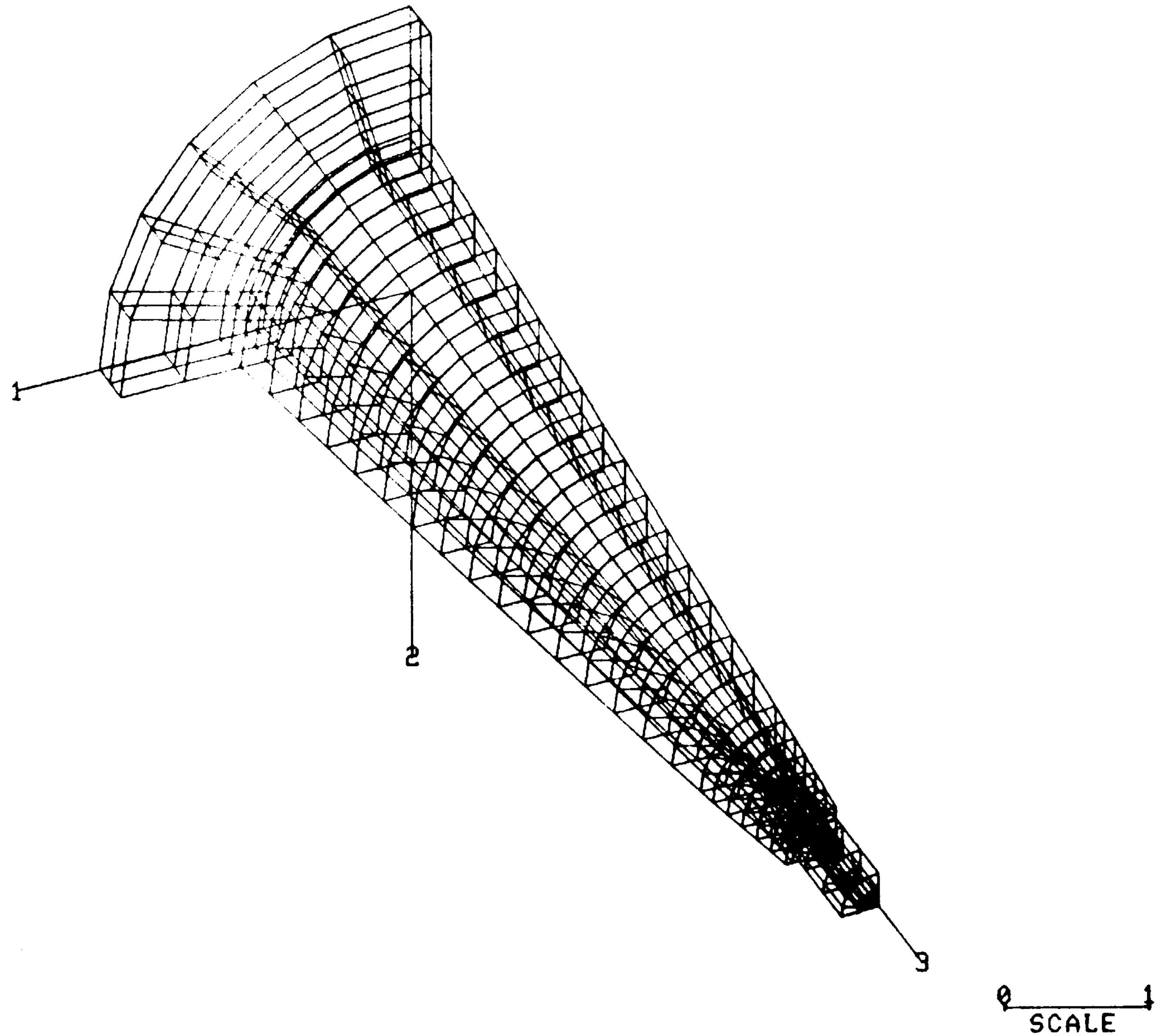

Figure 32. SSE trunnion SPAR quarter model.

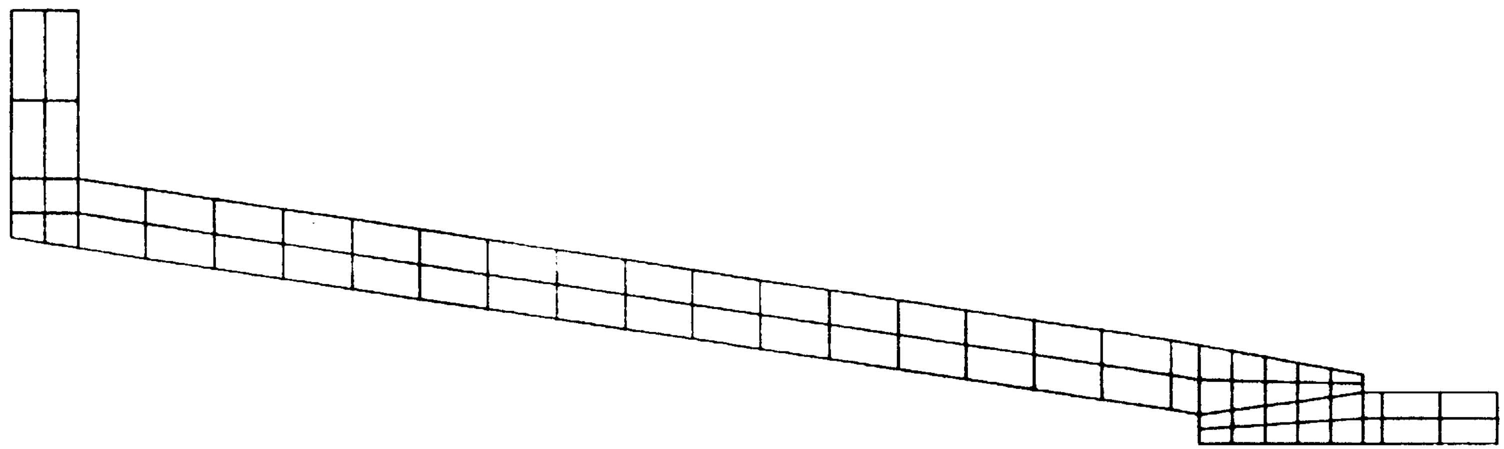

Figure 33. SSE trunnion SPAR quarter model side view.

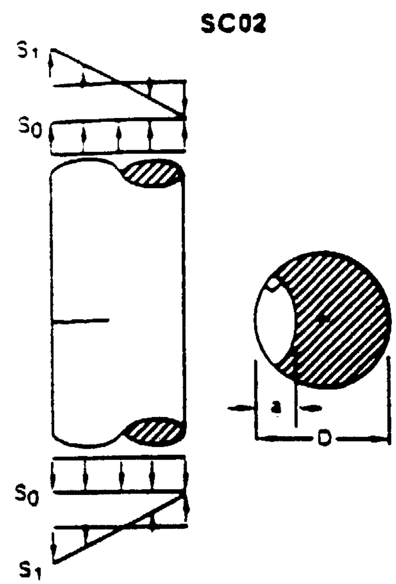

Figure 34. SSE NASA/FLAGRO surface crack in solid cylinder geometry model.

E. 270-Degree External Tank Attach Ring

The primary function of the external tank (ET) attach ring is to redistribute the strut loads on the SRB case. Three struts connect the ET to the SRB at SRB station 1511.0. The attach ring supports the integrated electronics assembly (IEA) box mounts and the wiring harness which connects the IEA box to the system tunnel. The redesign utilizes the baseline 360 design hardware between the 154 and 342 splices (Fig. 35, Structural Configuration). The new tapered sections attach directly to these splice plates. Both the cap and web are spliced. The new part is an integral cap and web design, in that it is machined out of one block of material. This eliminates the need for cap to web fasteners in this high stressed area. Figure 36 shows the 270-degree ring cross section [22].

1. Ring Cap

a. Stress Information

Loads spectra data that specified the load level, number of cycles at each level, and order of occurrence of each event that the structural part experienced were developed from References 22, 23, and 24. Table 8 contains the spectrum loading data used in the analysis of the ring cap segment. Table 9 gives an explanation of the spectrum steps given in Table 8 [23,24].

b. Material Properties

4340 Low Alloy Steel

K_{Ic} = 90 ksi-$\sqrt{in}$

K_c = 90 ksi-$\sqrt{in}$

ΔK_I = 15.03 ksi-$\sqrt{in}$

ΔK_0 = 4.0 ksi-$\sqrt{in}$

Ak = 0.75

Bk = 0

THk = 0.310

c = 0.791×10^{-8}

n = 1.984

p = q = 0.25

C_0 = 1.00

d = 0.50 .

c. Solution Model

The NASA/FLAGRO part-through crack at a hole solution model (Fig. 37) was used to analyze the portion of the ring cap segment shown in Figure 38.

W = 1.75 in

t = 0.56 in

D = 0.685 in

Minimum edge distance = 0.41 in.

d. Results

Two types of flaws were analyzed: (1) a semicircular flaw and (2) a long shallow flaw.

(1) a = c = 0.05

(2) a = 0.01 and c = 0.05.

The flaw in (1) survived one mission (one mission with a scatter factor of four = 4 blocklives) and the flaw in (2) survived 19 blocklives (4.75 missions).

Standard eddy-current NDE was recommended as the inspection technique for finding the above flaws.

2. Web Segment

The web segment (Fig. 39) was analyzed for different crack configurations, but only the embedded flaw will be highlighted here.

a. Stress Information

Loads spectra data that specified the load level, number of cycles at each level, and order of occurrence of each event that the structural part experienced was developed from References 22, 23, and 24. Table 10 contains the spectrum loading data used in NASA/FLAGRO.

b. Material Properties

4130 low alloy steel

K_{Ic} = 80.0 ksi-$\sqrt{in}$

$K_c = 80.0$ ksi-$\sqrt{in}$

$\Delta K_I = 9.86$ ksi-$\sqrt{in}$

$\Delta K_0 = 4.0$ ksi-$\sqrt{in}$

Ak = 0.75

Bk = 0

THk = 0.250

$c = 0.141 \times 10^{-7}$

n = 2.158

p = q = 0.25

$C_0 = 1.00$

d = 0.50 .

c. Solution Model

The NASA/FLAGRO embedded flaw geometry (Fig. 40) was used in the analysis.

Width W = 7.23 in

Thickness t = 0.25 in .

d. Results

A flaw of depth 2a = 0.124 and crack length 2c = 0.25 survived through 40 missions (40 x 4 = blocklives). Ultrasonic NDE was recommended as the inspection technique for finding this flaw.

TABLE 8. ET ATTACH RING – RING CAP SPECTRUM LOADING

Step No.	DESCRIPTION
1 THRU 4	EMPTY E.T. LOW CYCLE PRELAUNCH
5 THRU 8	EMPTY E.T. HIGH CYCLE PRELAUNCH
9 THRU 12	FULL E.T. LOW CYCLE PRELAUNCH
13 THRU 16	FULL E.T. HIGH CYCLE PRELAUNCH
17 THRU 18	BUILDUP
19 THRU 20	LIFTOFF
21 THRU 26	MAX Q
27 THRU 28	MAX G
29 THRU 30	PRESTAGING
31	WATER IMPACT

STEP NO.	CYCLES	MIN.STRESS	MAX. STRESS
1	1	0	1.5
2	20	1.5	2.2
3	1	-0.6	1.5
4	20	-0.6	0.3
5	1	0	0.1
6	2750000	0.11	0.16
7	1	-0.05	0.11
8	2750000	-0.05	0.02
9	1	-0.1	0
10	20	-0.2	-0.1
11	1	-1.5	-0.1
12	20	-1.5	-1.4
13	1	0	0.1
14	200000	0.1	0.16
15	1	-0.05	0.1
16	200000	-0.05	0
17	1	0	2.4
18	2	-2.3	2.4
19	1	46	60
20	14	36	59
21	1	41	53
22	70	31	53
23	175	31	53
24	1	41	47
25	70	35	47
26	175	35	47
27	1	24	36
28	1	15	36
29	1	3	5
30	1	1.6	5
31	1	-2.3	60

TABLE 9. ET ATTACH RING STRESS SPECTRA BREAKDOWN, STEP BY STEP

	A	B	C	D	E	F
1	ZERO TO MAX SS.+OSC.LOAD (P11,P12,P13)				PRELAUNCH CASES	
2	P11,P12,P13 MAX.SS+OSC.LOAD TO P8,P9,P10 MAXSS.-OSC.LOAD					
3	P11,P12,P13 MAX SS.+OSC.LOAD TO P8,P9,P10 MIN.SS-OSC.LOAD					
4	P8,P9,P10 MIN.-OSC.LOAD TO P11,P12,P13 MIN SS.+OSC.LOAD					
5	SAME EXPLANATION AS STEP ONE ABOVE					
6	SAME EXPLANATION AS STEP TWO ABOVE					
7	SAME EXPLANATION AS STEP THREE ABOVE					
8	SAME AS EXPLANATION AS STEP FOUR ABOVE					
9	SAME EXPLANATION AS STEP ONE ABOVE					
10	SAME EXPLANATION AS STEP TWO ABOVE					
11	SAME EXPLANATION AS STEP THREE ABOVE					
12	SAME AS EXPLANATION AS STEP FOUR ABOVE					
13	SAME EXPLANATION AS STEP ONE ABOVE					
14	SAME EXPLANATION AS STEP TWO ABOVE					
15	SAME EXPLANATION AS STEP THREE ABOVE					
16	SAME AS EXPLANATION AS STEP FOUR ABOVE					
17	P_ZERO BUILDUP TO PMAX.SS BUILDUP				BUILDUP CONDITIONS	
18	PMAX SS. BUILDUP TO PMIN.SS BUILDUP					
19	P_ZERO LIFTOFF TO PMAX.SS LIFTOFF				LIFTOFF LOAD CONDITIONS	
20	PMAX.SS+ LIFTOFF TO PMIN SS..LIFTOFF					
21	P_ZERO MAX Q. TO PMAX SS. MAX Q.				MAX Q. CONDITIONS	
22	PMAX.SS. MAX Q. TO PMIN.SS MAX Q.					
23	PMAX.SS. MAX Q. TO PMIN.SS. MAX Q.					
24	PMAX.SS. MAX Q. TO PMIN.SS. MAX Q.					
25	PMAX.SS. MAX Q. TO PMIN.SS.MAXQ					
26	PMAX .SS. MAX Q. TO PMIN.SS. MAX Q.					
27	P_ZERO MAX G. TO PMAX (MAXG.)				MAX.G CONDITONS	
28	PMAX.MAX G. TO PMIN. MAX G.					
29	P_ZERO PRESTAGING TO PMAX. PRESTAGING					
30	PMAX.PRESTAGING TO PMIN.PRESTAGING					
31	PMAX-ENTIRE SPECTRA TO PMIN .-ENTIRE SPECTRA				WATER IMPACT* * * * *	
	***** NO DATA READILY AVAILABLE : USED MAX. LIFTOFF STRESS AS MAX. AND					
	MIN.STRESS OF ALL CASES AS MIN. STRESS IMPACT					

TABLE 10. ET ATTACH RING – WEB SEGMENT LOADING SPECTRUM

STEP No.		CYCLES	MIN STRESS	MAX. STRESS
1:	1:	1:	-0.10:	0.00
2:	1:	20:	-0.35:	-0.10
3:	1:	1:	-0.26:	-0.10
4:	1:	20:	-0.26:	-0.04
5:	1:	1:	-0.01:	0.00
6:	1:	2750000:	-0.03:	0.00
7:	1:	1:	-0.02:	0.00
8:	1:	2750000:	-0.02:	0.00
9:	1:	1:	0.00:	0.13
10:	1:	20:	0.11:	0.13
11:	1:	1:	0.13:	0.15
12:	1:	20:	0.15:	0.17
13:	1:	1:	-0.01:	0.00
14:	1:	200000:	-0.03:	0.00
15:	1:	1:	-0.02:	0.00
16:	1:	200000:	-0.02:	0.00
17:	1:	1:	-0.12:	0.00
18:	1:	2:	-0.12:	0.12
19:	1:	1:	65.70:	66.00
20:	1:	14:	65.60:	66.00
21:	1:	1:	58.10:	58.50
22:	1:	70:	58.10:	58.14
23:	1:	175:	58.10:	58.14
24:	1:	1:	58.20:	58.50
25:	1:	70:	58.00:	58.20
26:	1:	175:	58.00:	58.20
27:	1:	1:	33.20:	34.00
28:	1:	1:	33.20:	34.10
29:	1:	1:	3.78:	4.00
30:	1:	1:	3.78:	3.90
31:	1:	1:	-0.12:	66.00

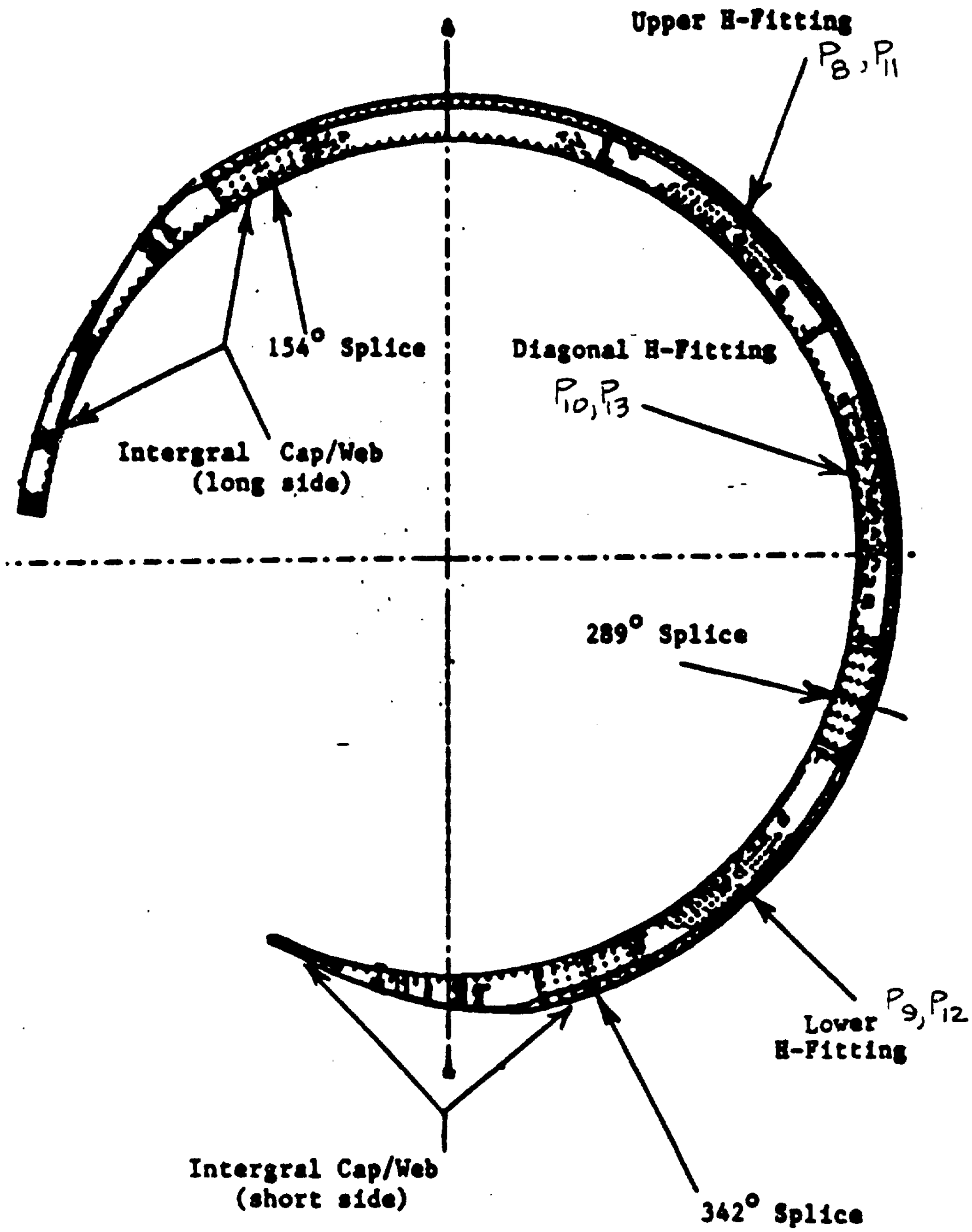

Figure 35. ET 270-degree attach ring.

ORIGINAL PAGE IS
OF POOR QUALITY

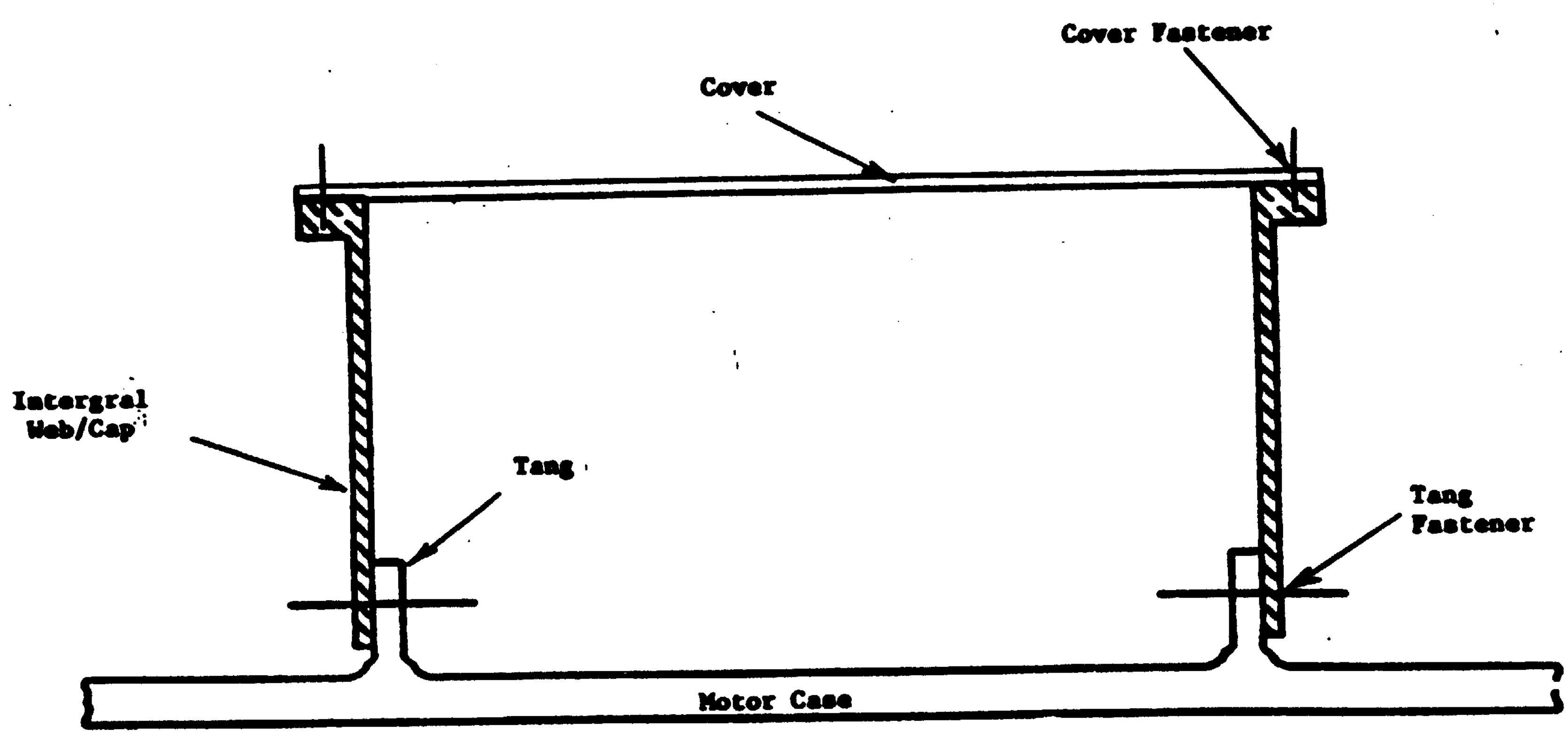

Figure 36. ET 270-degree attach ring cross section.

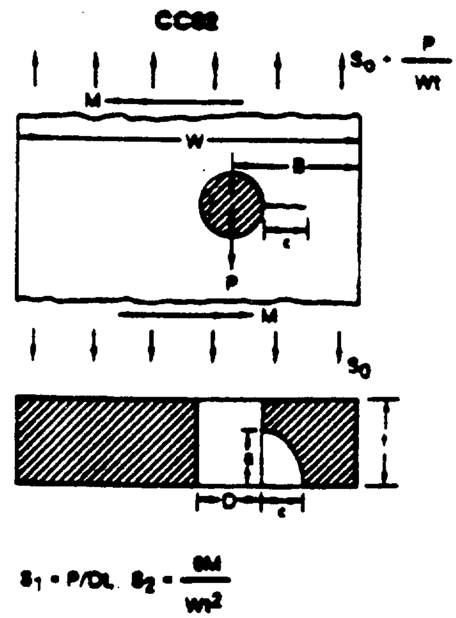

Figure 37. ET NASA/FLAGRO part-through crack at a hole.

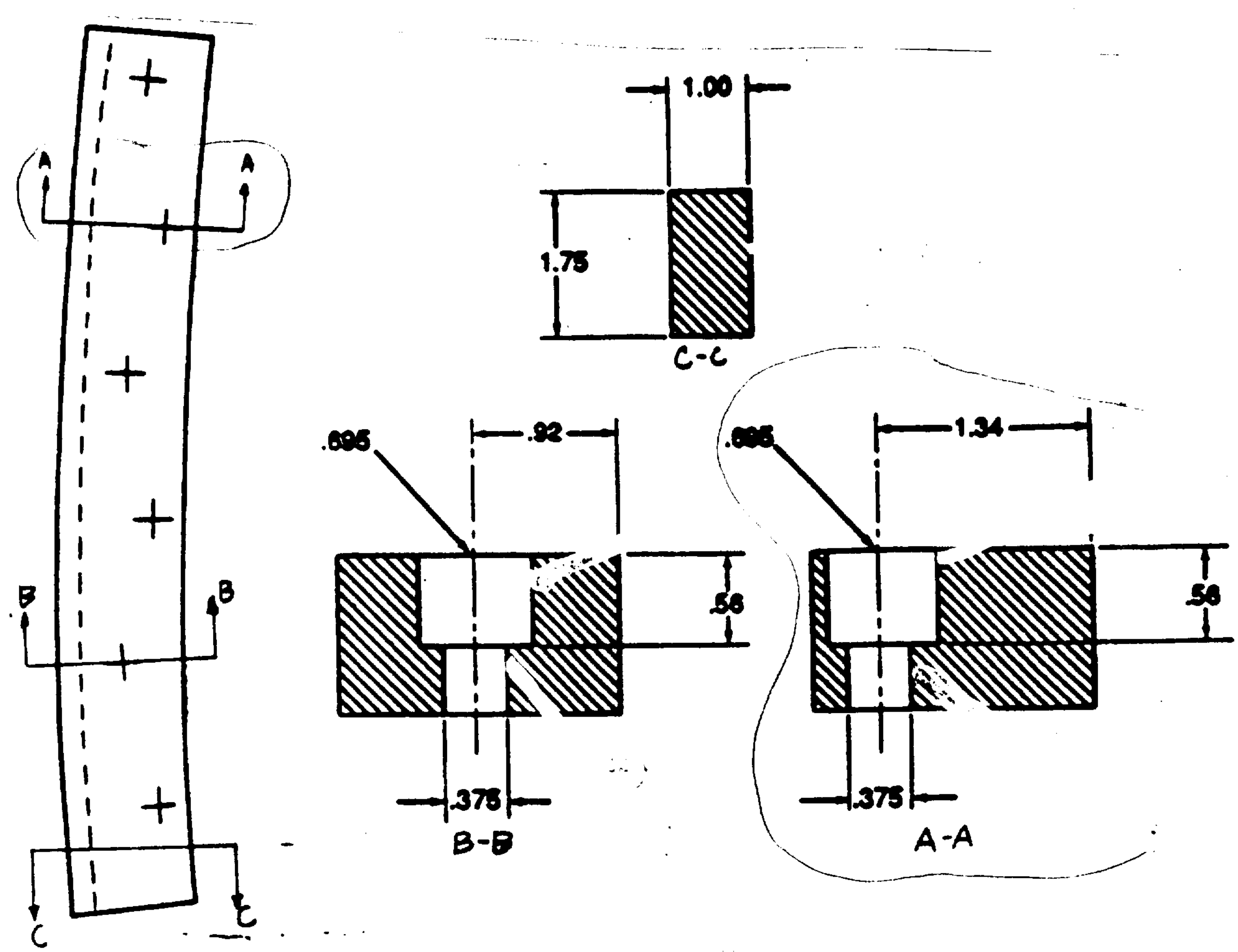

Figure 38. ET attach ring cap segment.

ORIGINAL PAGE IS
OF POOR QUALITY

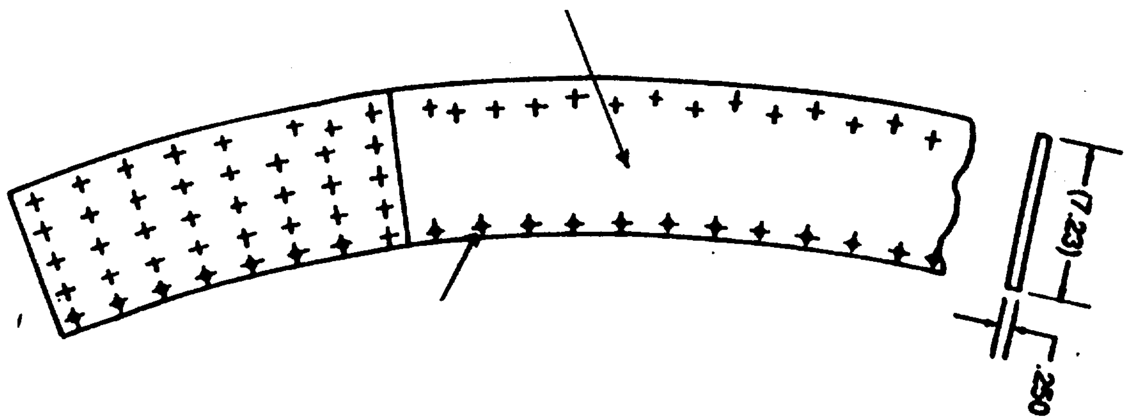

Figure 39. ET attach ring web segment.

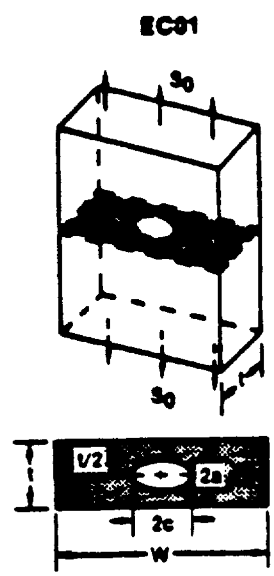

Figure 40. ET NASA/FLAGRO embedded flaw geometry.

F. B-1 Stand Lox Inner Tank

A leak before burst fracture mechanics analysis was performed on the B-1 stand LOX inner tank at the National Space Test Laboratory (NSTL), now known as the Stennis Space Center (SSC).

The LOX run tank was built in 1962 for Rocketdyne Santa Susanna Facility. The vessel was transported via land/water from Santa Susanna to NSTL in early 1984. The vessel remained on the barge during some modification work until installation on the B-1 stand in 1987. Figure 41 shows the LOX tank configuration. The tank has a 45,000 gallon volume and is made of 304 stainless steel. The thickness of the tank varies between 0.483 to 0.982 in. It has a 11.5-ft diameter and is 67.5 ft long. The tank had been ASME rated for 110 psig. A new operational condition of 130 psig had been imposed at the time of the analysis.

1. Leak Before Burst Analysis

A part-through crack in a thin walled pressure vessel may grow by fatigue or stress corrosion until it reaches the outer wall, then the vessel will be leaking and there is a good chance that detection follows. The possibility exists that fracture instability is initiated already by a surface flaw. If this fracture is arrested as soon as the crack pops through the wall, the vessel starts leaking and there is some time for crack detection before (through) cracks reach a critical crack size again. A vessel behaving in this manner satisfies the leak before burst criteria [7].

a. Tank Wall

Figure 42 shows a schematic of the tank varying wall thickness and the corresponding hydro head pressure, ullage vacuum head pressure, and stresses for each section of the tank.

b. Stress Information

It can be seen from Figure 42 that the minimum tank wall thickness section of 0.483 in has the maximum applied stress of 21,303 psi, therefore one analysis on the wall is necessary because this section is the thinnest and most highly stressed section. If this proved good then the other sections would be satisfactory.

c. Material Properties

304 Stainless steel

K_{Ic} = 100 ksi-$\sqrt{in}$

ΔK_{th} = 15 ksi-$\sqrt{in}$

n = 2.89

c = 4.127×10^{-4} .

d. Solution Model

The NASA/FLAGRO center panel part-through crack model shown in Figure 43 was used to evaluate the problem. It was also assumed that the cracks had propagated 90 percent through the thickness which added more conservatism to the analysis. Two types of flaws were analyzed: long shallow flaws (a/c = 0.1) and hemispherical flaws (a/c = 0.5). Table 11 contains the geometric parameters.

2. Analysis Results

Table 11, cases A1 and A2, show the analysis results for the tank wall analysis.

a. Cylinder

The cylindrical upper head section of 0.982 in is stressed to 20,681 psi. The maximum stress of 21,303 psi was used on this section also, which made this part of the analysis conservative. Adding more conservatism, the cracks were assumed to have propagated 90 percent through the thickness. The long shallow and hemispherical type flaws in a center crack part-through panel were used in this analysis. The same material properties noted above were used.

Table 11, cases A3 and A4, show the analysis results from the cylinder analysis [25].

Figure 44 shows a graph of the critical through crack length versus stress levels (Fig. 42) for each variable thickness section of the tank.

b. Welds

1) Fill penetration welds

2) Drain penetration welds.

Welds in the fill and drain penetrations of the LOX tank lower head were analyzed. Figure 45 shows a NASTRAN plot of the lower head [26].

c. Stress Information

A NASTRAN finite element model (Fig. 46) was used to obtain stresses in the fill and drain penetrations. The maximum stress for the fill and drain penetrations was found to be 26,470 and 17,330 psi, respectively.

d. Material Properties

Based on information supplied at the time of the analysis, the same properties used in the previous analysis were used here also.

e. Solution Model

The NASA/FLAGRO part-through center crack geometry model was used in the analysis. Note that the flaws were assumed to have propagated 90 percent through the thickness here also.

f. Results

Tables 12 and 13 show the analysis results for the fill and drain penetration welds, respectively.

TABLE 11. B-1 STAND LOX TANK WALL RESULTS

Case No.	Thickness	ksi	a in	c in	N_{leak} Cycles	N_{burst} Cycles	Type of Crack
A1	0.483	21.3	.435	2.175	1,971	27,963	Long Shallow
A2	0.483	21.3	.435	.435	NO GROWTH		Hemispherical
A3	0.982	21.3	.884	4.42	1,237	4,732	Long Shallow
A4	0.982	21.3	.884	.884	NO GROWTH		Hemispherical

TABLE 12. B-1 LOX TANK FILL PENETRATION WELD RESULTS

Case No.	Thickness	ksi	a in	c in	N_{leak} Cycles	N_{burst} Cycles	Type of Crack
B1	0.217	26.47	.195	.98	1,700	25,143	Long Shallow
B2	0.217	26.47	.195	.195	40,000	90,000	Hemispherical

TABLE 13. B-1 LOX TANK DRAIN PENETRATION WELD RESULTS

Case No.	Thickness	ksi	a in	c in	N_{leak} Cycles	N_{burst} Cycles	Type of Crack
C1	0.460	17.33	0.414	2.07	3,733	71,386	Long Shallow
C2	0.460	17.33	0.414	0.414	90,000+	-	Hemispherical

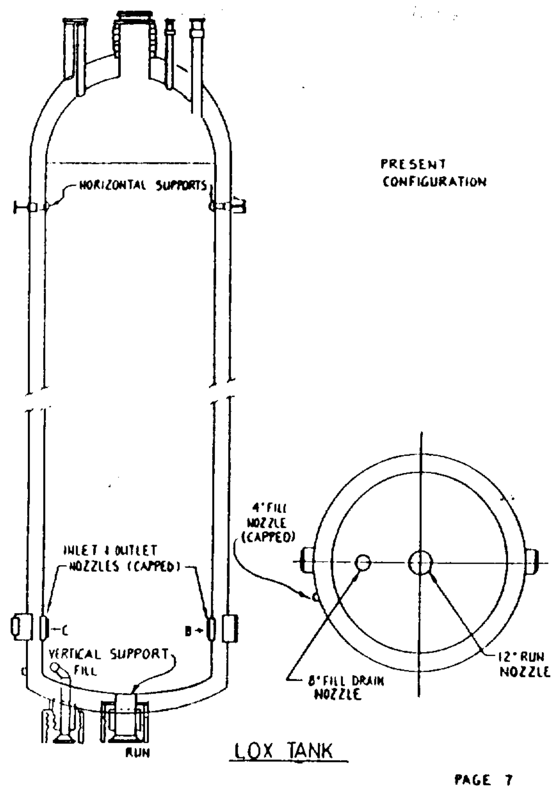

Figure 41. B-1 LOX tank configuration.

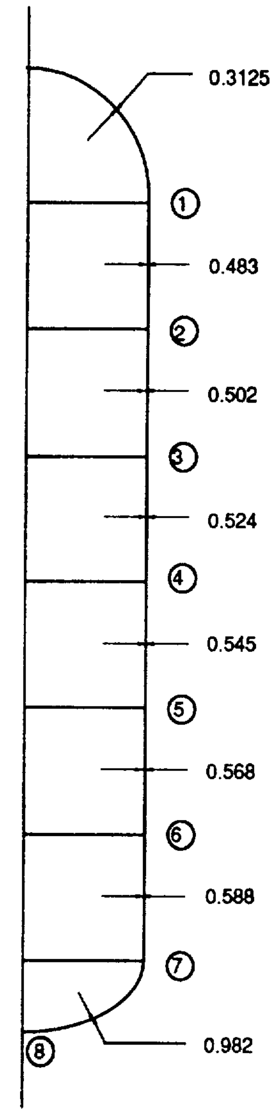

Location	Hydro. Head (psi)	Ullage+Vacuum +Head (psi)	Stress (psi)
1	0.0	144.7	15,989
2	3.8	148.5	21,303
3	8.6	153.3	21,163
4	13.4	158.1	20,913
5	18.3	163.0	20,734
6	23.2	167.9	20,497
7	28.0	172.7	20,369
8	29.0	173.7	20,681

Figure 42. B-1 schematic of tank.

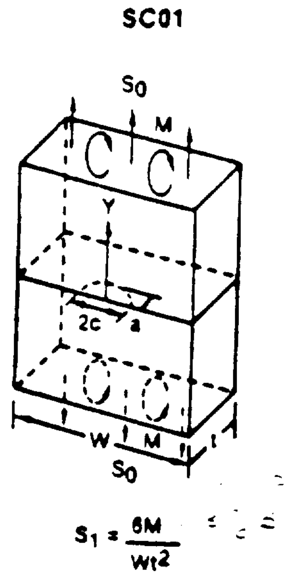

Figure 43. NASA/FLAGRO center crack panel.

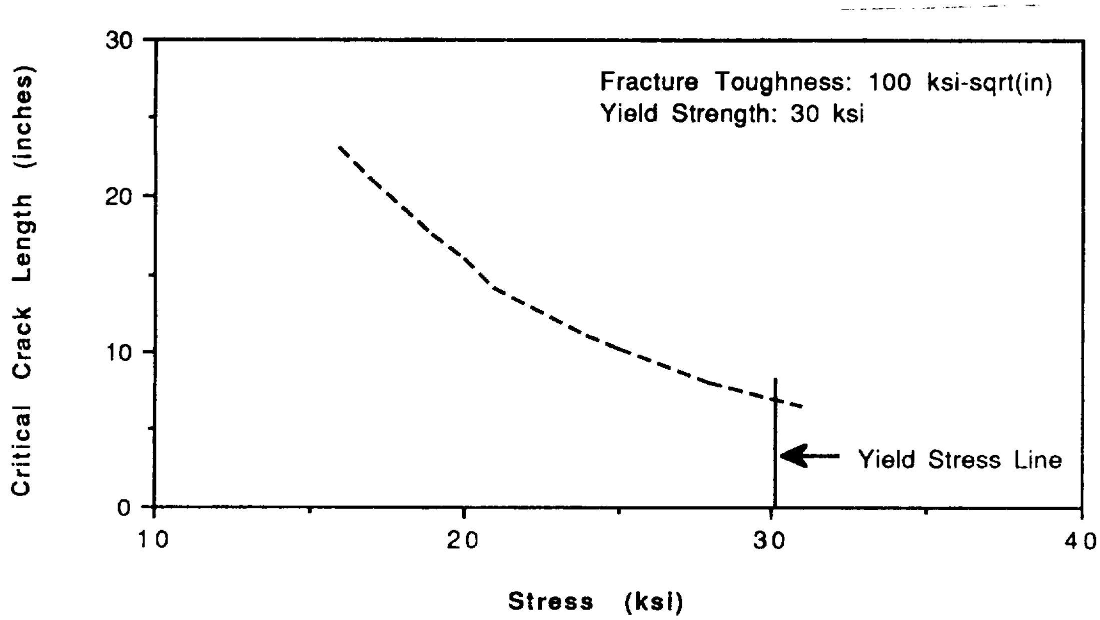

Figure 44. B-1 critical through crack length versus stress level.

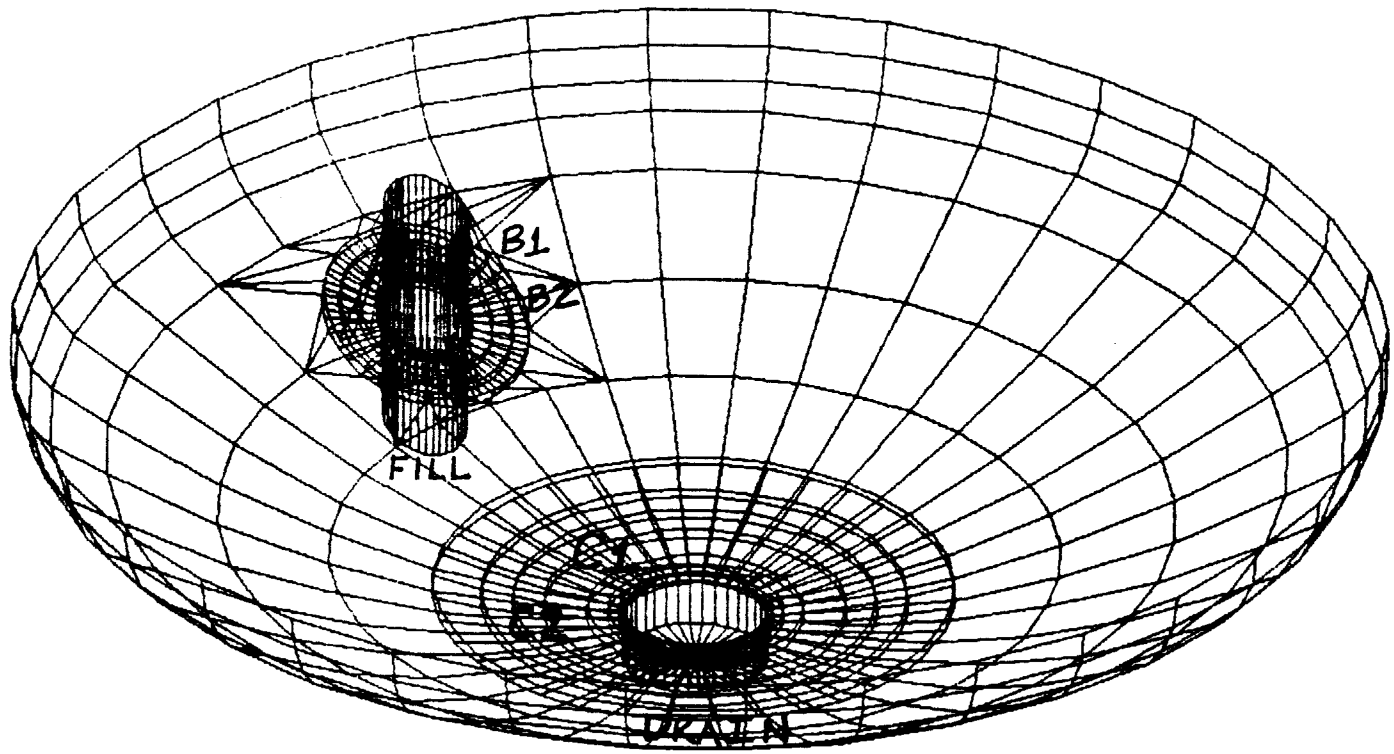

Figure 45. B-1 NASTRAN plot of lower head.

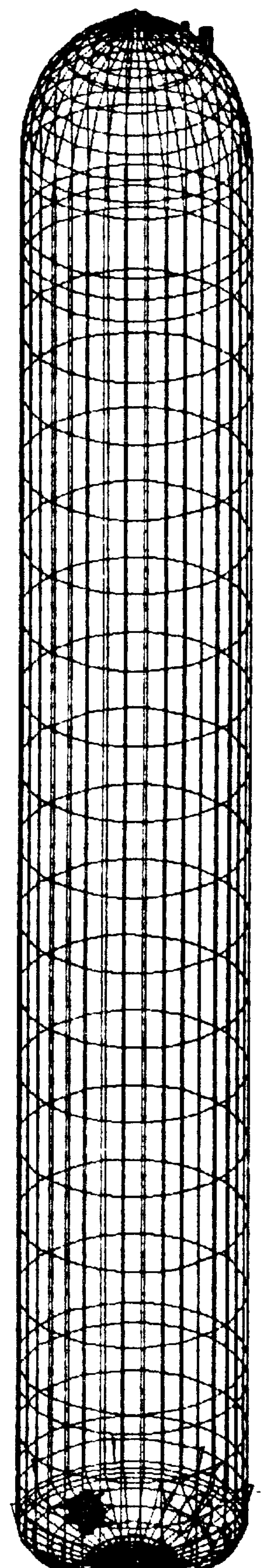

Figure 46. B-1 NASTRAN plot of LOX tank.

VIII. SUMMARY

The fracture mechanics problems highlighted in this paper were from real-time analysis problems. All of the analyses are conservative and in accordance with MSFC policy. Some of the problems presented here have been updated to account for changes in design, environmental effects, loads, stresses, etc. In analyzing the compendium of problems the analyst will obtain knowledge in working a versus K solutions, leak before burst analysis, time dependent analyses, life cycle analyses, and fail-safe analyses. The problems highlighted were analyzed using linear elastic fracture mechanic concepts and tools and the FLAGRO4, NASA/FLAGRO, and NASCRAC computer codes.

The fracture mechanics analyst problem solving scenario may involve interfacing with the stress analyst, materials engineer, and NDE engineer and the designer. Figure 47 which diagrams the fracture control sequence shows the interface between the different engineering operations and disciplines [27]. Once the fracture mechanics analysis (Fig. 48) has been completed, the results need to be documented in a complete fracture control report detailing all pertinent analyses and inspection results. A sample fracture mechanics reporting sheet, to be included in a fracture control report, is shown in Figure 49.

Along with the fail-safe analysis of the HST main ring, the Appendix section contains a safe life analysis of the SRB aft skirt. The SRB aft skirt analysis addresses the 1.375-in thick forging to skin welds and was performed according to MSFC-HDBK-1453, "Fracture Control Program Requirements," and USBI-10PLN-0023, "Solid Rocket Booster Fracture Control Plan." A basic requirement for the aft skirt is that detected flaws survive 40 flight uses times a service life factor of 4. Thus, a detected flaw must survive at least 160 flight uses as demonstrated by testing or analysis. Linear elastic fracture mechanics (LEFM) was performed using the NASA/FLAGRO computer program. The fracture mechanics analysis is detailed in the appendix section.

You may have noted in some of the analyses (post-1985) that the material constant, Bk, has been set equal to zero to ensure that a lower bound plane strain fracture toughness is used and adds to the conservatism of the analysis.

Fracture mechanics and fracture control are an integral part of providing safe space flight structures. The structural/fracture mechanics sector at MSFC is strongly committed to providing thorough, accurate, and complete fracture mechanics analysis and sound, detailed fracture control.

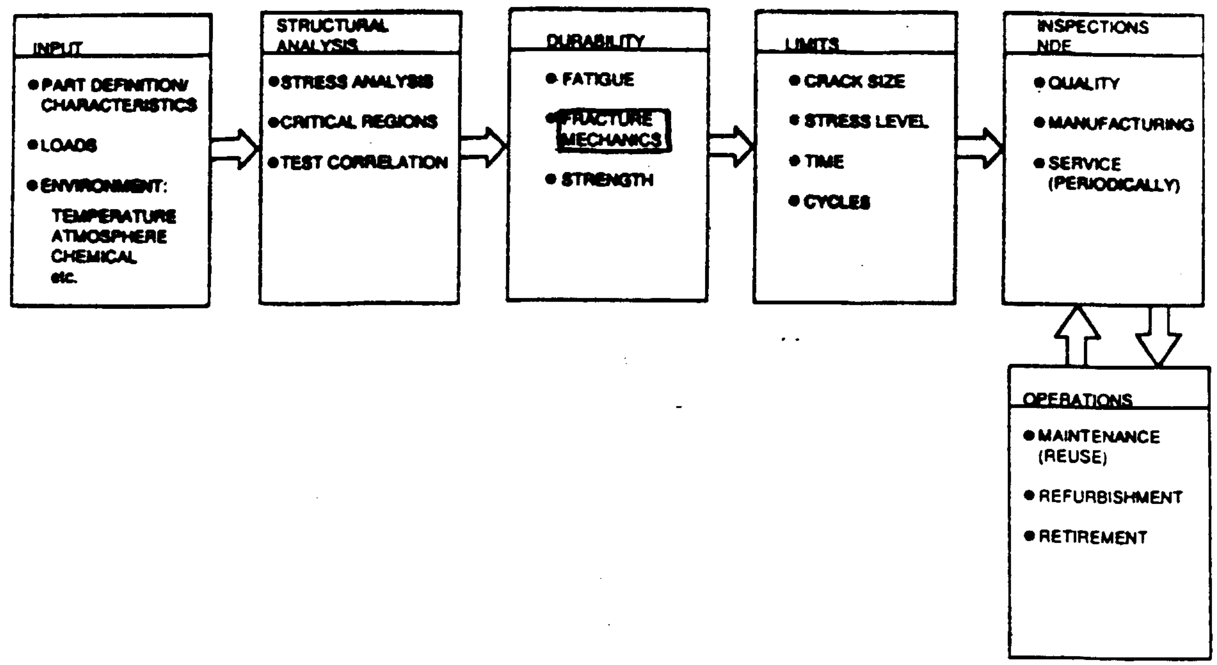

Figure 47. Fracture control sequence.

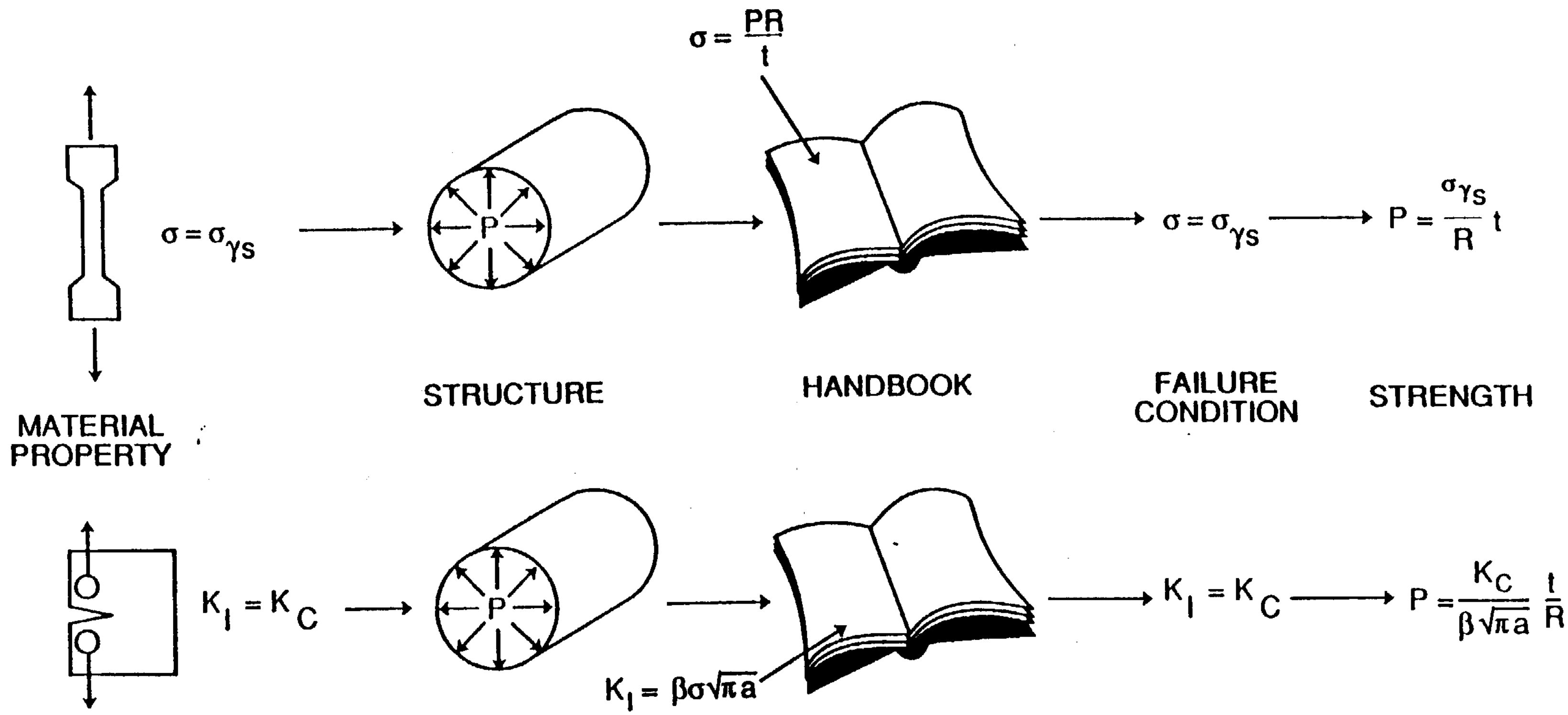

Figure 48. Fracture analysis sequence.

ASSEMBLY **OPTICAL TELESCOPE ASSEMBLY (OTA)**

SUBASSEMBLY **FINE GUIDANCE SENSOR KINEMATIC MOUNTS**

(KINEMATIC MOUNT #1)

PART NAME	PART NUMBER	PART SIZE (IN)*	MATERIAL	FLAW DEPTH (IN)	FLAW LENGTH (IN)	FLAW TYPE	TYPE NDE DONE	LIFE-TIME	STRESS (KSI)	S.F.	KEY
TOP HAT (OPTICAL BENCH END)	679-3495	t = 0.0625 w = 2.259	15-5PH ST. ST. AMS 5659 H-1025	0.0625	0.34	TC	UT ET	4	18.0	8.6	A
TOP HAT (KEEL END)	679-7249	t = 0.0625 w = 2.259	15-5 PH ST.ST. AMS 5659 H-1025	0.0625	0.34	TC	UT ET	4	18.0	8.6	B
TOP HAT FASTENERS	NAS1351N3	d = 0.1497	A-286 ST.	0.041	0.4703	C	UT ET	4	30.9	5.2	C
TUBE	679-3497	t = 0.117 w = 0.836	INVAR 36	0.117	0.31	TC	UT ET	4	20.4	3.2	D
FLEXURE (THREADED END)	679-3496	d = 0.2591	15-5 PH ST.ST. AMS 5659 H-1025	0.031	0.814	C	UT ET	4	22.1	7.0	E
FLEXURE (PLATE END)	679-3496	t = 0.10 w = 0.5937	15-5 PH ST.ST. AMS 5659 H-1025	0.038	0.038	PTE	UT ET	4	19.7	7.9	F

NOTES: *SIZE USED IN FRACTURE MECHANICS MODEL, t x w, DIAMETER, ETC.
TC = THROUGH CENTER
C = CIRCUMFERENTIAL AT THREAD ROOT
PTE = PART-THROUGH EDGE

UT = ULTRASONIC
ET = EDDY CURRENT

Figure 49. Sample fracture mechanics analysis reporting sheet.

APPENDIX

FAIL-SAFE ANALYSIS FOR THE MAIN RING SKINS

GWYN FAILE
EP42
NOVEMBER 21, 1983

TABLE OF CONTENTS

	PAGE
INTRODUCTION	1.0
FAIL-SAFE FACTORS OF SAFETY	3.0
A. SECTION PROPERTIES	
1. MAIN RING - FULL SECTION	4.0
2. MAIN RING - WITH FAILED CYLINDER	5.0
3. MAIN RING - WITH FAILED CHANNEL	6.0
B. MATERIAL PROPERTIES	7.0
C. MAIN RING STRESSES	7.0
D. MAIN RING FORCES, MOMENTS, AND TORQUES	
1. AXIAL LOAD	8.0
2. BENDING ABOUT 1-1 AXIS	8.0
3. BENDING ABOUT 2-2 AXIS	8.0
4. TORQUE	9.0
E. FAIL-SAFE STRENGTH CHECKS	
1. AXIAL LOAD	10.0
2. BENDING	10.0
3. SHEAR	11.0
4. PRINCIPAL STRESS CHECKS	12.0
F. FAIL-SAFE STABILITY CHECKS	
1. OUTER CYLINDER STABILITY CHECKS	13.0
a. COMPRESSION	14.0
b. SHEAR	16.0
c. INTERACTION	17.0
2. CHANNEL STABILITY CHECKS	18.0
a. IN-PLANE BENDING	18.0
b. SHEAR	21.0
c. TRANSVERSE COMPRESSION	22.0
d. INTERACTION	23.0

MAIN RING

FAIL-SAFE ANALYSIS FOR THE MAIN RING SKINS

INTRODUCTION

THE MAIN RING SKINS CONSIST OF OUTER AND INNER CYLINDERS RIVITED TO FORWARD AND AFT CHANNELS TO MAKE UP A RING WITH A RECTANGULAR CROSS SECTION AS SHOWN BELOW. IN THE FAIL-SAFE ANALYSIS IT IS ASSUMED THAT A CRACK HAS PROPAGATED ACROSS THE FULL WIDTH OF A CYLINDER OR CHANNEL. THE RESULTING CROSS SECTION, I.E., THE RING WITH ONE ELEMENT LOCALLY REMOVED, IS CHECKED TO DETERMINE IF IT WILL SUPPORT LIMIT LOAD WITH A FACTOR OF SAFETY OF ONE (1) AGAINST ULTIMATE STRENGTH. THE LOADS USED FOR THIS ANALYSIS ARE DETERMINED FROM THE SKIN MAXIMUM STRESSES WHICH WERE CALCULATED USING A FINITE ELEMENT MODEL OF THE MAIN RING. THE LOADS, AXIAL FORCES, MOMENTS, ETC, THAT ARE REQUIRED TO PRODUCE THE MAXIMUM STRESSES ARE BACKED OUT BY HAND FOR

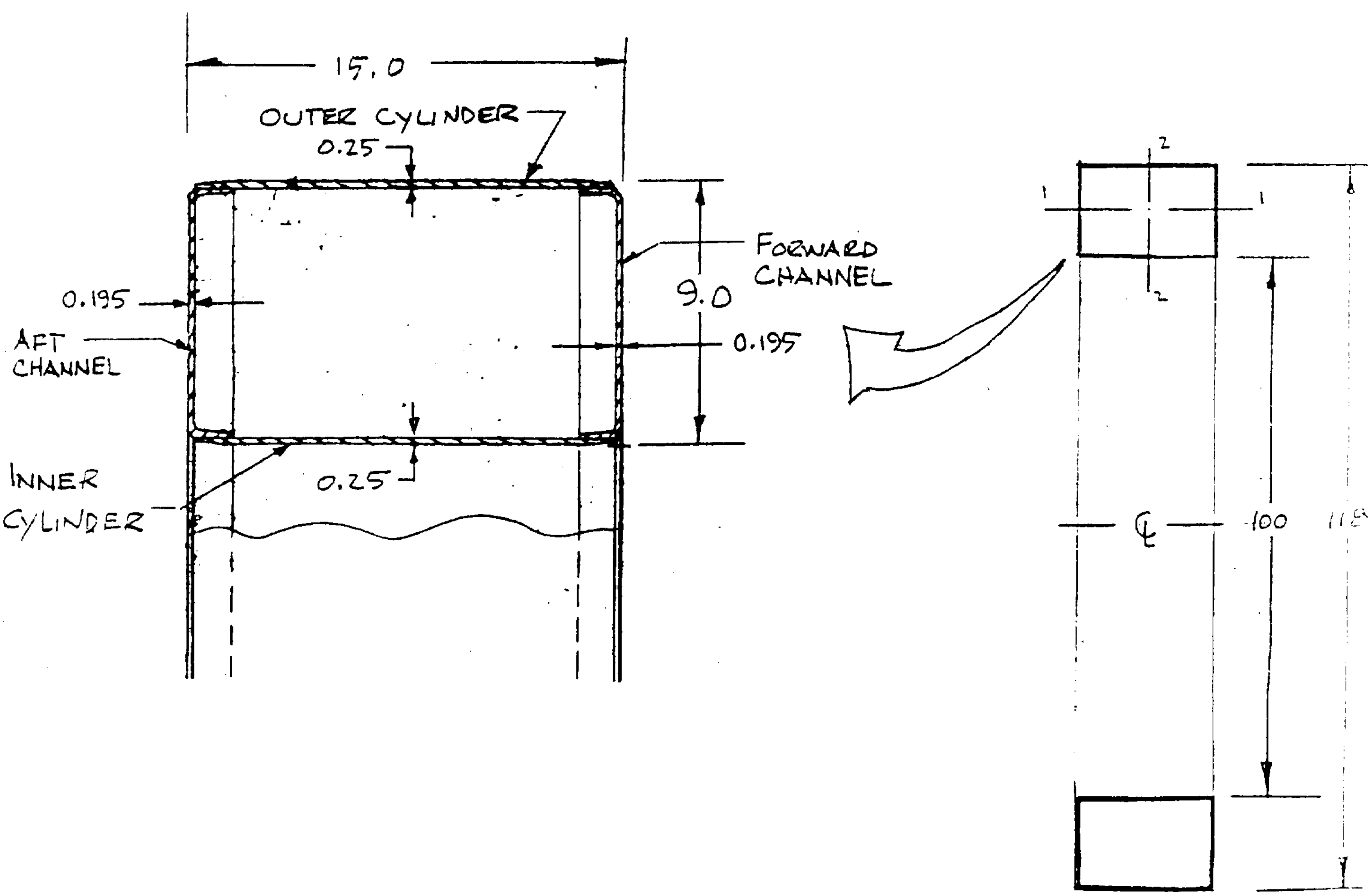

THE TOTAL CROSS SECTION AND THEN APPLIED TO THE REDUCED (RING WITH ONE ELEMENT LOCALLY REMOVED) CROSS SECTION. THE RESULTING STRESSES ON THE REDUCED SECTION ARE THEN CHECKED AGAINST ULTIMATE STRENGTH AND STABILITY.

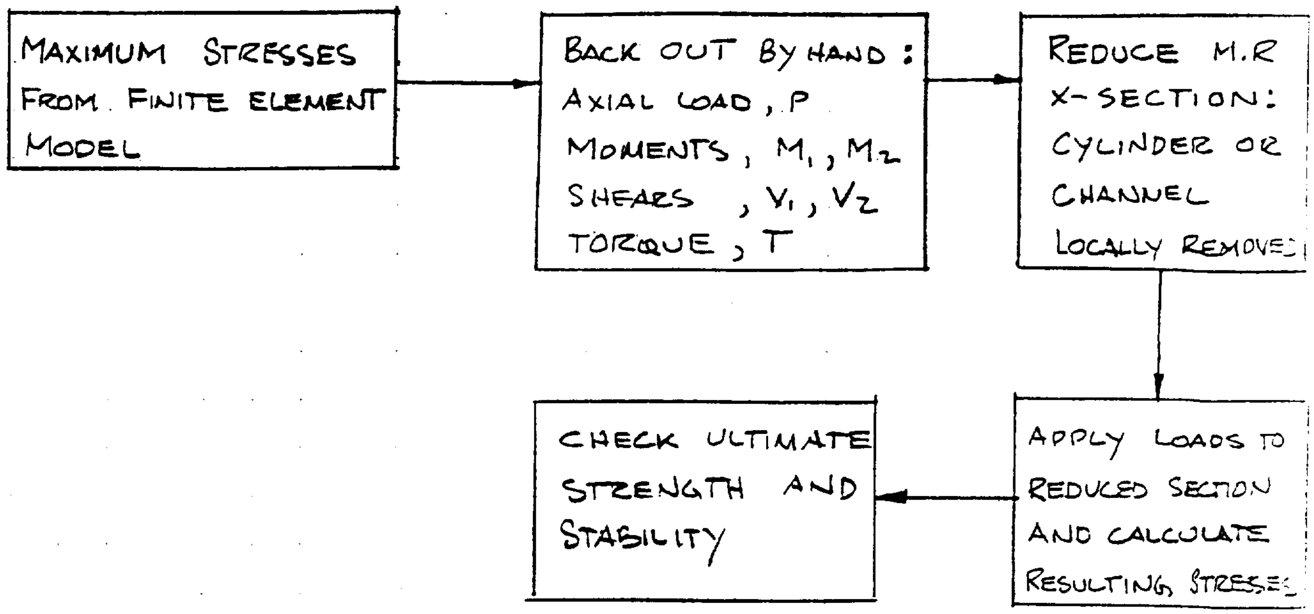

FAIL-SAFE FACTORS OF SAFETY

ITEM	CRACKED ELEMENT	MODE OF FAILURE	F.O.S.	PAGE
CYLINDER, CHANNEL	CYLINDER	TENSION	4.21	
CHANNEL	CYLINDER	TENSION/BEND.	1.51	
CHANNEL	CYLINDER	SHEAR	1.28	
CYLINDER	CHANNEL	SHEAR	1.64	
CHANNEL	CYLINDER	TEN./PRINCP.	1.03	
CHANNEL	CYLINDER	SHEAR/PRINCP.	1.19	
CYLINDER	CHANNEL	BUCKLING/COMP.	2.72	
CYLINDER	CHANNEL	BUCKLING/SHEAR	1.87	
CYLINDER	CHANNEL	BUCK./INT./C/C	1.09	
CYLINDER	CHANNEL	BUCK./INT/C/S	1.14	
CHANNEL	CYLINDER	BUCKLING/BEND.	1.95	
CHANNEL	CYLINDER	BUCKLING/SHEAR	1.59	
CHANNEL	CYLINDER	BUCKLING/COMP.	1.40	
CHANNEL	CYLINDER	BUCK./INT/B/S/C	>1.0	

NOTES: 1) REQUIRED FAIL-SAFE FACTOR OF SAFETY ≥ 1
2) THE CALCULATED FOS IS A CONSERVATIVE ESTIMATE AS OPPOSED TO AN EXACT VALUE.

ECF/EP42
9/19/83

A. SECTION PROPERTIES

1. MAIN RING CROSS SECTION [FULL SECTION]

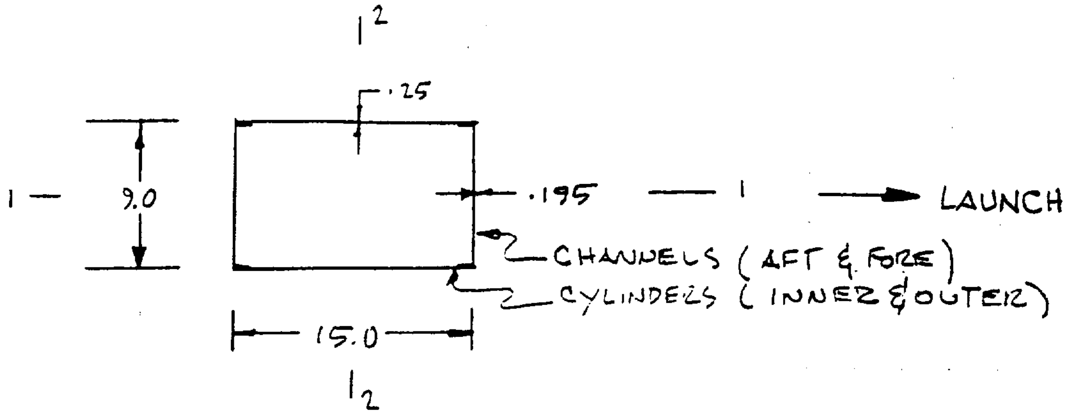

$A = (15.0)(9.0) - (14.61)(8.5)$

$A = 10.815 \text{ IN}^2$

$I_1 = \frac{1}{12}\left[(15)(9)^3 - (14.61)(8.5)^3\right]$

$I_1 = 163.553 \text{ IN}^4$

$I_2 = \frac{1}{12}\left[9(15)^3 - (8.5)(14.61)^3\right]$

$I_2 = 322.288 \text{ IN}^4$

2. MAIN RING CROSS SECTION [CYLINDER FAILED]

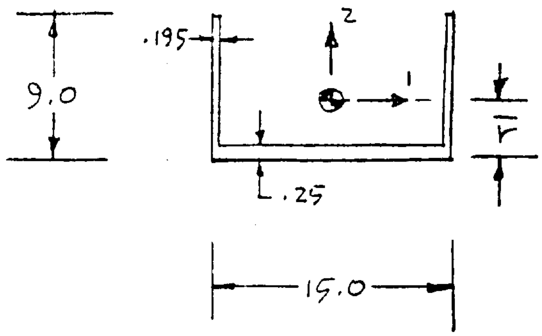

$$\bar{r} = \frac{2(.195)(9)(4.5) + (14.61)(.25)(.125)}{7.163}$$

$\bar{r} = 2.269$ IN

$A = (2)(.195)(9) + (.25)(14.61)$

$A = 7.163$ IN^2

$$I_1 = \frac{1}{12}\left[(2)(.195)(9)^3 + (14.61)(.25)^3\right] + 2(.195)(9)\left[4.5 - 2.269\right]^2 + (14.61)(.25)\left[2.269 - .125\right]^2$$

$I_1 = 57.972$ IN^4 , $\left(c/I_1\right)_{max} = \frac{6.731}{57.972} = .116$ $1/IN^3$

$$I_2 = \frac{1}{12}\left[(9)(15)^3 - (8.75)(14.61)^3\right]$$

$I_2 = 257.318$ IN^4 , $\left(c/I_2\right)_{max} = \frac{7.5}{257.318} = .0291$ $1/IN^3$

3. MAIN RING CROSS SECTION [CHANNEL FAILED]

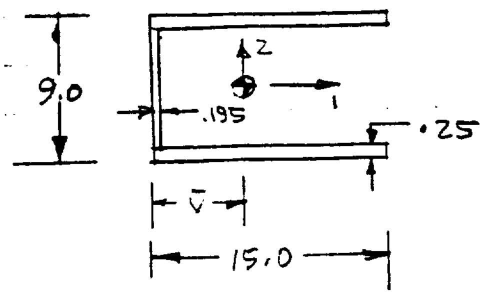

$$\bar{v} = \frac{2(15)(.25)(7.5) + (8.5)(.195)(.0975)}{9.158}$$

$$\bar{v} = 6.160 \text{ IN}$$

$$A = 2(.25)(15) + (.195)(8.5)$$
$$A = 9.158 \text{ IN}^2$$

$$I_1 = \frac{1}{12}\left[(15)(9)^3 - (14.805)(8.5)^3\right]$$

$$I_1 = 153.573 \text{ IN}^4, \quad \left(\frac{c}{I_1}\right)_{max} = \frac{4.5}{153.573} = .0293 \text{ }^1/_{IN^3}$$

$$I_2 = \frac{1}{12}\left[(2)(.25)(15)^3 + (8.5)(.195)^3\right] + (2)(.25)(15)\left[7.5 - 6.16\right]^2$$
$$+ (.195)(8.5)\left[6.16 - .0975\right]^2$$

$$I_2 = 215.017 \text{ IN}^4, \quad \left(\frac{c}{I_2}\right)_{max} = \frac{8.84}{215.017} = .0411 \text{ }^1/_{IN^3}$$

B. MATERIAL PROPERTIES

MAIN RING MATERIAL: TI-6AL-4V, ANNEALED

$F_{TU} = 130$ KSI	$E = 16.0$ MSI
$F_{TY} = 120$ KSI	$E_c = 16.4$ MSI
$F_{CY} = 126$ KSI	$G = 6.2$ MSI
$F_{SU} = 76$ KSI	$\mu = .31$

C. MAIN RING STRESSES

THE STRESSES USED ARE TAKEN FROM THE LMSC-HSV STRESS ANALYSIS FOR THE MAIN RING. LOAD CYCLE IS FOR MILC LOADS.

TENSION: $f_t = 20,468$ PSI L.O., L/C # 17, 180°-360°, EL# 802005

SHEAR: $f_s = 20,600$ PSI L.O., L/C # 17, 180°-360°, EL# 802005

THE TENSION STRESS GIVEN ABOVE INCLUDES TENSION PLUS BENDING AS FOLLOWS:

$$f_t = f_{t_1} + f_{b_1} \qquad f_{t_1} = 7,458 \text{ psi} \qquad f_{b_1} = 13,010 \text{ psi}$$

f_{t_1} COMES FROM AXIAL LOADS IN THE RING AND BENDIN[G] ABOUT THE RING CROSS SECTION, WHEREAS f_b IS BENDIN[G] ABOUT THE NEUTRAL AXIS OF THE SKINS. FOR THE FAIL-SAFE ANALYSIS IT IS GENERAL FAILURE OF THE RING (TOTAL COLLAPSE) THAT IS OF CONCERN AND THE LOADS, MOMENTS THAT PRODUCE THIS GENERAL FAILURE THAT WE WISH TO CALCULATE. THAT IS, WE HAVE GENERAL FORCES AND MOMENTS ACTING ON THE RING PLUS LOCAL EFFE[CTS]. LOCAL LOADS ARE ACCOMODATED BY A DIRECT PATH INTO THE INTERNAL FITTINGS.

THE f_t ABOVE IS THE STRESS WHICH HAS THE MAXIMUM MEMBRANE COMPONENT, AND THE TOTAL $(f_{t_1}+f_b)$ WILL BE USED TO BACK OUT A SET OF FORCES OR MOME[NTS] ACTING ON THE GENERAL RING CROSS SECTION. THIS IS CONSERVATIVE SINCE f_b IS A LOCAL EFFECT. THE MAXIMUM STRES[S]

IN THE RING IS A LOCAL BENDING STRESS ($f_b = 39{,}000$ PSI) IN THE RADIAL DIRECTION WHICH WILL NOT CAUSE M.R. SECTION FAILURE AND THEREFOR DOESNOT HAVE TO BE CONSIDERED IN THE FAIL-SAFE ANALYSIS.

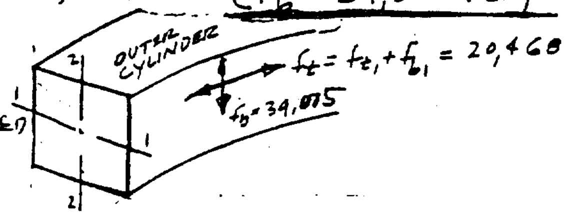

D. MAIN RING FORCES, MOMENTS AND TORQUES

1. ASSUME ALL THE LOAD IS AXIAL:

$$F_t = \frac{P}{A}$$

$$P = AF_t$$

$$= (10.815)(20{,}468)$$

$$P = 221{,}361 \text{ LBS} \longleftarrow$$

2. ASSUME BENDING ABOUT M.R. 1-1 AXIS

$$f_b = \frac{M_1 C_2}{I_1}$$

$$M_1 = \frac{I_1}{C_2} f_b$$

$$= \frac{163.553}{4.5}(20{,}468)$$

$$M_1 = 743{,}912 \text{ IN-LB} \longleftarrow$$

3. ASSUME BENDING ABOUT MR. 2-2 AXIS

$$M_2 = \frac{I_2}{C_1} f_b$$

$$= \frac{322.288}{7.5}(20{,}468)$$

$$M_2 = 879{,}545 \text{ IN·LB} \longleftarrow$$

4. ASSUME TORSION GENERATES f_s

$$f_s = \frac{T}{2t\,(a-t)\,(b-t_1)}$$

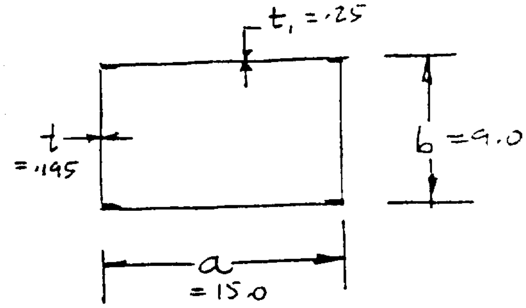

$$T = 2t(a-t)(b-t_1)\,f_s$$

$$= 2(.195)(15.0-.195)(9.0-.25)(20,600)$$

$$T = 1,040,754 \text{ IN}\cdot\text{LB}$$

THIS TORQUE GENERATES f_s AT MIDPOINT OF THE SHORT SIDE AN LARGER THAN THE TORQUE REQUIR TO GENERATE f_s AT THE LONG SIDE THUS IT IS THE MORE CONSERVATIVE OF THE TWO POSSIBLE CHOICES.

E. FAIL-SAFE STRENGTH CHECKS

1. AXIAL LOAD STRENGTH CHECK

ASSUME THAT A CYLINDER HAS FAILED (A.2.) THIS REPRESENTS THE GREATER LOSS OF AREA.

$$f_t = P/A$$

P FROM D.1.
A FROM A.2.

$$= \frac{221361}{7.163}$$

$$f_t = 30{,}903$$

$$F.S. = \frac{130{,}000}{30{,}903} = \underline{\underline{4.21 > 1}}$$

2. BENDING MOMENT STRENGTH CHECK

FROM THE C/I VALUES (A.2. AND A.3.) AND THE MOMENTS (D.2. AND D.3.) IT CLEAR THAT THE WORST CASE IS BENDING ABOUT THE 1-1 AXIS WITH A FAILED CYLINDER.

$$f_b = \frac{M_1 c}{I_1}$$

$M_1 = 743{,}912$ IN·LB (D.2.)
$c/I_1 = .116$ 1/IN3 (A.2.)

$$= (743912)(.116)$$

$$f_b = 86{,}294 \text{ PSI}$$ (OCCURS ON A CHANNEL)

$$F.S. = \frac{130{,}000}{86{,}294} = \underline{\underline{1.51 > 1}}$$

3. SHEAR (DUE TO TORSION) STRENGTH CHECK

SINCE THERE WILL BE END RESTRAINTS PROVIDED BY THE CLOSED TUBE AT THE CRACK INTERFACE, THE TORSION CAN BE CARRIED BY DIFFERENTIAL BENDING (SHEAR FORCES V). THUS WE NEED TO SHOW THAT THE SIDEWALLS HAVE SUFFICIENT SHEAR CAPABILITY TO CARRY V.

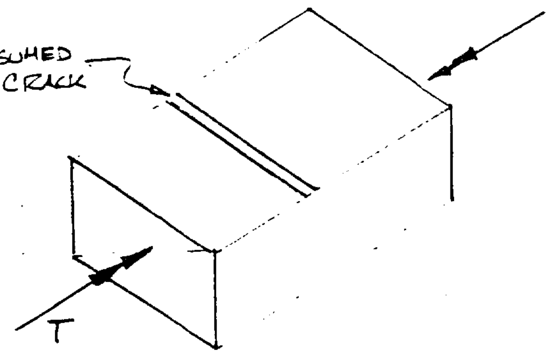

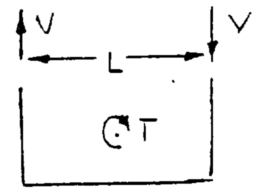

$V = \frac{T}{L}$

SECTION AT CRACK

$T = 1{,}040{,}754$ IN·LB (D.4.)

a) ASSUME A CRACKED CYLINDER

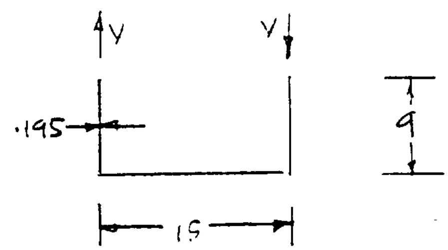

$$V = \frac{1{,}040{,}754}{15}$$

$$V = 69{,}384 \text{ LB}$$

$$f_{s_{MAX}} = \frac{69{,}384}{(.195)(9)}(1.5)$$

$$f_{s_{MAX}} = 59{,}303 \text{ PSI}$$ (OCCURS ON A CHANNEL)

$$F.S. = \frac{76{,}000}{59{,}303} = \underline{1.28 > 1}$$

b) ASSUME A CRACKED CHANNEL

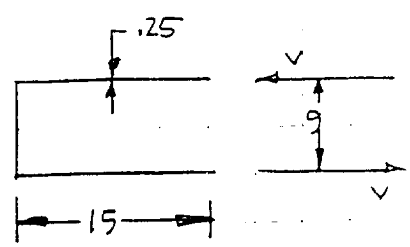

$$V = \frac{1{,}040{,}754}{9}$$

$$V = 115\,639 \text{ LB}$$

$$f_{s_{MAX}} = \frac{115\,639}{(.25)(15)}(1.5)$$

$$f_{s_{MAX}} = 46{,}256 \text{ PSI}$$ (OCCURS ON A CYLINDER)

$$F.S. = \frac{76{,}000}{46{,}256} = \underline{1.64 > 1}$$

4. PRINCIPAL STRESS CHECK

ASSUME THAT ALL THE MAXIMUM STRESSES ABOVE OCCUR AT THE SAME POINT (VERY CONSERVATIVE).

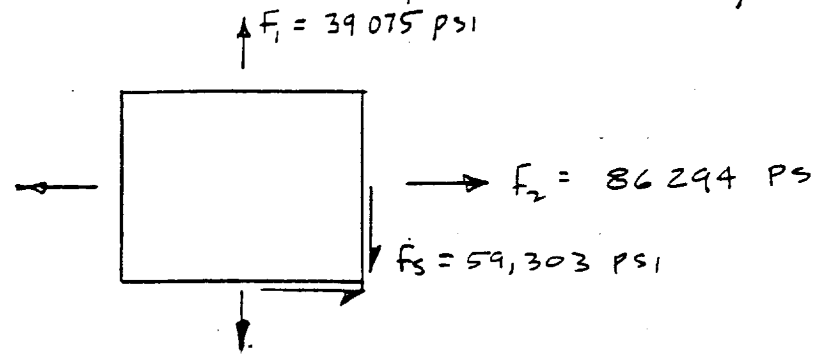

$$f_{t_{max}} = \frac{f_1 + f_2}{2} + \sqrt{\left(\frac{f_1 - f_2}{2}\right)^2 + f_s^{\,2}}$$

$$= \frac{39\,075 + 86\,294}{2} + \sqrt{\left[\frac{39\,075 - 86\,294}{2}\right]^2 + (59\,303)^2}$$

$$= 62\,685 + 63\,830$$

$f_{t_{max}} = 126,515$ psi (OCCURS ON A CHANNEL)

$$F.S. = \frac{130,000}{126,515} = 1.03 > 1$$

MAXIMUM TENSION (VERY CONSERVATIVE)

$f_{s_{max}} = 63,830$ psi (OCCURS ON A CHANNEL)

$$F.S. = \frac{76,000}{63,830} = 1.19 > 1$$

MAXIMUM SHEAR

F. FAIL-SAFE STABILITY CHECKS

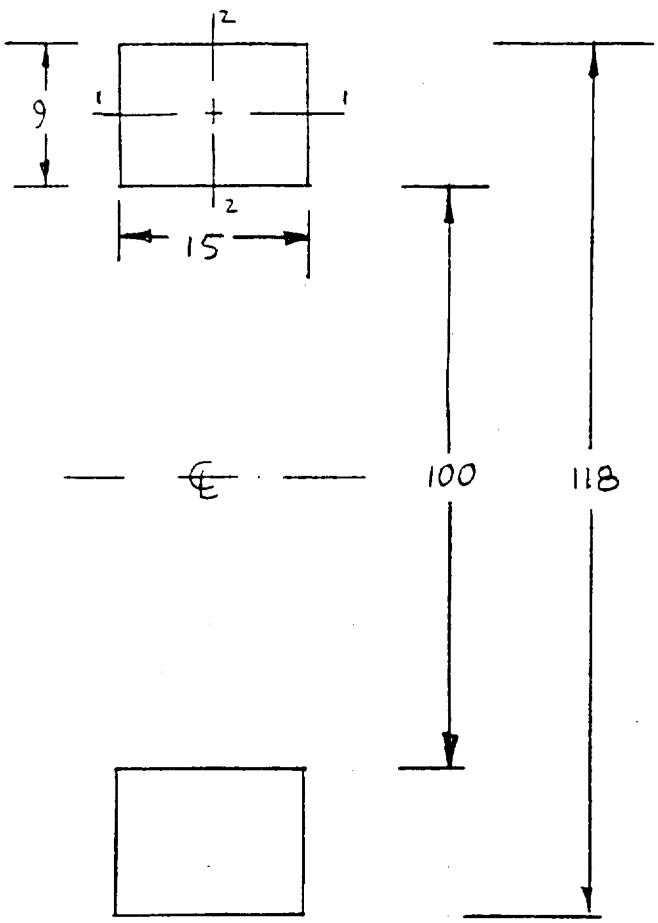

1. OUTER CYLINDER STABILITY CHECK

THE MAXIMUM INTERNAL FITTING SPACING IS 15°. THEREFORE THE MAXIMUM UNSUPPORTED DIMENSION IS

$$S = \frac{(59)(15)\pi}{180} = 15.45 \text{ IN}$$

HENCE FOR THE STABILITY CHECK OF THE OUTER CYLINDER CONSIDER A SQUARE PLATE 15" × 15".

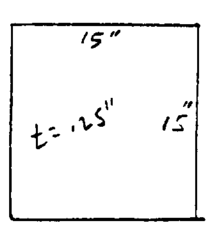

a. COMPRESSION (ULTIMATE)

BENDING ABOUT THE 2-2 AXIS IN CONFIGURATION A.3. WILL PRODUCE THE HIGHEST STRESS IN THE OUTER CYLINDER.

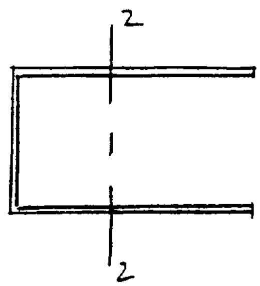

$$\left(c/I_2\right)_{max} = .0411 \ 1/IN^3$$

SINCE THE LOCAL BENDING STRESS WILL NOT BE AFFECTED BY A REDUCTION IN CROSS SECTIONAL AREA, IE, A CRACK, THE BENDING MOMENT THAT DOES CAUSE AN INCREASE IN THE CYLINDER STRESS MAY BE FOUND AS FOLLOWS.

$$M_2 = \left(\frac{I_2}{c}\right) f_{t1}$$

$\frac{I_2}{c}$ FOR TOTAL SECTION

f_{t1} FROM SEC. C.

$$= \frac{322.288}{7.5}(7,458)$$

$$M_2 = 320,483 \text{ IN·LB}$$

THEN THE STRESS TO CONSIDER IS

$$f_c = M_2 \frac{c}{I_2} + f_{b1}$$

$\frac{c}{I_2}$ FOR A FAILED CHANNEL

f_{b1} FROM SECTION C.

$$= (320,483)(.0411) + 13010$$

$$= 13,172 + 13,010$$

$$\underline{f_c = 26,182 \text{ PSI}}$$

THIS IS ACTUALLY A BENDING (IN-PLANE) TYPE STRESS ON THE CYLINDER BUT WILL BE CONSIDERED AS A COMPRESSIVE STRESS FOR ADDED CONSERVATIVISM.

THE ULTIMATE CAPABILITY FOR A SQUARE PLATE IN COMPRESSION IS GIVEN BY

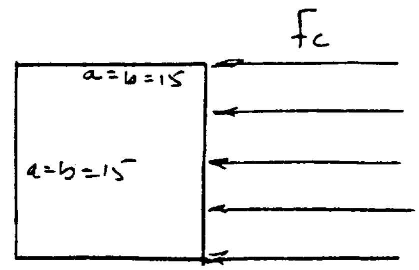

$$F_{c_{ULT}} = \tfrac{1}{2}F_{cy} + \tfrac{1}{2}\sigma_c$$

WHERE

$$\sigma_c = \frac{\pi^2 E t^2}{3(1-\nu^2)b^2}, \quad t = \text{THICKNESS} = .125 \text{ IN}$$

AND THE SIDES ARE SIMPLY SUPPORTED.

REFERENCE: "BUCKLING OF METAL STRUCTURES", FRIEDRICH BLEICH, 1952. P.P. 459 - 473

$$\sigma_c = \frac{\pi^2 (16.4\times10^6)(.25)^2}{3(1-.31^2)(15)^2}$$

$$\sigma_c = 16,581 \text{ psi}$$

$$F_{c_{ULT}} = \frac{126,000}{2} + \frac{16581}{2}$$

$$= 63,000 + 8291$$

$$F_{c_{ULT}} = 71,291 \text{ psi}$$

$$F.S. = \frac{71291}{26182} = 2.72 > 1$$

b. SHEAR

MAXIMUM AVERAGE SHEAR STRESS IN OUTER CYLINDER IS

$\frac{46,256 \text{ PSI}}{1.5} = 30837$ PSI SEE SECT. E.3.b

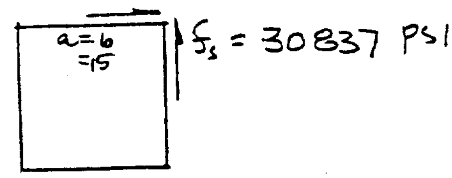

INITIAL BUCKLING CAPABILITY PER LMSC STRESS MEMO 80

FIXED EDGES

$k_3 = .0637$

$n = 35$

$F_{0.7} = 133.09$ KSI

$\sqrt{K} = 3.68$

$\left(\frac{b}{t}\right)_e = (b/t)/\sqrt{K} = \left(\frac{15}{.25}\right)/3.68 = 16.3$

$B = k_3\left(\frac{b}{t}\right)_e = (.0637)(16.3) = 1.04$

$F/F_{0.7} = .87$

$F_{s_{cr}} = .5\, F_{0.7} \times \frac{F}{F_{0.7}}$

$= (.5)(133.09)(.87)$

$F_{s_{cr}} = 57.894$ KSI $= 57,894$ PSI

$F.S. = \frac{57\,894}{30\,837} = 1.87 > 1$

THIS IS AGAINST INITIAL BUCKLING. ULTIMATE FAI INCLUDING TENSION FIE ACTION WOULD BE GRE THUS THIS IS A CONSE ANSWER.

c. INTERACTION FOR OUTER CYLINDER BUCKLING

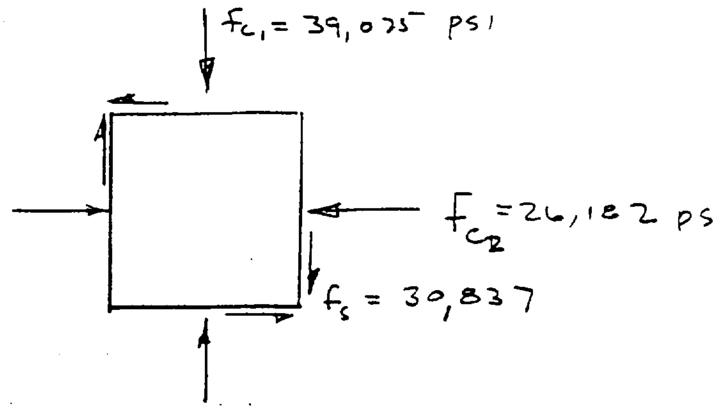

$$R_{c_1} = \frac{39075}{71291} = .548$$

$$R_{c2} = \frac{26182}{71291} = .367$$

$$R_s = \frac{30837}{57894} = .533$$

REF: ASM FIG A3.5.0-1 and TABLE A3.5.0-1

R_{c1} & R_{c2} : $$F.S. = \frac{1}{.548 + .367} = \underline{\underline{1.09}}$$

R_{c1} & R_s : $$F.S. = \frac{2}{R_{c1} + \sqrt{R_{c_1}^2 + 4R_s^2}}$$

$$= \frac{2}{.548 + \sqrt{.548^2 + 4(.533)^2}}$$

$$F.S. = \underline{\underline{1.14}}$$

2. CHANNEL STABILITY CHECKS

THE MAXIMUM SPACING BETWEEN INTERNAL RING FITTINGS IS:

15.45 IN AT OUTSIDE DIAMETER

$\frac{50}{59} \times 15.45$ IN = 13.09 IN AT INSIDE DIAMETER

$$\text{AVERAGE} = \frac{15.45 + 13.09}{2} = 14.27$$

PLATE DIMENSIONS TO CONSIDER FOR CHANNEL STABILITY CHECKS -

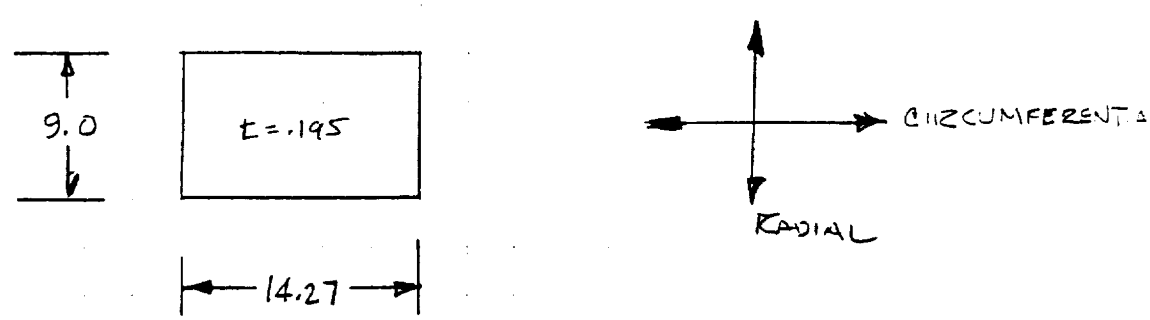

a) IN-PLANE BENDING

BENDING ABOUT THE 1-1 AXIS IN CONFIGURATION A.2. WILL PRODUCE THE HIGHEST STRESS IN THE CHANNEL.

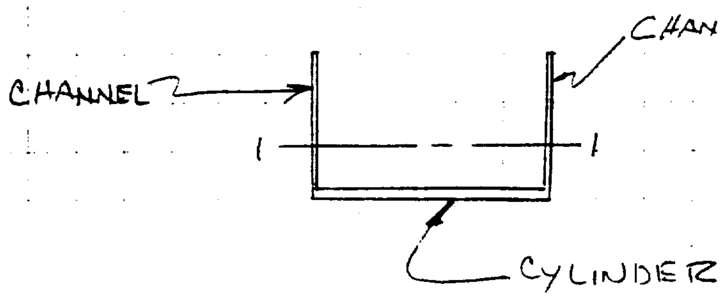

$$\left(\frac{c}{I_1}\right)_{max} = .116 \ 1/\text{IN}^3$$

SINCE THE LOCAL BENDING STRESS WILL NOT BE AFFE[CTED] BY A REDUCTION IN CROSS SECTIONAL AREA DUE TO A CRACK[ED] CYLINDER, THE BENDING MOMENT OF INTEREST MA[Y] BE CALCULATED AS FOLLOWS:

$$M_1 = \left(\frac{I_1}{c}\right) f_{t1}$$

$\frac{I_1}{c}$ FOR TOTAL SECTION
f_{t1} FROM SECTION C.

$$= \frac{163.553}{4.5}(7458)$$

$$M_1 = 271{,}062 \text{ IN·LB}$$

THEN THE STRESS TO CONSIDER ON THE CHANNEL IS

$$f = \pm M_1\left(\frac{c}{I_1}\right) + f_{b1}$$

c/I_1 FOR A FAILED CYLINDER
f_{b1} FROM SECTION C.

$$= \pm(271{,}062)(.116) + 13\,010$$

$$f = \pm 31443 + 13\,010$$

$$= \begin{cases} 44\,453 \text{ PSI MAX} \\ -18\,433 \text{ PSI MIN} \end{cases}$$

IN-PLANE BENDING TYPE OF DISTRIBUTION

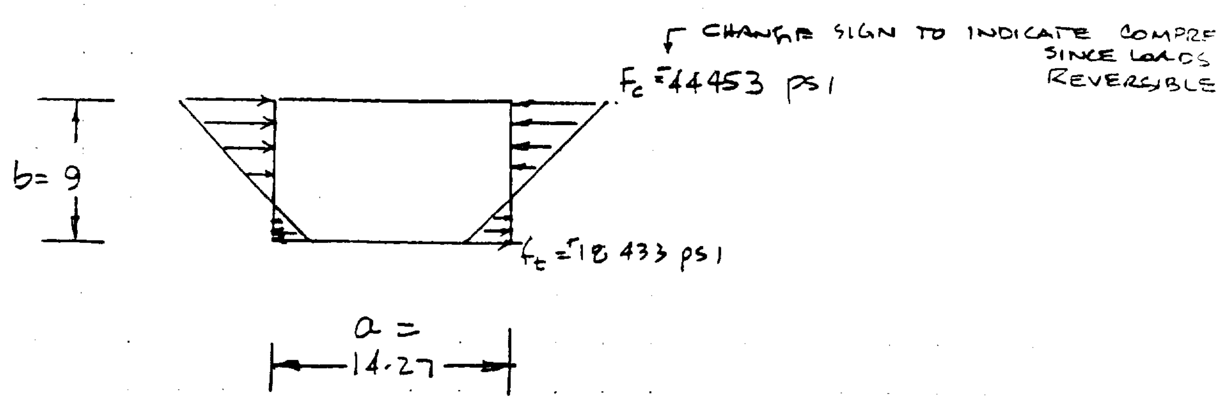

BENDING CAPABILITY PER LMSC STRESS MEMO 80 C.

$k_2 = .0901$

$n = 35$

$F_{0.7} = 133.09$ KSI

$\sqrt{K} = 3.35$

$\alpha = \frac{f_c}{f_c - f_t} = \frac{44453}{44453+18433} = .$

$a/b = \frac{14.27}{9} = 1.59$

$(b/t)_e = (b/t)/\sqrt{K} = (9/.145)/3.35 = 13.8$

$B = k_2(b/t)_e = (.0901)(13.8) = 1.24$

$F/F_{0.7} = .65$

$F_{bcr} = F_{0.7} \times \frac{F}{F_{0.7}}$

$= (133.09)(.65)$

$F_{bcr} = 86,508$ KSI

$F_{bcr} = 86,508$ PSI

$F.S. = \frac{86508}{44453} = \underline{\underline{1.95}}$

b) SHEAR

MAXIMUM AVERAGE SHEAR IN CHANNEL IS

$\frac{59\,303}{1.5} = 39\,535$ PSI. SEE SECTION E.3.a.

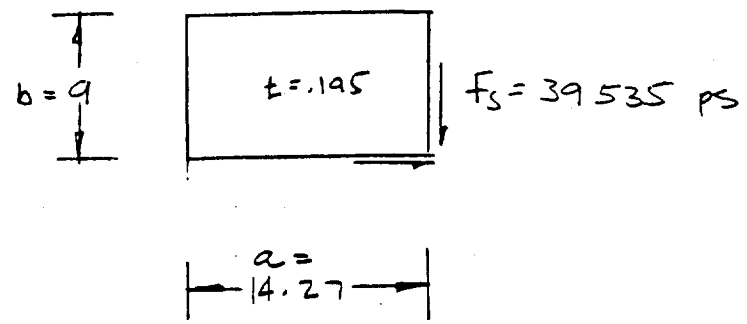

INITIAL BUCKLING CAPABILITY PER LMSC STRESS MEMO 80C.

FIXED EDGES

$k_3 = .0637$ $\qquad$ $b/a = 9/14.27 = .63$

$n = 35$

$F_{0.7} = 133.09$ KSI

$\sqrt{K} = 3.3$

$(b/t)_e = (b/t)/\sqrt{K} = \left(\frac{9}{.195}\right)/3.3 = 13.99$

$B = k_3\,(b/t)_e = (.0637)(13.99) = .89$

$\frac{F}{F_{0.7}} = .95$

$F_{s_{CR}} = .5\,F_{0.7} \times \frac{F}{F_{0.7}}$

$= (.5)(133.09)(.95)$

$F_{s_{CR}} = 63.218$ KSI

$F_{s_{CR}} = 63\,218$ PSI

$F.S. = \frac{63\,218}{39\,535} = \underline{\underline{1.59}}$

THIS IS CONSERVATIVE, SINCE ULTIMATE FAILURE CONSIDERING TENSION FIELD ACTION WOULD BE GREATER.

C. TRANSVERSE COMPRESSION

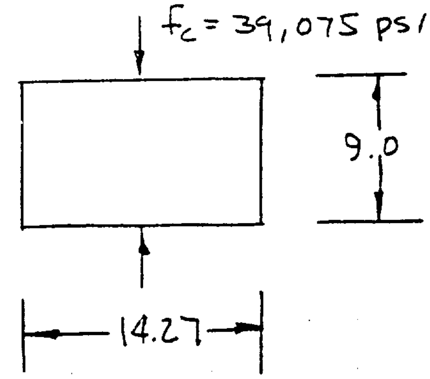

REF: "BUCKLING OF METAL STRUCTURES," FRIEDRICH BLEICH, 1952
P.P. 473 - 475

$a = 9.0$ IN
$b = 14.27$ IN
$\beta = b/a = 1.586$

$$\sigma_c = \frac{\pi^2 E}{12(1-\nu^2)} \left(\frac{t}{b}\right)^2 \left(\beta + \frac{1}{\beta}\right)^2$$

$$= \frac{\pi^2 (16.4 \times 10^6)}{12(1 - .31^2)} \left(\frac{.195}{14.27}\right)^2 \left(1.586 + \frac{1}{1.586}\right)^2$$

$\sigma_c = 13,686$ PSI

ULTIMATE CAPABILITY IS GIVEN BY

$$F_{c_{ULT}} = \frac{1+\beta^4}{1+3\beta^4} F_{cy} + \frac{2\beta^4}{1+3\beta^4} \sigma_c$$

$$= \frac{1+(1.586)^4}{1+3(1.586)^4} (126,000) + \frac{2(1.586)^4}{1+3(1.586)^4} (13,686)$$

$$= (.367)(126,000) + .633(13,686)$$

$$= 46242 + 8663$$

$F_{c_{ULT}} = 54,905$ PSI

$$F.S. = \frac{54905}{39075} = 1.4 > 1$$

d. INTERACTION FOR CHANNEL BUCKLING

$$R_b = \frac{44453}{86508} = .514$$

$$R_s = \frac{39535}{63218} = .625$$

$$R_c = \frac{39075}{54905} = .712$$

R_s AND R_b ARE PLOTTED ON THE FOLLOWING PAGE WHICH WAS TAKEN FROM THE MSFC ASM. IT CAN BE SEEN THAT FOR THE GIVEN VALUES OF R_s AND R_b, R_c COULD BE GREATER THAN 0.8. THEREFORE THE ABOVE RATIOS ARE ACCEPTABLE.

A 3.5.0 (Cont'd) Buckling of Rectangular Flat Plates under Combined Loading

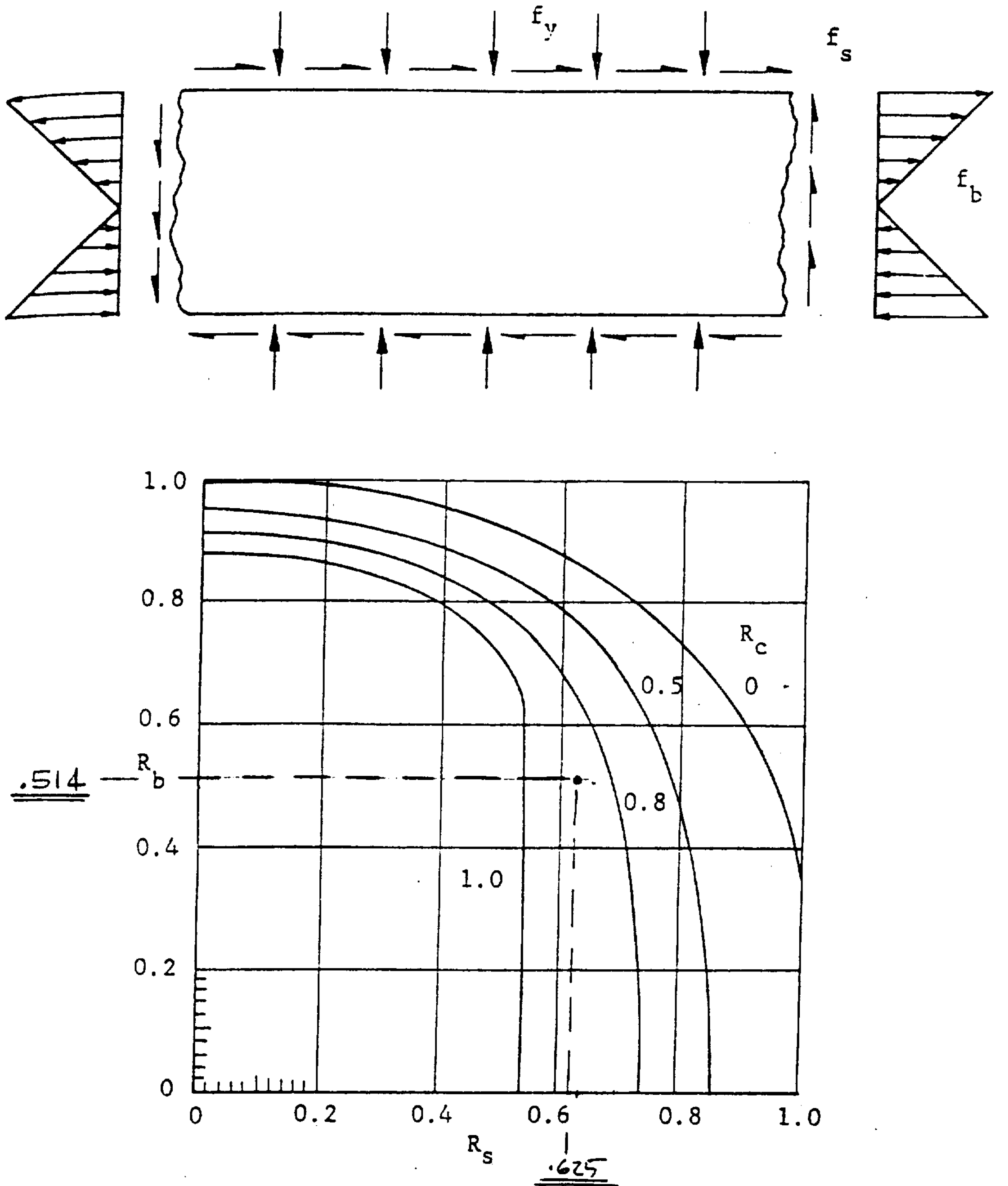

Interaction Curves for Simply Supported Long Flat Plates
Under Various Combinations of Shear, Bending, and Transverse Compression

Fig. A 3.5.0-3

SOLID ROCKET BOOSTER (SRB) AFT SKIRT

The following analysis was done by United Space Boosters Incorporated analyst.

The Solid Rocket Boosters (SRB) are used for approximately 123 seconds to supplement the orbiter thrust during the launch and ascent phases of flight. Prior to and including launch, the entire Space Transportation System (STS) is supported by two SRB aft skirts attached to the Mobile Launch Platform (MLP) by four holddown posts on each aft skirt.

During shuttle transportation on the crawler and Space Shuttle Main Engine (SSME) thrust buildup, a hold-down system is required in the SRB aft skirt to resist prelaunch and launch holddown loads at the MLP. Thrust buildup loads are critical for the aft skirt during the manned flight phase.

After burnout, the SRB's are jettisoned and moved away from the shuttle by booster separation motors located in the aft skirt and frustrum. SRB descent is braked by parachutes. The frustum is separated from the SRB and descends on a drogue chute while the SRB descends on the main parachutes. Water impact and cavity collapse loads are critical for unmanned loading of the aft skirt. After splashdown in the ocean, the frustum and SRB are recovered and refurbished for reuse.

STRUCTURAL DESCRIPTION

The SRB aft skirt is a stiffened conical shell fabricated from 2219-T852 aluminum plate and forging alloy. Figure G.1 shows a cut-away view of the aft skirt. The diameters of the base and forward end of the aft skirt are approximately 207 and 146 inches, respectively. The conical shell angle is 18.67° from the vertical. The height of the aft skirt is 86.5 inches. An aluminum ring forging is welded circumferentially to a 1.375-inch thick skin at the forward end of the conical shell. The four hold-down post forgings are welded longitudinally along the cone axis to a 1.375-inch thick aluminum skin.

STRESS HISTORY/LOAD SPECTRUM DEVELOPMENT

The load spectrum used in this report was developed using a 180 degree symmetric NASTRAN model of the SRB aft skirt. Loads were developed for conditions prior to and including launch. These loads were then used in a static analysis to determine the state of stress in aft skirt welds. All stresses are calculated at limit load, i.e., 100% load level for fracture analysis.

The load spectrum is given in Table G.1. Loads considered significant for crack growth include wind loads experienced on the launch pad, SSME thrust buildup for a flight readiness firing (FRF), rebound from FRF and SSME thrust buildup for launch. This particular spectrum reflects the sequence of events for STS-26 return to flight.

A more detailed load spectrum was developed specifically for flaws on "tension posts". Tension posts are holddown posts which carry the large tensile loads during SSME thrust buildup. Because the aft skirt is cone shaped, this tensile load produces a compressive stress across the longitudinal weld. However, during an FRF or on-pad abort, these stresses are reversed and a lower level of tensile stresses is produced. An example of this spectrum is given in the following analyses.

INSPECTIONS

Prior to the Challenger accident, aft skirt welds were inspected only once by x-ray following fabrication. No other inspections were performed between flights. In an effort to improve flight safety, reburbishment inspections were implemented prior to aft skirt reuse. Critical weld areas were identified and ultrasonic inspection now takes place after fabrication and after each flight. Because of these inspections, critical weld areas have a single flight use minimum requirement and are evaluated prior to each fight.

ANALYSIS

The holddown post forging-to-skin longitudinal weld is shown in Figure G.2. There are two weld seams per post, for a total of eight weld seams per aft skirt. The forward ring-to-skin circumferential weld is shown in Figure G.3 The aft skirt welds have been analyzed using detailed NASTRAN finite element models and strain gage data from a structural qualification test of the aft skirt. The aft skirt longitudinal weld failed under structural test conditions at approximately 128% of prelaunch loads. Because of this, strain gages were mounted on flight skirt welds to monitor strains during liftoff.

Fracture analysis of the weld seams falls into one of three categories. 1) Worst case finite element stresses are used to evaluate flaws in low stress areas. 2) Strain gage data is used in highly stressed areas and for large flaws which must be evaluated using actual test data. 3) The longitudinal weld experiences strains at or above yield at limit load in some local areas. When flaws are detected in these areas, flawed specimen tests must be performed to demonstrate adequate safe life. An example of each type of analysis follows.

1) WELD SEAM ANALYSIS - LOW STRESS REGIONS

The low stress area is analyzed by selecting worst case stresses from NASTRAN model data and calculating crack growth to failure. Linear elastic fracture mechanics (LEFM) is applicable. Detected flaws in this area can then be plotted on the crack growth curve and its remaining safe life determined. Because this region is not highly stressed, inspections are performed only once. Therefore, safe life for this region must be at least 160 mission uses. An example of this analysis is given in section 1 using the following procedure:

a) Refer to inspection data sheet for location and size of flaw. The sample inspection sheet shows flaws on a longitudinal weld only.

b) Crack growth is plotted using worst case stresses from the finite element model.

c) Safe life for each detected flaw is determined according to flaw size on the crack growth plot.

2) WELD SEAM ANALYSIS - STRAIN GAGE DATA

Flaws are assessed individually with strain gage data when they cannot be shown good using conservative model stresses or are located in a high stress gradient area. Finite elements may not correctly reflect the actual stress distribution where large stress gradients exist. These areas are considered critical and are therefore inspected before each use. Safe life requirements are assessed on a flight-by-flight basis. An example of this analysis is given in section 2 using the following procedure:

a) Refer to inspection data sheet for location and size of flaw. The sample inspection sheet shows flaws on a longitudinal weld only.

b) Follow procedure for locating proper strain gage corresponding to the desired flaw location. This is necessary because test data corresponds to a left hand skirt. Therefore flaws on right hand skirts must be correlated by symmetry to á left hand skirt location. The enclosed procedure also mentions the use of strain gage data for flaws in the circumferential weld.

c) Calculate safe life using appropriate strain gage values.

LONGITUDINAL WELD - TEST RESULTS

3) In a few limited areas, stresses exceed yield for the weld heat affected zone. Flaws in these areas can only be assessed by performing precracked specimen tests. Results from these tests are given in Tables G.2 and G.3. Test specimens were prepared from plate-to-plate 2219 aluminum alloy welds (t=1.375) using the same weld schedule as is used in the fabrication of the aft skirt. Two inch wide dogbone type specimens shown in figure G.4 were cut from the welded plates. Surface flaws were introduced and the specimens were then cycled at low stress to initiate fatigue crack growth. A cyclic axial stress spectrum from 0 to limit stress was then applied for 160 cycles. This represents 40 flights with a service life factor of 4 with one application of load per flight. This does not include FRF. If failure did not occur proir to 160 cycles, the specimens were then pulled to failure to determine residual strength. Two specimens were tested in bending. One survived the cyclic stress and the other was accidentally overloaded. No residual strength is reported for the bending specimens.

The first series of tests were intended to demonstrate adequate safe life for the maximum undetectable flaw size. An initial surface crack goal was 0.080 inches deep, 0.160 inches long. Specimens were cycled to a stress of 38 ksi, estimated as the worst case weld stress at 100% prelaunch loads. Results are given in Table G.2 and are considered successful since all specimens survived a goal of 160 cycles.

Another series of tests were performed to demonstrate adequate safe life for a detected flaw on aft skirt S/N 20032. The precrack size goal was 0.130 inches deep, 0.260 inches long. Specimens were cycled to a stress of 38 ksi as in the previous test series. This is conservative since the actual stress at this location is estimated at 28.9 ksi. Test results are given in Table G.3. Results are listed in order of increasing initial crack size. The largest precrack survived only 5 cycles, but is significantly larger than the desired precrack size.

At the time this paper went to print, another series of tests were planned to assess a flaw on aft skirt S/N 20023. The detected flaw is located on a tension post and experiences a compressive stress above yield during prelaunch. If an on-pad abort or FRF occurs, cyclic tensile stresses follow the compression cycle. These tests will observe the effect of a compression overload on fatigue crack growth. ASTM test procedure E647 will be followed to measure da/dN versus delta-K with a periodic compression overload cycle. Compact tension test specimens will be cut from forging to plate weldments. Previous fracture test specimens were machined from plate-to-plate welds.

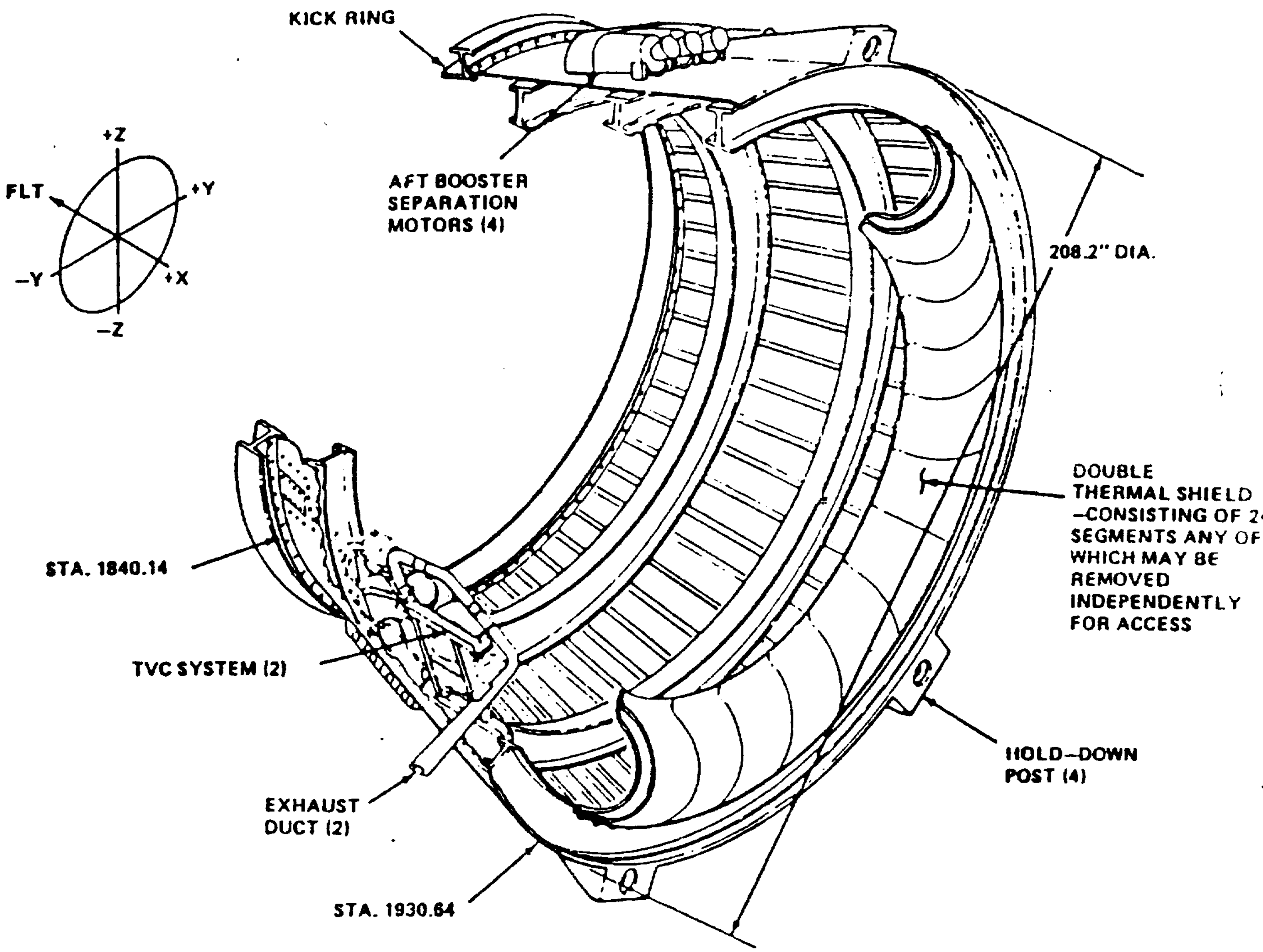

Figure G.1 SRB Aft Skirt Assembly

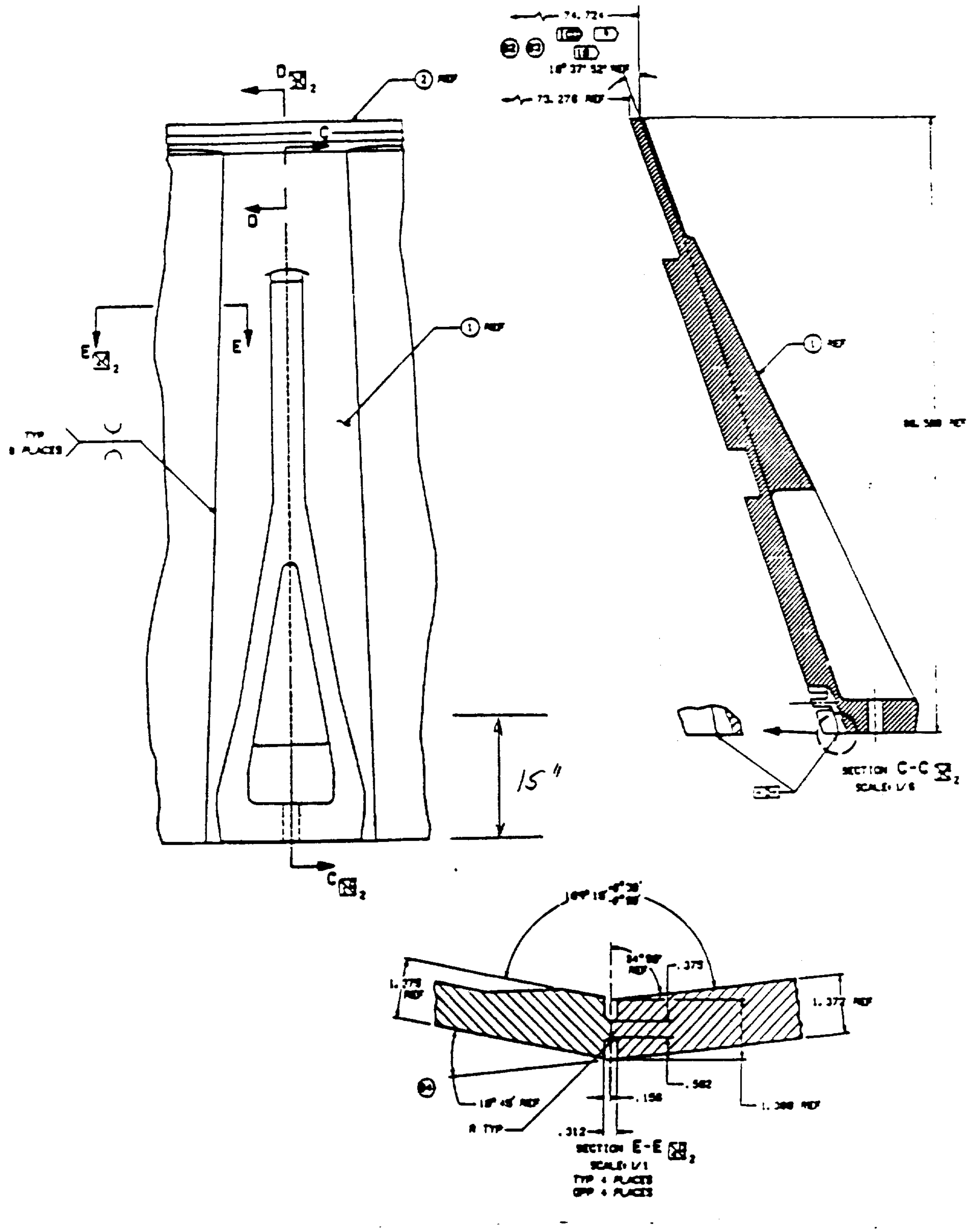

Figure G.2 SRB Holddown Post Longitudinal Weld

ORIGINAL PAGE IS
OF POOR QUALITY

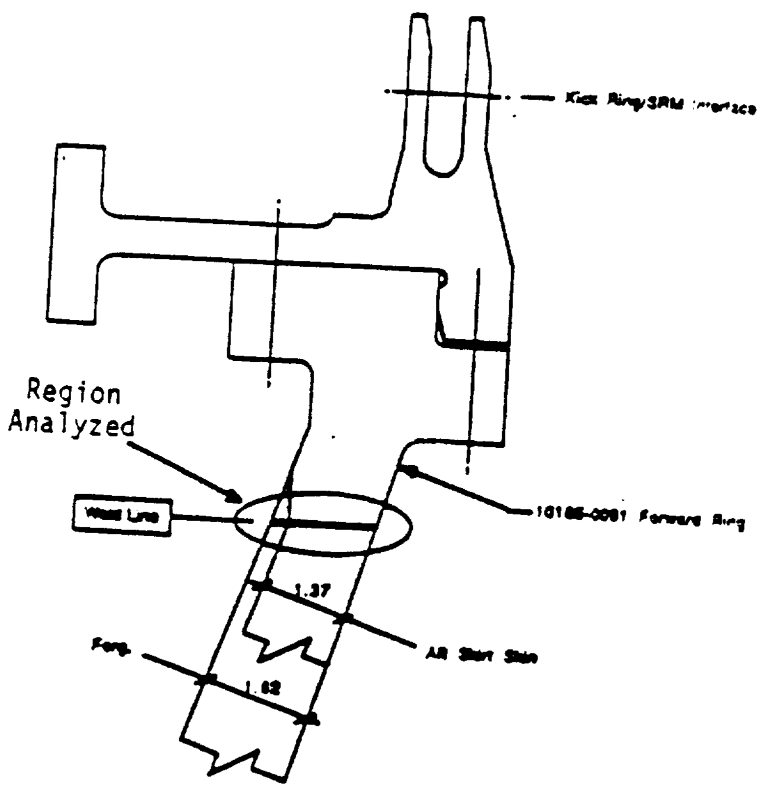

Figure G.3 SRB Forward Ring Weld

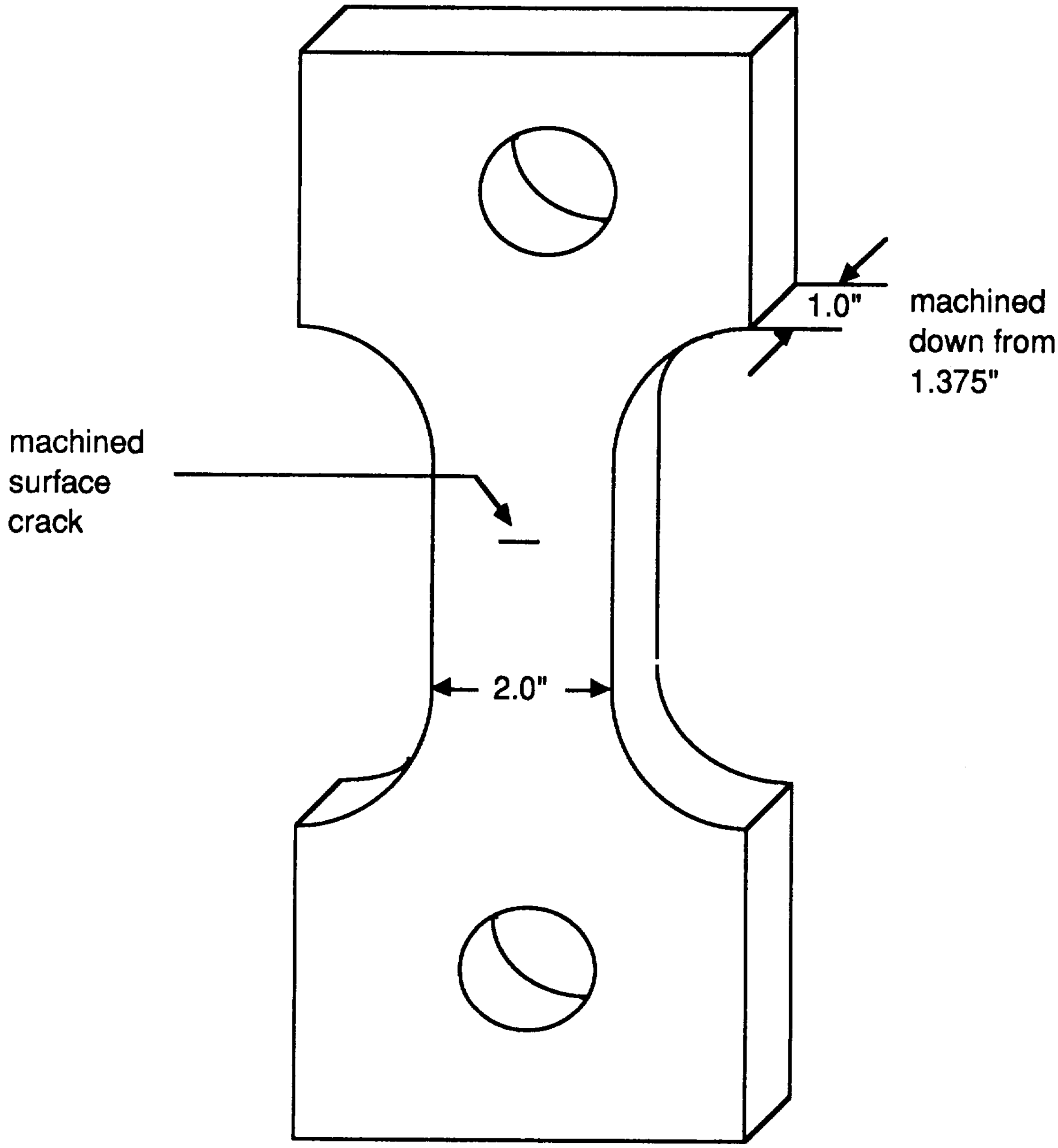

Figure G.4 Surface Crack Tensile Specimen

Table G-1 SRB Load Spectrum

SPECTRUM		REDUCED SPECTRUM			
				LOAD CASE	
EVENT	CYCLES	EVENT	CYCLES	MAX	MIN
E.T EMPTY, 60.4 KT WIND	105	E.T. EMPTY, 60.4 KT WIND	1155	FM11	FM12
E.T EMPTY, 50.2 KT WIND	315				
E.T EMPTY, 35.5 KT WIND	735				
E.T FULL, 47KT WIND	105	E.T. FULL, 47KT WIND	903	FM17	FM18
E.T FULL, 40.7KT WIND	210				
E.T FULL, 33.2KT WIND	252				
E.T FULL, 23.5KT WIND	336				
FRF, SSME BUILDUP	4	FRF, SSME BUILDUP	4	FM25	FM26
FRF, BUILDUP/REBOUND	1	FRF, BUILDUP/REBOUND	1	FM35	FM36
FRF REBOUND 1	10	FRF REBOUND 1	40	FM27	FM28
FRF REBOUND 2	10				
FRF REBOUND 3	10				
FRF REBOUND 4	10				
SSME BUILDUP, LIFTOFF	1	SSME BUILDUP, LIFTOFF	1	FM37	FM38

Table G-2 SRB Test Results

Specimen Number	Flaw* Location	Flaw Size (in)** Precrack Depth	Length	Flaw Size (in) After 160 Cycles Depth	Length	(in) Δ Depth	(in) Δ Length	Residual Strength (KSI)
23-2	OD	.0900	.1618	.1063	.2012	.0163	.0394	49.20
25-1	OD	.0915	.1611	.1165	.2001	.025	.039	49.98
25-2	ID	.0890	.1738	.1641	.2327	.0751	.0589	41.60
29-1	OD	.1025	.1595	.1158	.1831	.0133	.0236	48.60
30-1 (Bend)	OD	.0693	.1502	.081	.1852	.0117	.035	-----
30-2	OD	.0900	.1629	.1045	.1836	.0145	.0207	48.00
31-1	OD	.0884	.1587	.1058	.1922	.0174	.0335	46.00
31-2	OD	.1123	.1927	.1332	.2566	.0209	.1039	45.00

* Tests Run for 160 Cycles at 38 KSI

** Precrack Aim was .16" X .08" - Maximum Undetectable Flaw Size

Table G-3 SRB Test Results

SPECIMEN #	STRESS (KSI)	** PRECRACK (in)	# of cycles	UTS after 160 cycles (KSI)
D	38.2	0.273 X 0.145	160	45.89
B	38.2	0.274 X 0.1573	160	40.946
C	38.2	0.2934 X 0.1586	160	43.445
F	38.2	0.3019 X 0.1624	160	41.983
E	38.2	0.3049 X 0.1639	5	N/A

* ALL FLAWS ON O.D. SIDE (LOW YIELD STRENGTH)

** PRECRACK Aim was .260" X .130"

SECTION 1

Longitudinal Weld

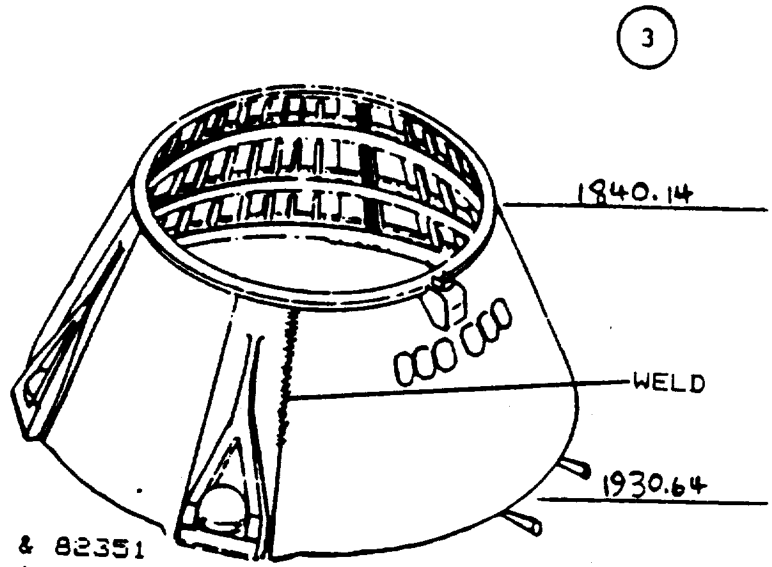

POST:	6
SEAM:	3
GRIDPOINT:	82357 & 82351 82327 & 82321
ELEVATION:	86.500 " 79.247 "
CRACK MODEL:	TC01
P-THICKNESS:	1.372 "
PLATE WIDTH:	5.000 "
EMBED DEPTH:	SURFACE
STRESS:	NORM-X (HOOP) NORM-Y (LONG)
SPECTRUM:	AXIAL & BENDING
COMPONENT:	HDP FORGING - SKIN INTERFACE
PART NR:	N/A
SERIAL NR:	N/A
REF DWG:	10165-0087/0088/0089/0090
MATERIAL:	AL ALLOY 2219-T87 WELDMENT
NDE TYPE:	ULTRASONIC (A) assumed
computed:	NASA/FLAGRO, 1986 Aug version, 1987 Jul rev.)

SKIN TO FORGING INTERFACE

FIG 7.3.2 TYPICAL INTERFACE CONNECTION

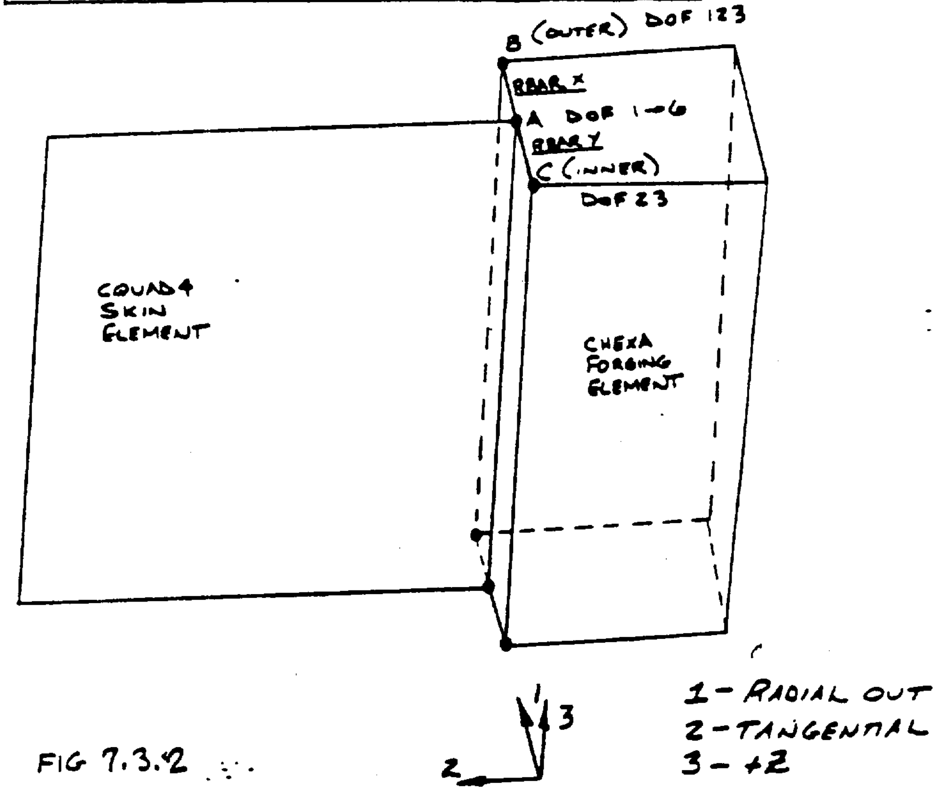

FIG 7.3.2

ALL 6 INDEPENDENT DOF. AT GRID A OF THE CQUAD4 SKIN ELEMENT ARE TRANSFERRED TO THE 3 TRANSLATIONAL D.O.F. OF THE OUTER GRID B, AND TRANSLATIONAL D.O.F. 2 AND 3 OF THE INNER GRID C, OF THE CHEXA FORGING ELEMENT. SEE THE ABOVE FIGURE.

EXAMPLE NASTRAN BULK DATA:

RBAR	X	A	B	123456	X	X	123
RBAR	Y	A	C	123456	X	X	23

Spectrum:

axbend82

BENDING/AXIAL COMPONENTS
100% NORMAL-X STRESS
COMPONENT: UPPER LONGITUDINAL WELD

FM	STRESS INNER	STRESS OUTER	fa axial	fb bending	SUM fa+fb check
11	-3.00	-10.02	-6.51	-3.51	-10.02
12	-0.84	-5.38	-3.11	-2.27	-5.38
17	-1.98	-10.10	-6.04	-4.06	-10.10
18	-0.49	-6.95	-3.72	-3.23	-6.95
25	7.47	7.32	7.40	-0.07	7.32
26	1.06	-3.41	-1.18	-2.24	-3.41
35	-4.45	-13.61	-9.03	-4.58	-13.61
36	7.40	7.53	7.47	0.06	7.53
27	3.76	-0.04	1.86	-1.90	-0.04
28	-4.75	-13.86	-9.31	-4.56	-13.86
37	7.47	7.32	7.40	-0.07	7.32
38	-0.61	-6.29	-3.45	-2.84	-6.29

$$fa = \frac{So + Si}{2} \qquad fb = \frac{So - Si}{2}$$

Crack Case:

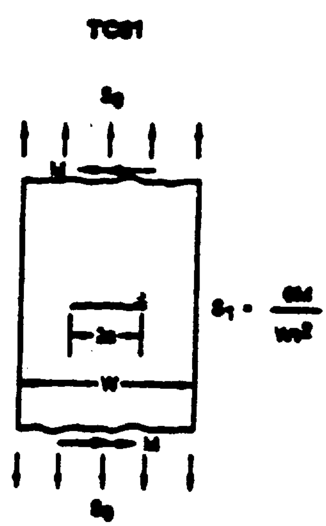

$t = 1.372$
$W = 5.00$
$a_i = 0.75$

```
                    FATIGUE CRACK GROWTH ANALYSIS
                    -----------------------------
   (computed: NASA/FLAGRO, 1986 Aug version, 1987 Jul rev.)
      U.S. customary units [inches, ksi, ksi sqrt(in)]

PROBLEM TITLE
-------------
AFT SKIRT UPPER LONGITUDINAL WELD FRACTURE ANALYSIS

GEOMETRY
--------
MODEL: TC01-Through crack in center of plate.

Plate Thickness, t =    1.3720
  "   Width, W     =    5.0000

FLAW SIZE:

a   (init.) =  0.7500



MATERIAL
--------

MATL 1: 2219-T87 AL, WELDMENTS [BK=0]

Material Properties:

:Matl:  YS  : K1e : K1c : Ak  : Bk  :  Thk  :  Kc  : K1scc:
: No.:      :     :     :     :     :       :      :      :
:----:------:-----:-----:-----:-----:-------:------:------:
:  1 : 32.0: 30.0: 20.0: 0.75: 0.00: 1.372: 20.0:        :

:Matl:              Crack Growth Eqn Constants (closure)              :
: No.:    C    : n  : p  : q  : DKo : Co : d  : DK1 :Alpha:Smax/:
:    :         :    :    :    :     :    :    :     :     :SIGo :
:----:---------:----:----:----:-----:----:----:-----:-----:-----:
:  1 :0.348D-06:1,858:1.00:1.00: 2.50:1.00:1.00: 5.90: 1.75: 0.30:
```

AFT SKIRT UPPER LONGITUDINAL WELD FRACTURE ANALYSIS
MODEL: TC01

FATIGUE SPECTRUM STRESS TABLE

NORMAL-X GRIDPOINT STRESS GP:82357/82351 P:6 SE:20

STEP	MAT	NUMBER OF FATIGUE CYCLES	S0 (ksi) t1	S0 (ksi) t2	S1 (ksi) t1	S1 (ksi) t2
1	1	1155.0000	-3.11	-6.51	-2.27	-3.51
2	1	903.0000	-3.72	-6.04	-3.23	-4.06
3	1	4.0000	-1.18	7.40	-2.24	-0.07
4	1	1.0000	7.47	-9.03	0.06	-4.58
5	1	40.0000	-9.31	1.86	-4.56	-1.90
6	1	1.0000	-3.45	7.40	-2.84	-0.07

Environmental Crack Growth Check for Sustained Stresses
(Kmax less than KIscc): NOT SET

AFT SKIRT UPPER LONGITUDINAL WELD FRACTURE ANALYSIS
MODEL: TC01

FATIGUE SPECTRUM INPUT TABLE

NORMAL-X GRIDPOINT STRESS GP:82357/82351 P:6 SE:20

[Note: Stress = Input Value * Stress Factor]
Stress Factors SF0, SF1: 1.00 1.00

STEP	MAT	NUMBER OF FATIGUE CYCLES	S0 t1	S0 t2	S1 t1	S1 t2
1	1	1155.0000	-3.11	-6.51	-2.27	-3.51
2	1	903.0000	-3.72	-6.04	-3.23	-4.06
3	1	4.0000	-1.18	7.40	-2.24	-0.07
4	1	1.0000	7.47	-9.03	0.06	-4.58
5	1	40.0000	-9.31	1.86	-4.56	-1.90
6	1	1.0000	-3.45	7.40	-2.84	-0.07

Environmental Crack Growth Check for Sustained Stresses
(Kmax less than KIscc): NOT SET

AFT SKIRT UPPER LONGITUDINAL WELD FRACTURE ANALYSIS
MODEL: TC01

ANALYSIS RESULTS: $a_i = 0.75''$ (X)

BLOCK STEP	FINAL FLAW SIZE A	K MAX A-TIP
10	0.753545	12.231897
20	0.757139	12.268146
30	0.760783	12.304908
40	0.764479	12.342200
50	0.768227	12.380037
60	0.772030	12.418436
70	0.775890	12.457415
80	0.779806	12.496993
90	0.783783	12.537188
100	0.787820	12.578021
110	0.791921	12.619514
120	0.796087	12.661688
130	0.800321	12.704569
140	0.804624	12.748180
150	0.808998	12.792549
160	0.813448	12.837703
170	0.817974	12.883672
180	0.822580	12.930487
190	0.827268	12.978182
200	0.832043	13.026791
210	0.836906	13.076353
220	0.841862	13.126907
230	0.846913	13.178496
240	0.852065	13.231165
250	0.857321	13.284963
260	0.862686	13.339942
270	0.868164	13.396158
280	0.873761	13.453671
290	0.879481	13.512545
300	0.885332	13.572851
310	0.891319	13.634664
320	0.897449	13.698065
330	0.903729	13.763145
340	0.910168	13.829999
350	0.916774	13.898733
360	0.923557	13.969463
370	0.930528	14.042317
380	0.937697	14.117435
390	0.945077	14.194972
400	0.952683	14.275100
410	0.960530	14.358011
420	0.968635	14.443922
430	0.977018	14.533073
440	0.985699	14.625740
450	0.994705	14.722233
460	1.004062	14.822910
470	1.013804	14.928184
480	1.023967	15.038532

AFT SKIRT UPPER LONGITUDINAL WELD FRACTURE ANALYSIS
MODEL: TC01

ANALYSIS RESULTS: ai = 0.75" (X) cont

BLOCK STEP	FINAL FLAW SIZE A	K MAX A-TIP
490	1.034594	15.154516
500	1.045738	15.276802
510	1.057457	15.406185
520	1.069827	15.543631
530	1.082936	15.690331
540	1.096896	15.847774
550	1.111847	16.017866
560	1.127975	16.203110
570	1.145525	16.406888
580	1.164843	16.633961
590	1.186433	16.891382
600	1.211091	17.190366
610	1.240205	17.550708
620	1.276647	18.013894
630	1.328905	18.704331

FINAL RESULTS:
Unstable crack growth, max stress intensity exceeds critical value:
K max = 20.07 K cr = 20.00
AT CYCLE NO. 4. OF LOAD STEP NO. 3 OF BLOCK NO. 638
CRACK SIZE A = 1.44970

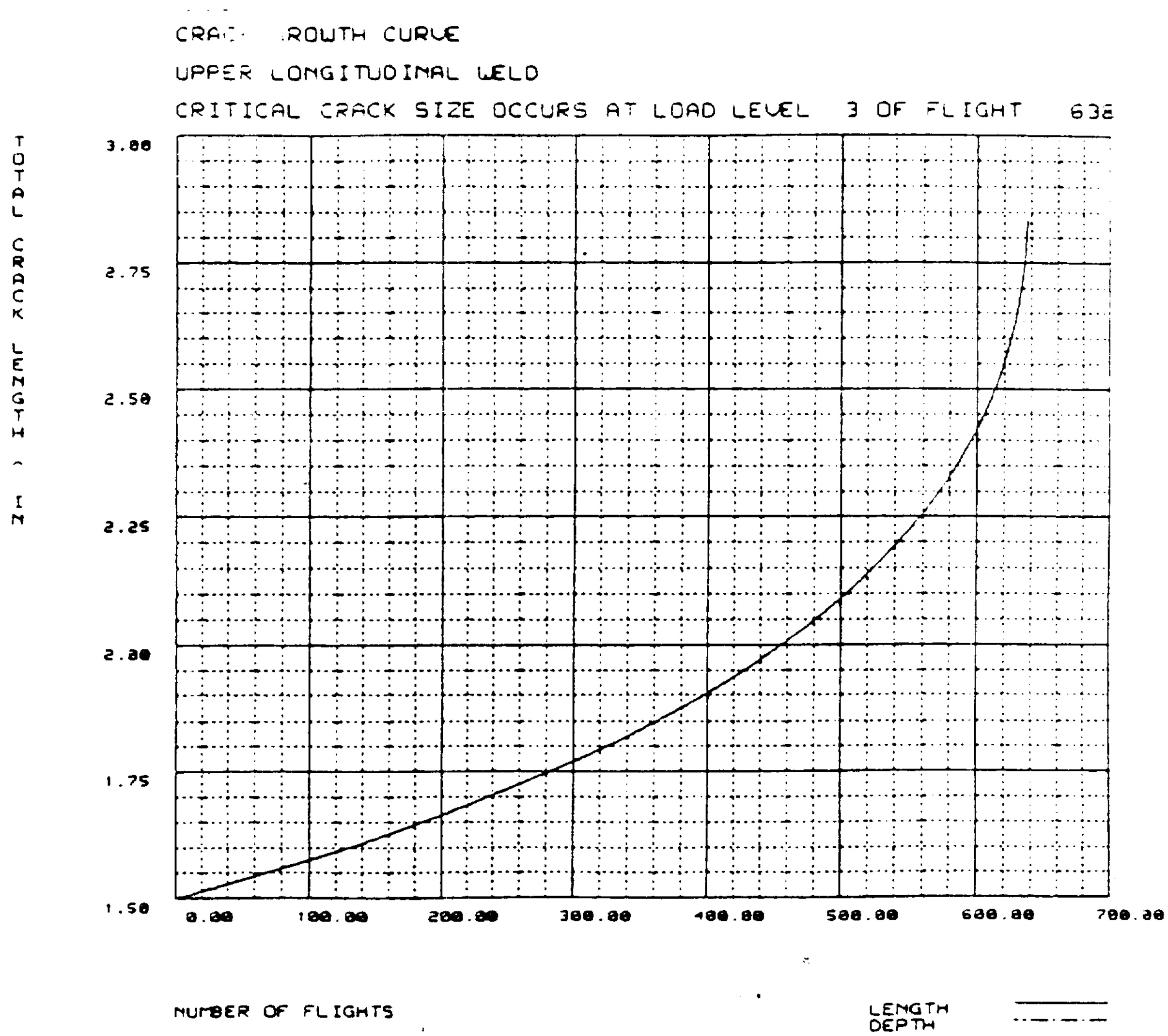

CONCLUSION: FOR A THROUGH CRACK WITH INITIAL LENGTH EQUAL TO 1.50 INCHES IT REQUIRES 630 FLIGHTS TO REACH THE CRITICAL SIZE.

CRACK MODEL : TC01 - Through Crack in finite width plate is assumed. For a given initial crack length (larger than minimum specified in MSFC- STD -1249) along the circumference of the weldment, the analysis is to determine the final critical crack length and the number of flights at which the flaw reaches the critical size.

Thickness = 1.451 in.
Width = 5.0 in.

a = 0.2 in. (this specifies initial crack length of 0.4 inches.)
(MSFC- STD -1249 specifies minimum detectable length of 0.15 inches using Penetrant Inspection Method)

TC01

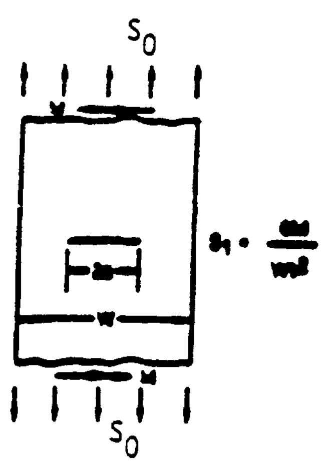

STRESS SPECTRUM : Area which has maximum tension stress (identified from Ref. [1], Aft Skirt Recertification Report) is considered to be the fracture critical location. Grid point stresses at 42801, 42803 (θ=-22.375°, real side) are used for this analysis.

Load Case	σ_{42801}	σ_{42803}	S_0	S_1
FM11	-18.54	-7.19	-12.87	-5.68
FM12	-9.98	-3.56	-6.77	-3.21
FM17	-18.71	-6.90	-12.81	-5.90
FM18	-12.80	-4.38	-8.59	-4.21
FM25	13.99	7.17	10.58	3.41
FM26	-6.52	-1.63	-4.06	-2.45
FM27	0.32	0.83	0.58	-0.26
FM28	-25.81	-9.91	-17.86	-7.95
FM35	-25.31	-9.83	-17.57	-7.74
FM36	14.36	7.29	10.83	3.54
FM37	13.99	7.17	10.58	3.41
FM38	-11.56	-3.95	-7.76	-3.81

unit in ksi.

where

$$S_0 = \frac{\sigma_{42801} + \sigma_{42803}}{2}$$

$$S_1 = \frac{\sigma_{42801} - \sigma_{42803}}{2}$$

RESULT:

The result shows that for given initial flaw of 0.4 inches, the Aft Skirt Forward Ring/Skin Interface Weldment is capable of sustaining 727 cycles before reaching the critical flaw length of 1.45 inches. Figure 12.5.2 plots the fracture growth versus number of flights. The NASA/FLAGRO output is attached below.

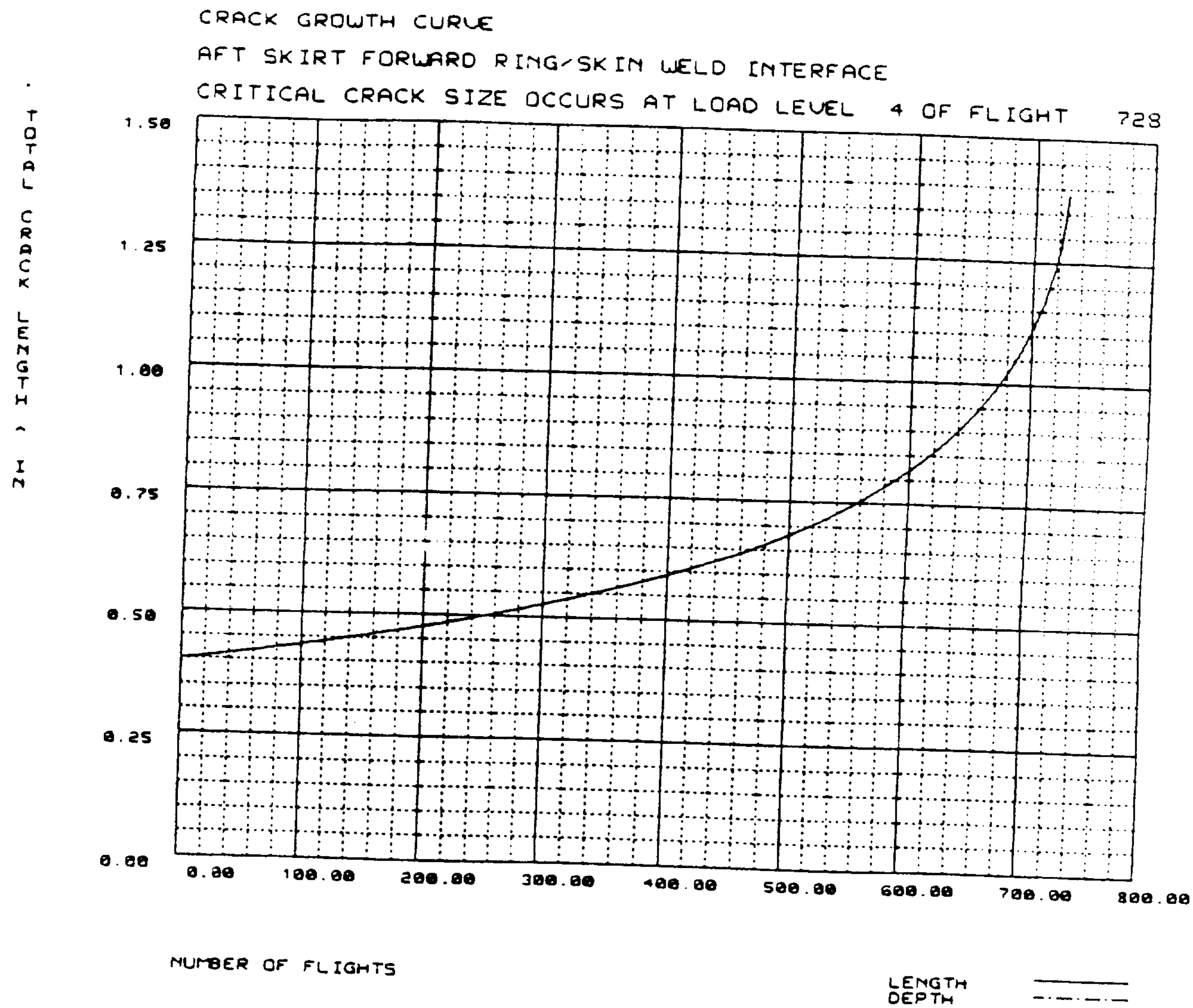

Figure 12.5.2 Crack Growth Curve for Skin to Forward Ring Weld

FATIGUE CRACK GROWTH ANALYSIS

(computed: NASA/FLAGRO, 1986 Aug version, 1987 Jul rev.)
U.S. customary units [inches, ksi, ksi sqrt(in)]

PROBLEM TITLE

AFT SKIRT FORWARG RING/SKIN INTERFACE WELD

GEOMETRY

MODEL: TC01-Through crack in center of plate.

Plate Thickness, t = 1.4510
" Width, W = 5.0000

FLAW SIZE:

a (init.) = 0.2000

MATERIAL

MATL 1: 2219-T87 AL, WELDMENTS

Material Properties:

Matl No.	YS	K1e	K1c	Ak	Bk	Thk	Kc	KIscc
1	32.0	30.0	20.0	0.75	0.00	1.451	20.0	

Matl No.	C	n	p	q	DKo	Co	d	DK1	Alpha	Smax/SIGo
	Crack Growth Eqn Constants (closure)									
1	0.3480-06	1.858	1.00	1.00	2.50	1.00	1.00	5.90	1.75	0.30

AFT SKIRT FORWARG RING/SKIN INTERFACE WELD
MODEL: TC01

FATIGUE SPECTRUM STRESS TABLE

STEP	MATL	NUMBER OF FATIGUE CYCLES	S0 (ksi) t1	S0 (ksi) t2	S1 (ksi) t1	S1 (ksi) t2
1	1	1155.0000	-12.87	-6.77	-5.68	-3.21
2	1	903.0000	-12.81	-8.59	-5.90	-4.21
3	1	4.0000	-4.06	10.58	-2.45	3.41
4	1	1.0000	-17.57	10.83	-7.74	3.54
5	1	40.0000	-17.86	0.58	-7.95	-0.26
6	1	1.0000	-7.76	10.58	-3.81	3.41

Environmental Crack Growth Check for Sustained Stresses
(Kmax less than KIscc): NOT SET

ORIGINAL PAGE IS
OF POOR QUALITY

AFT SKIRT FORWARG RING/SKIN INTERFACE WELD
MODEL: TC01

ANALYSIS RESULTS:

BLOCK STEP	FINAL FLAW SIZE A	K MAX A-TIP
20	0.203195	10.108162
40	0.206499	10.191403
60	0.209921	10.276943
80	0.213467	10.364907
100	0.217143	10.455426
120	0.220959	10.548645
140	0.224923	10.644721
160	0.229046	10.743825
180	0.233337	10.846145
200	0.237810	10.951888
220	0.242476	11.061281
240	0.247351	11.174576
260	0.252452	11.292053
280	0.257795	11.414025
300	0.263402	11.540840
320	0.269296	11.672894
340	0.275503	11.810632
360	0.282054	11.954563
380	0.288982	12.105268
400	0.296328	12.263422
420	0.304139	12.429808
440	0.312469	12.605347
460	0.321384	12.791133
480	0.330964	12.988478
500	0.341303	13.198983
520	0.352522	13.424624
540	0.364770	13.667894
560	0.378242	13.932001
580	0.393194	14.221191
600	0.409977	14.541269
620	0.429093	14.900522
640	0.451297	15.311469
660	0.477828	15.794591
680	0.510961	16.387677
700	0.555855	17.176683
720	0.631866	18.486420

FINAL RESULTS:
Unstable crack growth, max stress intensity exceeds critical value:
K max = 20.02 K cr = 20.00
AT CYCLE NO. 2. OF LOAD STEP NO. 4 OF BLOCK NO. 728
CRACK SIZE A = 0.722099

SECTION 2

DATA MATRIX FOR STRUCTURAL WELD NONDESTRUCTIVE EVALUATION

AFT SKIRT S/N's 20016 & 20024

- THIS STRUCTURAL DATA MATRIX PACKAGE CONTAINS FINDINGS OF NONDESTRUCTIVE EVALUATION (ULTRASONIC & X-RAY INSPECTIONS) OF SRB AFT SKIRT WELDS PERFORMED BY USBI & MDAC.
- INDICATIONS FROM REVIEW OF MDAC X-RAY FILMS ARE IDENTIFIED ALPHABETICALLY AND BY SOLID SQUARES.
- INDICATIONS FROM USBI ULTRASONIC & X-RAY INSPECTION ARE IDENTIFIED NUMERICALLY AND BY CIRCLES.
- INDICATION LOCATION & MDAC WELD SEAM CORRELATION ARE ESTABLISHED BASED ON MDAC SHOP PROCEDURE REQUIREMENTS AND ADDITIONAL TIE-IN X-RAY OPERATIONS PERFORMED BY USBI. TOLERANCES ON LOCATION INFORMATION ARE AS FOLLOWS:
  - INDICATIONS IN CIRCUMFERENTIAL RING WELDS.
    - ± .5" FOR INDICATIONS LYING WITHIN 6" OF VERTICAL SEAMS.
    - ± 6" FOR ALL OTHER INDICATIONS.
  - INDICATIONS IN VERTICAL HOLD-DOWN POST WELDS
    - ± .5" FOR INDICATIONS LYING WITHIN THE BOTTOM 30" OF VERTICAL SEAMS.
    - ± 2" FOR ALL OTHER INDICATIONS.
  - INDICATION DEPTH AND THROUGH-WALL DIMENSIONS ARE DETERMINED FOR ULTRASONIC INDICATIONS ONLY.

BIO(TBD) – AFT SKIRT S/N20016 – (TBD)HAND

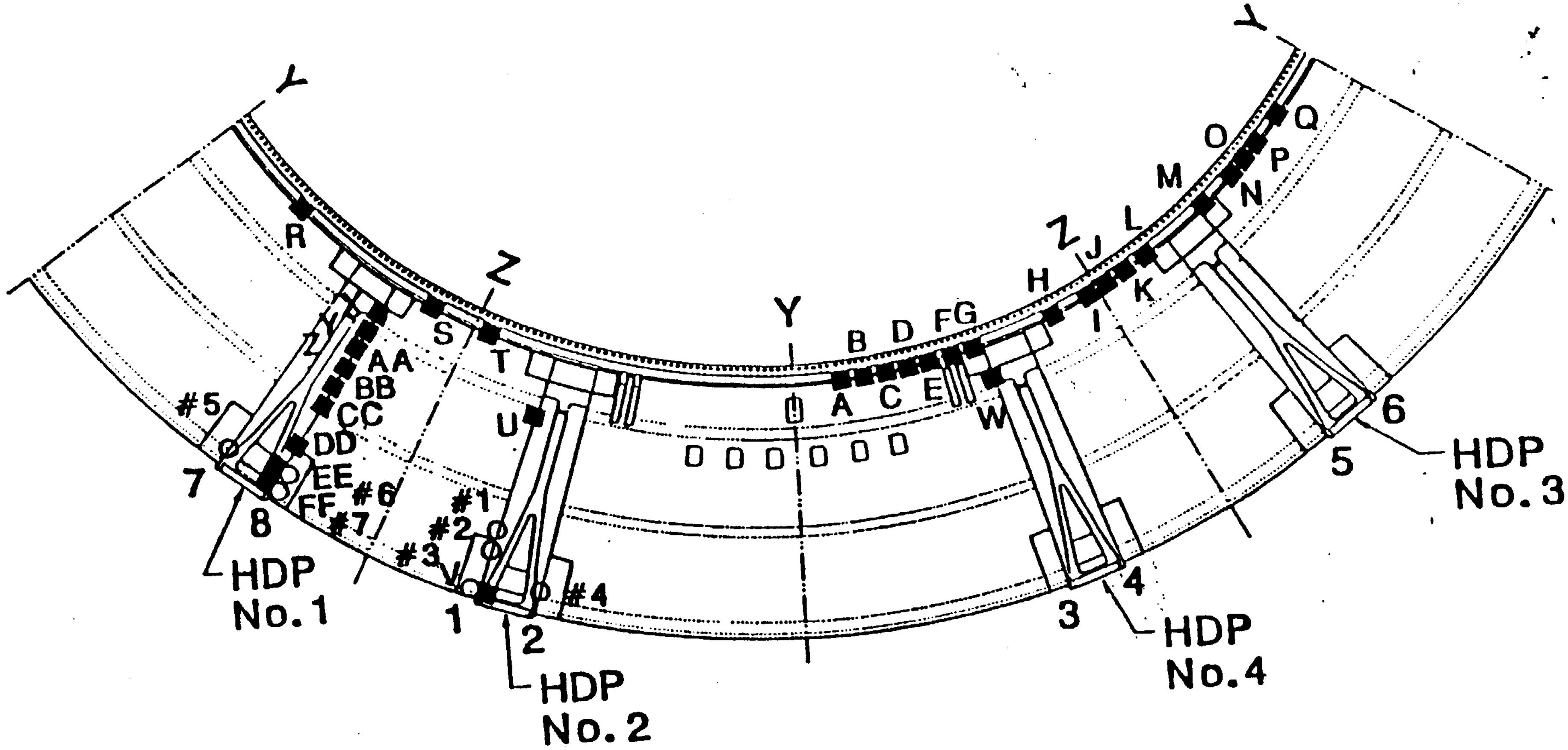

○ :USBI NDT (UT & X-RAY)

■ :MDAC FILM REVIEW

BIO(TBD) – AFT SKIRT S/N20016 – (TBD)HAND

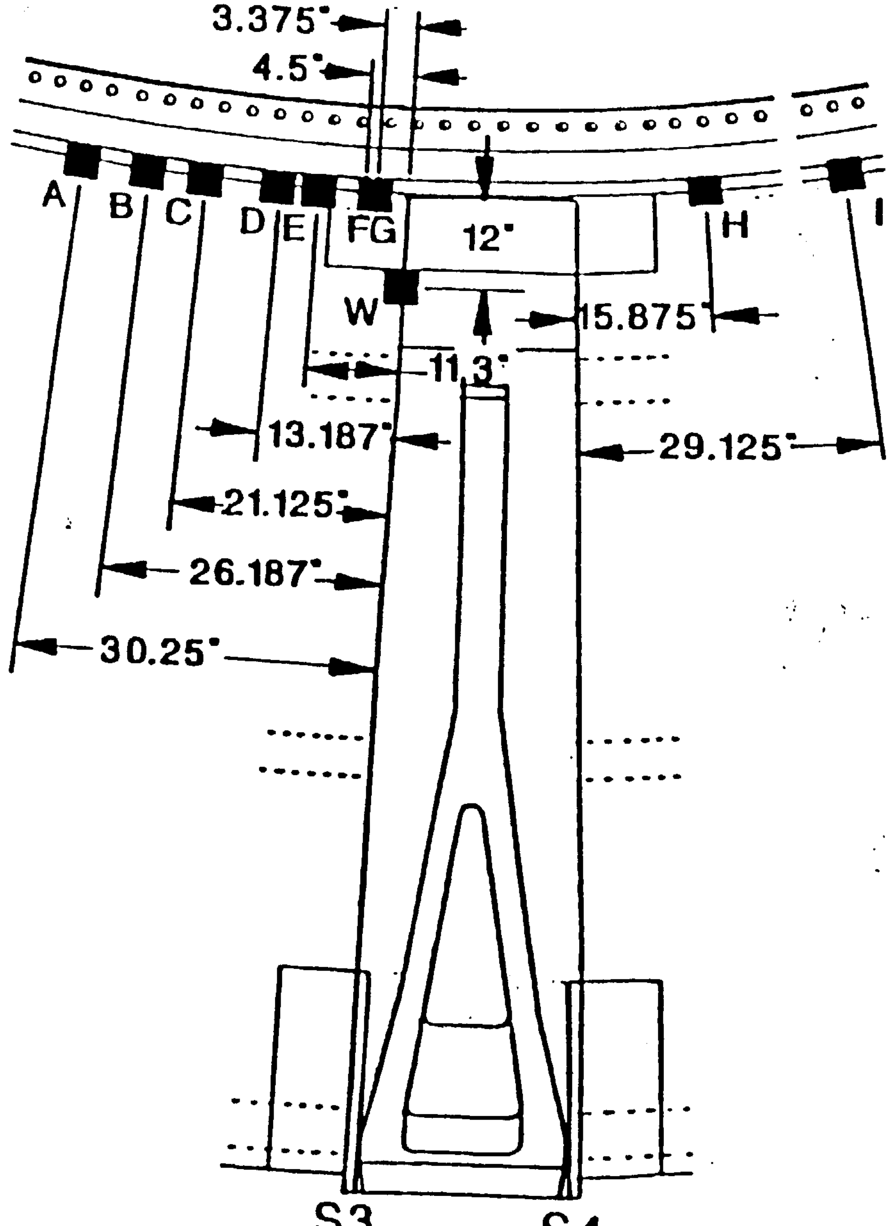

BIO(TBD) - AFT SKIRT S/N20016 - (TBD)HAND

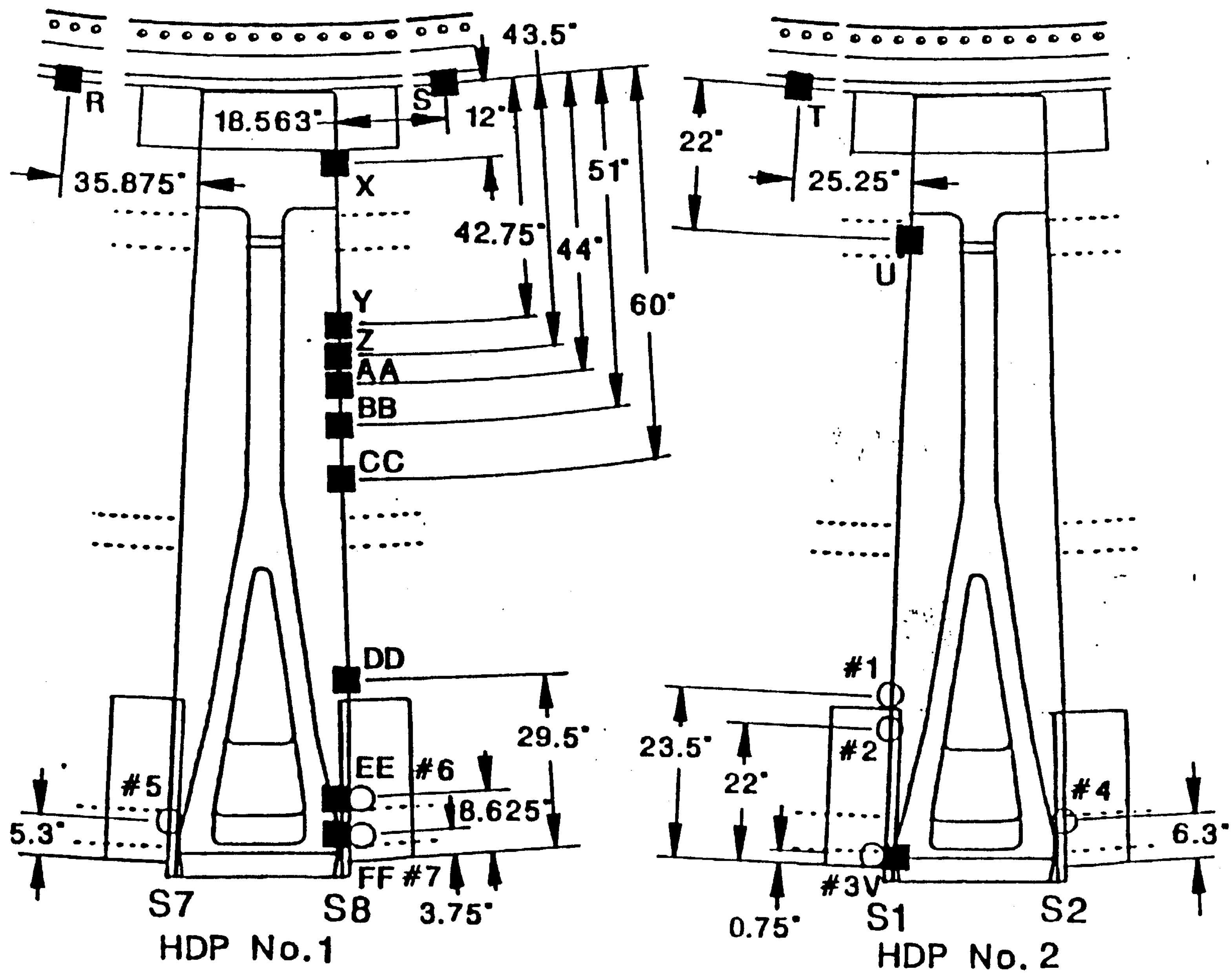

BIO(TBD) - AFT SKIRT S/N20016 - (TBD)HAND

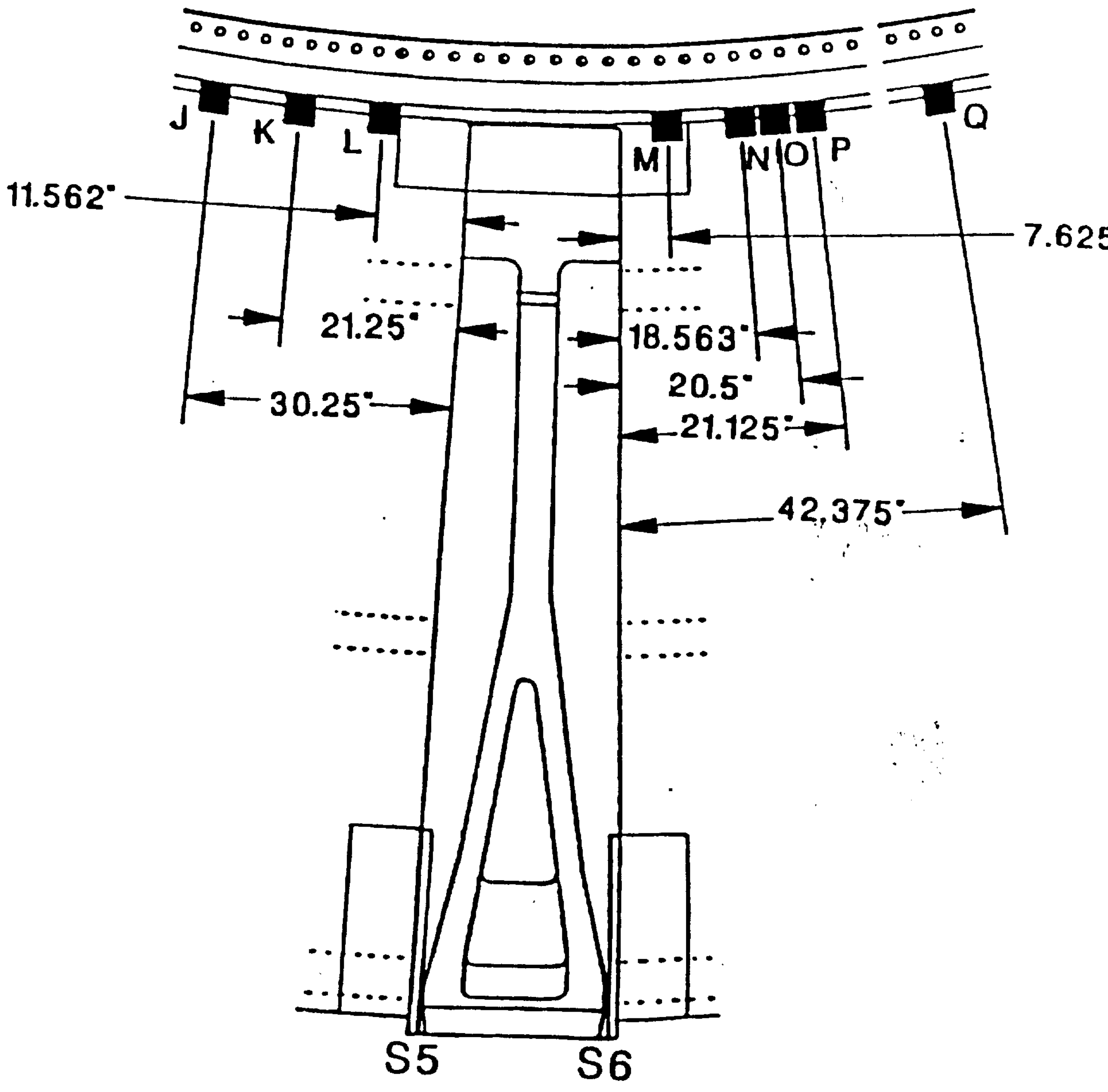

HDP No. 3

BIO(TBD) - AFT SKIRT S/N20016 - (TBD)HAND

WELD SEAM	ANOMALLY	USBI ULTRASONIC	USBI X-RAY	MDAC X-RAY	LOCATION		SIZE		REMARKS
					SURFACE DIM.	DEPTH FROM SURFACE	LENGTH	THRU WALL DIM.	
RING	A			■	30.25" LEFT OF SEAM 3	NA	0.225"	NA	LINEAR INDICATION
RING	B			■	26.187" LEFT OF SEAM 3	NA	0.200"	NA	LINEAR INDICATION
RING	C			■	21.125" LEFT OF SEAM 3	NA	0.820"	NA	LINEAR INDICATION
RING	D			■	13.187" LEFT OF SEAM 3	NA	1.700"	NA	LINEAR INDICATION
RING	E			■	11.5" LEFT OF SEAM 3	NA	0.285"	NA	LINEAR INDICATION
RING	F			■	4.5" LEFT OF SEAM 3	NA	4.562"	NA	LINEAR INDICATION
RING	G			■	3.375" LEFT OF SEAM 3	NA	0.260"	NA	LINEAR INDICATION
RING	H			■	15.875" RIGHT OF SEAM 4	NA	0.375"	NA	LINEAR INDICATION
RING	I			■	29.125" RIGHT OF SEAM 4	NA	2.625"	NA	LINEAR INDICATION
RING	J			■	30.25" LEFT OF SEAM 5	NA	0.115"	NA	PORE WITH TAIL

BIO(TBD) - AFT SKIRT S/N20016 - (TBD)HAND

WELD SEAM	ANOMALLY	USBI ULTRASONIC	USBI X-RAY	MDAC X-RAY	LOCATION		SIZE		REMARKS
					SURFACE DIM.	DEPTH FROM SURFACE	LENGTH	THRU WALL DIM.	
RING	L			■	11.56" LEFT OF SEAM 5	NA	0.400"	NA	CURVILINEAR INDICATION
RING	K			■	21.25" LEFT OF SEAM 5	NA	2.375"	NA	INTERMITTENT LINEAR INDICATION
RING	M			■	7.625" RIGHT OF SEAM 6	NA	0.300"	NA	CLUSTER OF 4 VOIDS
RING	N			■	18.563" RIGHT OF SEAM 6	NA	0.130"	NA	CLUSTER OF 3 CONNECTED VOIDS
RING	O			■	20.5" RIGHT OF SEAM 6	NA	0.350"	NA	VOID WITH TAIL
RING	P			■	21.125" RIGHT OF SEAM 6	NA	0.100"	NA	VOID WITH TAIL
RING	Q			■	42.375" RIGHT OF SEAM 6	NA	0.570"	NA	LINEAR INDICATION
RING	R			■	35.875" LEFT OF SEAM 7	NA	0.275"	NA	ALIGNED POROSITY
RING	S			■	18.563" RIGHT OF SEAM 8	NA	0.275"	NA	ALIGNED POROSITY
RING	T			■	25.25" LEFT OF SEAM 1	NA	0.350"	NA	ALIGNED POROSITY

BIO(TBD) - AFT SKIRT S/N20016 - (TBD)HAND

WELD SEAM	ANOMALLY	USBI ULTRASONIC	USBI X-RAY	MDAC X-RAY	LOCATION		SIZE		REMARKS
					SURFACE DIM.	DEPTH FROM SURFACE	LENGTH	THRU WALL DIM.	
8	AA			■	44" BELOW RING	NA	0.180"	NA	PORE WITH TAIL
8	BB			■	51" BELOW RING	NA	0.100"	NA	ELONGATED VOID
8	CC			■	60" BELOW RING	NA	0.155"	NA	SHARP VOID
8	DD			■	29.5" FROM BOTTOM	NA	0.125"	NA	ELONGATED VOID
8	#6 EE	○	○	■	8.625" FROM BOTTOM	0.5"	0.175"	0.12"	ELONGATED VOID
8	#7 FF		○	■	3.75" FROM BOTTOM	NA	0.230"	NA	FAINT OXIDE WITH TAIL

BIO(TBD) - AFT SKIRT S/N20016 - (TBD)HAND

DATE: 8-30-88
REV: A
PAGE: 8

WELD SEAM	ANOMALLY	USBI ULTRASONIC	USBI X-RAY	MDAC X-RAY	LOCATION		SIZE		REMARKS
					SURFACE DIM.	DEPTH FROM SURFACE	LENGTH	THRU WALLDIM.	
1	U			■	22" BELOW RING	NA	0.250"	NA	PORE WITH TAIL
1	#1	○	○		23.5" FROM BOTTOM	0.4"	0.090"	0.35"	POROSITY WITH TAIL
1	#2	○	○		22" FROM BOTTOM	0.4"	0.105"	0.5"	POROSITY WITH TAIL
1	#3 V	○	○	■	0.75" FROM BOTTOM	0.51"	0.175"	<0.1"	SINGLE PORE
2	#4	○	○		6.3" FROM BOTTOM	0.53"	0.160"	0.2"	POROSITY WITH TAIL
3	W			■	12" BELOW RING	NA	0.165"	NA	ELONGATED VOID
7	#5	○	○		5.3" FROM BOTTOM	0.43"	0.20"	0.35"	LINEAR INDICATION
8	X			■	12" BELOW RING	NA	0.100"	NA	LINEAR INDICATION
8	Y			■	42.75" BELOW RING	NA	0.135"	NA	PORE WITH TAIL
8	Z			■	43.5" BELOW RING	NA	0.310"	NA	PORE WITH TAIL

UNITED TECHNOLOGIES USBI

PROCEDURE FOR LOCATING APPROPRIATE STRAIN GAGE:

USE FIGURE TO SELECT PROPER POST-SEAM IN MODEL (LH SRB).

PAGES 4-7 CONTAINS LIST OF ALL GAGES ON ALL SEAMS, AND X-DISTANCE FROM BOTTOM OF SKIRT.

PAGES 8-9 CONTAINS LIST OF ALL GAGES ON FWD RING-TO-SKIN WELD, DIVIDED BY POST NR, AND θ-LOCATION ON MODEL. (θ BASED ON RADIUS AT THAT POINT OF 74.878", & THUS CIRCUMFERENCE OF 470.5")

$$\frac{d}{470.5} = \frac{\theta}{360°} \qquad \theta = \frac{360}{470.5} d \qquad d = \text{distance in inches}$$

ANOMALIES ARE LOCATED BY θ ON FWD RING WELD & BY X FROM BOTTOM ON VERTICAL WELD. SEE PAGES 10-13. APPROPRIATE GAGE IS DETERMINED BY MATCHING GAGE LOCATION (θ_{GAGE} OR X_{GAGE}) WITH LOCATION OF ANOMALY (θ_{ANOM} OR X_{ANOM}). CLOSEST GAGE, OR HIGHEST STRAINED OF TWO EQUAL-DISTANCE GAGES IS USED FOR PARTICULAR ANOMALY.

GAGE LOCATIONS FROM 10183-0085.

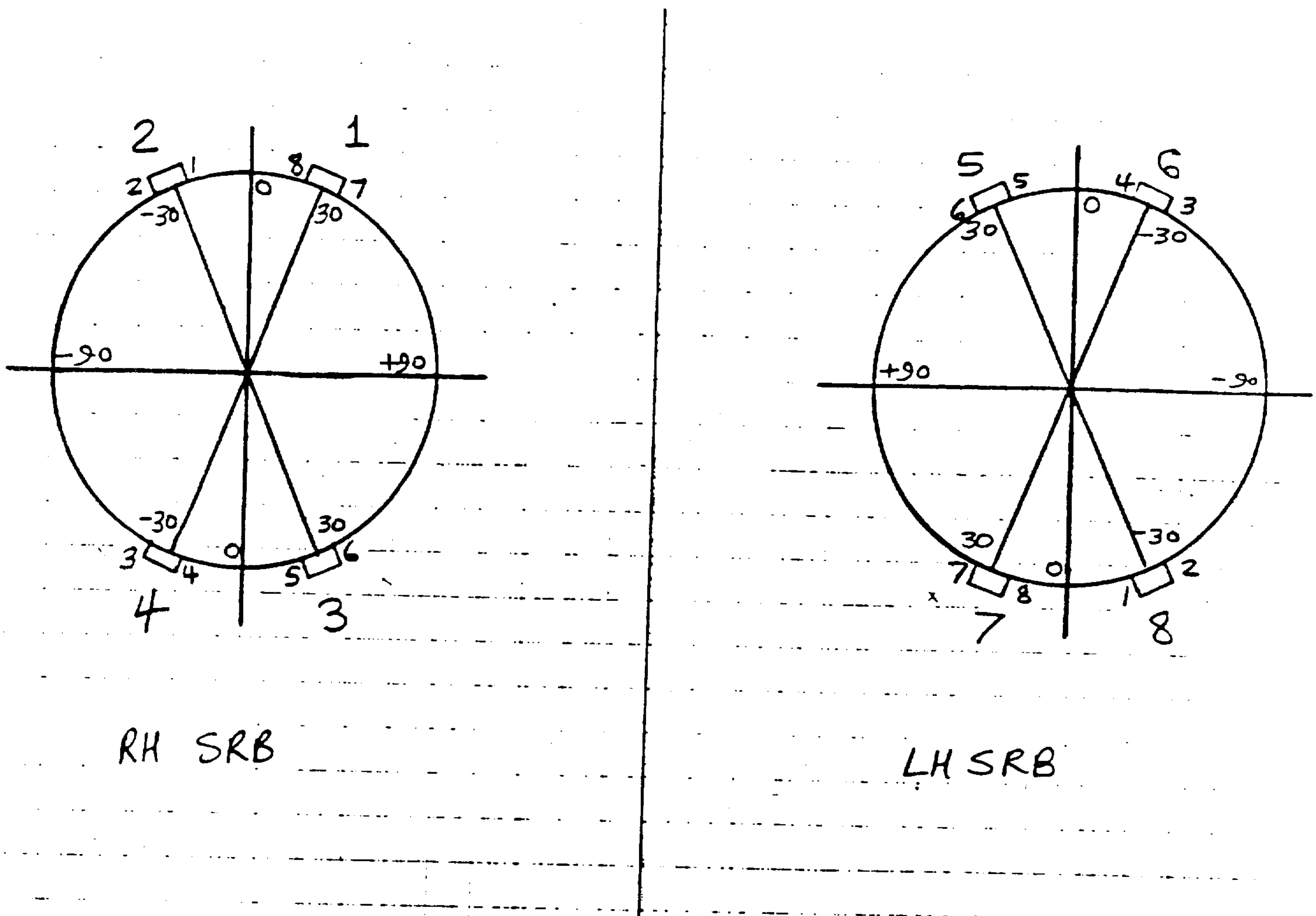

FIGURE 1 POST-SEAM CORRELATION

NOTES:

1. SEAMS ON RH SRB DO NOT MATCH SEAMS ON LH SRB ; SEE NEXT PAGE.
2. MATCH POSTS AS FOLLOWS FOR STRESS OUTPUT:

   1→5 3→7
   2→6 4→8

3. APPROPRIATE GAGE ON RING WELD DETERMINED BY θ LOCATION OF ANOMALY.
4. DISTANCE FROM BOTTOM DETERMINES APPROPRIATE GAGE FOR VERTICAL WELD.
5. WELD SEAMS ON FORGING OCCUR AT ±24° & ±36°; SIGN CONVENTION TO MATCH POST.

SEAM INFO FROM NDE SHEETS & PREVIOUS FLAGRO ANALYSES.

RH SRB SEAM-POST		→	LH SRB SEAM-POST	
1 2	2	→	4 3	6
3 4	4	→	2 1	8
5 6	3	→	8 7	7
7 8	1	→	6 5	5

REF LENGTH = 86.5'

VERTICAL WELD GAGES

8

REF SEAM 1 [POST 8-L] | SEAM 2 [POST 8-R]

GAGE-NS	GAGE-(FS)	X FROM BOTTOM	GAGE-NS	GAGE-(FS)
T6073	T6704	0.25	T6075	T6076
S5369	S5370	2.21	S5373	S5374
T6071	—	4.42	T6072	—
S5857	—	≈ 5.92	S5858	—
T6063	T6064	7.42	T6069	T6070
S5850	S5851	≈ 14.00	S5852	S5853
S5362	S5363	15.11	S5364	S5365
S5356	S5357	20.45	S5358	S5359
S5351	—	36.48	S5353	—
S5608	S5609	47.64	S5610	S5611
T6061	—	58.79	T6062	—
T6059	—	69.95	T6060	—
T6053	T6054	77.48	T6057	T6058
T6250	T6251	81.24	T6254	T6255
T6047	T6048	85.00	T6051	T6052

REF LENGTH = 86.5"

VERTICAL WELD GAGES:

6

REF SEAM 3 [POST 6-L] SEAM 4 [POST 6-R]

GAGE-NS	GAGE-(FS)	X FROM BOTTOM	GAGE-NS	GAGE-(FS)
T6030	T6031	0.25	T6032	T6033
$5304	$5305	2.21	$5308	$5309
T6026	—	4.42	T6029	—
$5292	$5293	7.42	$5300	$5301
$5288	$5289	15.11	$5290	$5291
T6022	T6023	20.45	T6024	T6025
$5279	—	36.48	$5281	—
$5274	$5275	53.22	$5277	$5278
$5271	—	69.95	$5273	—
T6018	T6019	85.00	T6020	T6021

REF LENGTH = 86.5"

VERTICAL WELD GAGES

5

REF SEAM 5 [POST 5-L] SEAM 6 [POST 5-R]

GAGE-NS	GAGE-(FS)	X FROM BOTTOM	GAGE-NS	GAGE-(FS)
T6043	T6044	0.25	T6045	T6046
S5341	S5342	2.21	S5345	S5346
T6040	—	4.42	T6042	—
S5329	S5330	7.42	S5337	S5338
S5325	S5326	15.11	S5327	S5328
S5315	S5316	21.95	S5323	S5324
S5606	—	32.06	S5607	—
S5602	S5603	51.01	S5604	S5605
S5310	—	69.95	S5312	—
T6036	T6037	85.00	T6038	T6039

REF LENGTH = 86.5"

VERTICAL WELD GAGES

7

REF SEAM 7 [POST 7-L] SEAM 8 [POST 7-R]

GAGE-NS	GAGE-(FS)	X FROM BOTTOM	GAGE-NS	GAGE-(FS)
T6101	T6102	0.25	T6103	T6104
S5414	S5415	2.21	S5418	S5419
T6099	—	4.42	T6100	—
S5403	S5404	7.42	S5407	S5408
S5397	S5398	15.11	S5401	S5402
S5393	S5394	20.45	S5395	S5396
S5389	—	36.48	S5390	—
S5384	S5385	47.64	S5387	S5388
S5379	S5380	58.79	S5382	S5383
T6092	—	69.95	T6094	—
T6085	T6086	77.48	T6089	T6090
T6079	T6080	85.00	T6083	T6084

R= 74.878 IN
C= 470.5 IN.

FWD RING WELD SEAM GAGES

REF POST 5 (+30°)

GAGE-NS	GAGE-FS	LOCATION	Θ
T6189	T6190	+Z AXIS	0°
T6193	T6194	18.30 FM +Z AXIS	+14°
T6198	T6199	2.25 FM SEAM 5	+22.3°
T6203	T6204	2.25 FM SEAM 6	+37.7°
T6306	T6307	29.73 FM +Y AXIS	+67.3°
T6205	T6206	+Y AXIS	+90°

REF POST 6 (-30°)

GAGE-NS	GAGE-FS	LOCATION	Θ
T6189	T6190	+Z AXIS	0°
T6186	T6187	18.30 FM +Z AXIS	-14°
T6184	T6185	2.25 FM SEAM 4	-22.3°
T6171	T6172	2.25 FM SEAM 3	-37.7°
T6302	T6303	39.54 FM -Y AXIS	-59.7°
S5487	S5488	-Y AXIS	-90°

FWD RING WELD SEAM GAGES

R = 74.878 IN
C = 470.5 IN

REF POST 7 (+30°)

GAGE - NS	GAGE - FS	LOCATION	θ
T6246	T6247	-Z AXIS	0°
T6239	T6240	18.30 FM -Z AXIS	+14°
T6236	T6237	24.19 FM -Z AXIS	+18.5°
T6231	T6232	2.25 FM SEAM 8	+22.3°
T6216	T6217	2.25 FM SEAM 7	+37.7°
T6207	T6208	57.50 FM +Y-AXIS	+46°
T6312	T6313	29.73 FM +Y AXIS	+67.3°
T6205	T6206	+Y AXIS	+90°

REF POST 8 (-30°)

GAGE - NS	GAGE - FS	LOCATION	θ
T6246	T6247	-Z AXIS	0°
T6121	T6122	9.48 FM -Z AXIS	-7.3°
T6125	T6126	15.36 FM -Z AXIS	-11.8°
T6127	T6128	24.19 FM -Z AXIS	-18.5°
T6136	T6137	2.25 FM SEAM 1	-22.3°
T6159	T6160	2.25 FM SEAM 2	-37.7°
T6163	T6164	53.66 FM -Y AXIS	-48.9°
T6295	T6296	29.73 FM -Y AXIS	-67.3°
S5487	S5488	-Y AXIS	-90°

CHECK OF PR PV 4025190 R4 SKIRT S/N 16

ANOM	WELD	Δd	DIR – SEAM	REF POST	Δθ	θ-REF (Deg)	θ ANOM (Deg)	σ POST
A	RING	30.25	L-3	4	23.15	-36	-59.15	8
B	"	26.187	L-3	4	20.04	-36	-56.04	8
C	"	21.125	L-3	4	16.16	-36	-52.16	8
D	"	13.187	L-3	4	10.09	-36	-46.09	8
E	"	11.5	L-3	4	8.80	-36	-44.80	8
F	"	4.5	L-3	4	3.44	-36	-39.44	8
G	"	3.375	L-3	4	2.58	-36	-38.58	8
H	"	15.875	R-4	4	12.15	-24	-11.85	8
I	"	29.125	R-4	4	22.29	-24	-1.71	8
J	"	30.25	L-5	3	23.15	24	0.85	7
L	"	11.562	L-5	3	8.85	24	15.15	7
K	"	21.25	L-5	3	16.26	24	7.74	7
M	"	7.625	R-6	3	5.83	36	41.83	7
N	"	13.563	R-6	3	14.20	36	50.20	7
Ø	"	20.5	R-6	3	15.69	36	51.69	7
P	"	21.125	R-6	3	16.16	36	52.16	7

ANOM	WELD	Δd	DIR-SEAM	REF POST	$\Delta\theta$	θ-REF(Deg)	θ-ANOM(Deg)	σ POST
Q	RING	42.375	R-6	3	32.42	36	68.42	7
R	"	35.875	L-7	1	27.45	36	63.45	5
S	"	18.563	R-8	1	14.20	24	9.80	5
T	"	25.25	L-1	2	19.32	-24	-4.68	6

ANOMALY	STRAIN GAGE	ANOMALY	STRAIN GAGE
A	T6295/96 or T6163/64	—	—
B	T6163/64		
C	"		
D	"		
E	"		
F	T6159/60		
G	"		
H	T6125/26		
I	T6246/47		
J	"		
K	T6246/47 OR T6239/40		
L	T6239/40		
M	T6216/17 OR T6207/08		
N	T6207/08		
Ø	"		
P	"		
Q	T6312/13		
R	T6306/07		
S	T6193/94		
T	T6189/90		

↑ closest gage:

Where given choice, choose highest strained.

ANOMALY	RH SRB SEAM	LH SRB SEAM	MODEL POST	LOCATION - FM*	GAGE TO USE
U	1	4	6	22" ↓ R (64.5↑)	S5273
#1	1	4	6	23.5" ↑ B	T6024/25
#2	1	4	6	22" ↑ B	"
#3, V	1	4	6	0.75" ↑ B	T6032/33
#4	2	3	6	6.3" ↑ B	S5292/93
W	3	2	8	12" ↓ R (74.5↑)	T6060 or T6057/52
#5	7	6	5	5.3" ↑ B	T6042 or S5337/38
X	8	5	5	12" ↓ R (74.5↑)	S5310
Y	8	5	5	42.75" ↓ R (42.75↑)	S5602/03 or S56[illegible]
Z	8	5	5	43.5" ↓ R (43↑)	"
AA	8	5	5	44" ↓ R (42.5↑)	"
BB	8	5	5	51" ↓ R (35.5↑)	S5606
CC	8	5	5	60" ↓ R (26.5↑)	S5606 or S5315/16
DD	8	5	5	29.5" ↑ B	S5606
#6, EE	8	5	5	8.625" ↑ B	S5329/30
#7, FF	8	5	5	3.75" ↑ B	T6040 or [illegible]

* R = RING B = BOTTOM

STRAIN-STRESS DATA

ANOMALY		GAGES	PRELAUNCH ϵ	PRELAUNCH σ	REBOUND ϵ	REBOUND σ
#3, V		1T6032 (T)	530	(T) -3.30	-189	(T) -0.04
	NS	2T6032	-552	(A) -26.87	335	(A) 5.89
		3T6032 (A)	-2455		562	
		1T6033 (T)	-101	(T) 0.78	201	(T) -0.49
	FS	2T6033	228	(A) 5.58	-51	(A) -7.89
		3T6033 (A)	507		-736	
#4	NS	S5292 (T)	-3111	-29.5†	2335	24.52
	FS	S5293	1238	13.00	-750	-7.88
#5		1T6042 (A)	-98	(A) -18.33	-393	(A) 6.77
	NS	2T6042	-1475	(T) -52.42	1325	(T) 33.01
		3T6042 (T)	-4416	ϵ = -4992 (use ←)	2931	ϵ = 3144 (use ←)
		or				
	NS	S5337 (T)	-3404	-32.0†	2088	29.5†
	FS	S5338	1019	10.70	-723	-7.59
#6, EE	NS	S5329 (T)	-1705	-17.90	213	2.24
	FS	S5330	462	4.85	86	0.90
#7, FF		1T6040 (A)	136	(A) -7.96	-392	(A) -3.37
	NS	2T6040	-1431	(T) -28.43	-930	(T) 2.26
		3T6040 (T)	-2458	ϵ = -2708	321	ϵ = 215 (use ←)
		or				
	NS	S5341	-2713	-28.49	-183	2.26
	FS	S5342	736	7.73	-590	-6.20

NS= NEAR SIDE GAGE   FS= FAR SIDE GAGE
(T) = TANGENTIAL OR HOOP   (A) = AXIAL OR VERTICAL
† - AT STRAINS ABOVE YIELD, σ-ε CURVE FOR FORGING IS USED.
USB 0644A (88/06) STRAIN DATA FROM GAGE OUTPUT

CALCULATION OF AXIAL & BENDING STRESSES: TANGENTIAL DIR.

	PRELAUNCH				REBOUND			
ANOMALY	σ_{NS}	σ_{FS}	S_0	S_1	σ_{NS}	σ_{FS}	S_0	S_1
#3, V	-3.30	0.78	-1.26	-2.04	-0.04	-0.49	-0.27	0.23
#4	-29.5	13.00	-8.25	-21.25	24.52	-7.88	8.32	16.20
#5	-32.0	10.70	-10.65	-21.35	29.5	-7.59	10.96	18.55 ←
#6, EE	-17.90	4.85	-6.52	-11.38	2.24	0.90	1.57	0.67
#7, FF	-28.49	7.73	-10.38	-18.11	2.26	-6.20	-1.97	4.23

$$S_0 = \frac{\sigma_{NS} + \sigma_{FS}}{2} \qquad S_1 = \frac{\sigma_{NS} - \sigma_{FS}}{2}$$

MAXIMUM CRACK GROWTH AT ANOMALY #5:

S_0		S_1	
t_1	t_2	t_1	t_2
-10.65	10.96	-21.35	18.55

t_1 = PRELAUNCH
t_2 = REBOUND

FLAGRO RUN USING THESE VALUES IN FATIGUE SPECTRUM...

Crack model - NASA/FLAGRO Analysis

Two cases were run

(1) ECØ1 - Embedded crack in finite plate

Initial flaw $2a \times 2c = 0.4'' \times 0.4''$

(max. flaw size of 0.35" is reported on PR PV4025190)

(2) SCØ1 - Surface Crack in finite plate

Initial flaw $a \times 2c = 0.2'' \times 0.4''$

Material Properties:

2219-T852 Forging properties were used

$Y.S = 30.5$ ksi

$B_K = 0$

$K_2 = K_c = 22.0$ ksi-in$^{1/2}$ (Conservative)

RESULTS:

∴ FROM CURVES, p.18-19, ~~SAFE~~ FLIGHT LIFE IS 20 FLIGHTS.

DESIGN SAFE LIFE $= \frac{20}{4} = 5$

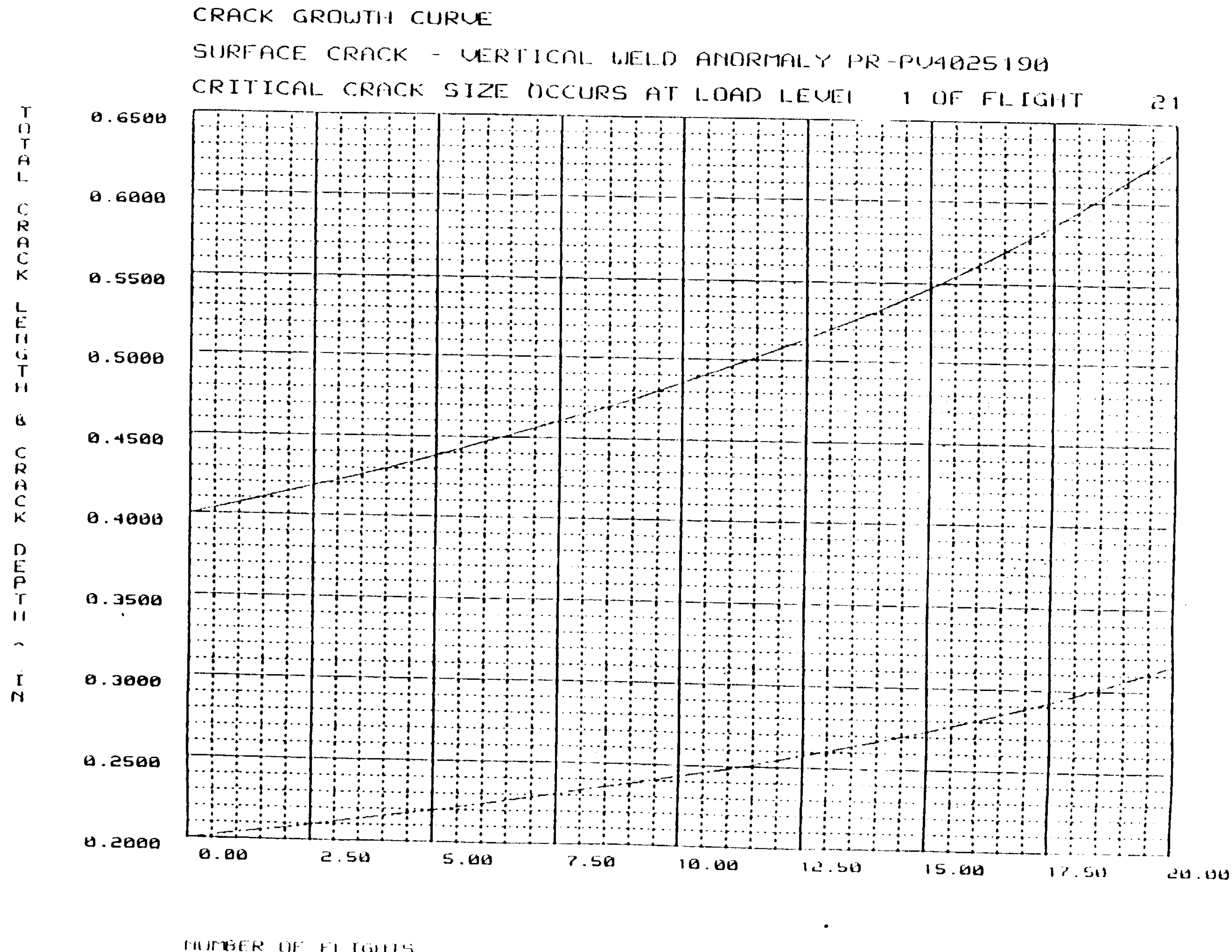
CRACK GROWTH CURVE
SURFACE CRACK - VERTICAL WELD ANORMALY PR-PV4025190
CRITICAL CRACK SIZE OCCURS AT LOAD LEVEL 1 OF FLIGHT 21
TOTAL CRACK LENGTH & CRACK DEPTH (IN
0.6500
0.6000
0.5500
0.5000
0.4500
0.4000
0.3500
0.3000
0.2500
0.2000
0.00
2.50
5.00
7.50
10.00
12.50
15.00
17.50
20.00
NUMBER OF FLIGHTS

CRACK GROWTH CURVE

EMBEDDED CRACK IN PLATE

CRITICAL CRACK SIZE OCCURS AT LOAD LEVEL 1 OF FLIGHT 21

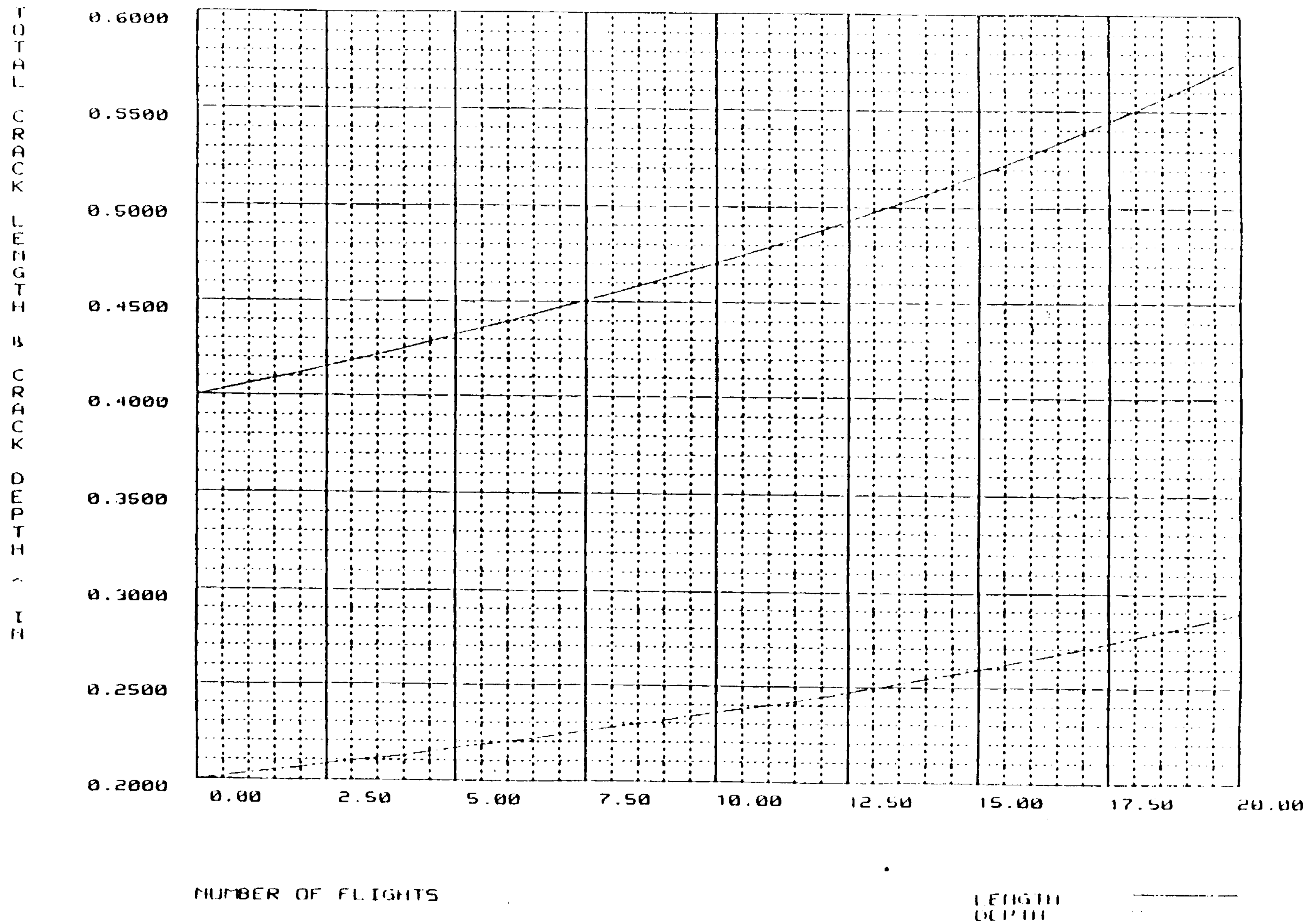

FATIGUE CRACK GROWTH ANALYSIS

(computed: NASA/FLAGRO, 1986 Aug version, 1987 Jul rev.)
U.S. customary units [inches, ksi, ksi sqrt(in)]

PROBLEM TITLE

AFT SKIRT VERTICAL WELD ANOMLY: PR PV4025190

GEOMETRY

MODEL: EC01-Embedded crack in plate (2D)

Thickness, t = 1.3750
Width, W = 7.5000

FLAW SIZE:

a (init.) = 0.2000
c (init.) = 0.2000
a/c (init.) = 1.000

MATERIAL

MATL 1: 2219-T852 AL, FORGING [BK=0]

Material Properties:

Matl: No.	YS	K1e	K1c	Ak	Bk	Thk	Kc	KIscc
1	30.5	22.0	22.0	0.75	0.00	1.375	22.0	

Matl: No.	Crack Growth Eqn Constants (closure) C	n	p	q	DKo	Co	d	DK1	Alpha	Smax/SIGo
1	0.1580-06	2.729	0.50	0.50	2.50	1.00	1.00	6.23	1.75	0.30

AFT SKIRT VERTICAL WELD ANOMLY: PR PV4025190
MODEL: EC01

FATIGUE SPECTRUM INPUT TABLE

MAXIMUM STRESS SPECTRUM

(Note: Stress = Input Value * Stress Factor)
Stress Factor SF0: 29.5

STEP	MAT	NUMBER OF FATIGUE CYCLES	S0 t1	S0 t2
1	1	1.0000	-1.00	1.00
2	1	1.0000	-0.95	0.95
3	1	1.0000	-0.90	0.90
4	1	1.0000	-0.86	0.86
5	1	1.0000	-0.82	0.82
6	1	1.0000	-0.78	0.78
7	1	1.0000	-0.74	0.74
8	1	1.0000	-0.71	0.71
9	1	1.0000	-0.67	0.67
10	1	1.0000	-0.64	0.64
11	1	1.0000	-0.61	0.61
12	1	1.0000	-0.58	0.58
13	1	1.0000	-0.55	0.55
14	1	1.0000	-0.52	0.52
15	1	1.0000	-0.50	0.50
16	1	1.0000	-0.47	0.47
17	1	1.0000	-0.45	0.45
18	1	1.0000	-0.43	0.43
19	1	1.0000	-0.41	0.41
20	1	1.0000	-0.39	0.39
21	1	1.0000	-0.37	0.37
22	1	1.0000	-0.35	0.35
23	1	1.0000	-0.33	0.33
24	1	1.0000	-0.32	0.32
25	1	1.0000	-0.30	0.30

Environmental Crack Growth Check for Sustained Stresses
(Kmax less than KIscc): NOT SET

AFT SKIRT VERTICAL WELD ANOMLY: PR PV4025190
MODEL: EC01

FATIGUE SPECTRUM STRESS TABLE

MAXIMUM STRESS SPECTRUM

S : T : E : P	M: A: T: L:	NUMBER OF FATIGUE CYCLES	SO (ksi) t1	SO (ksi) t2
1:	1:	1.0000	-29.50	29.50
2:	1:	1.0000	-28.02	28.02
3:	1:	1.0000	-26.55	26.55
4:	1:	1.0000	-25.37	25.37
5:	1:	1.0000	-24.19	24.19
6:	1:	1.0000	-23.01	23.01
7:	1:	1.0000	-21.83	21.83
8:	1:	1.0000	-20.95	20.95
9:	1:	1.0000	-19.77	19.77
10:	1:	1.0000	-18.88	18.88
11:	1:	1.0000	-18.00	18.00
12:	1:	1.0000	-17.11	17.11
13:	1:	1.0000	-16.23	16.23
14:	1:	1.0000	-15.34	15.34
15:	1:	1.0000	-14.75	14.75
16:	1:	1.0000	-13.86	13.86
17:	1:	1.0000	-13.27	13.27
18:	1:	1.0000	-12.69	12.69
19:	1:	1.0000	-12.10	12.10
20:	1:	1.0000	-11.50	11.50
21:	1:	1.0000	-10.92	10.92
22:	1:	1.0000	-10.32	10.32
23:	1:	1.0000	-9.74	9.74
24:	1:	1.0000	-9.44	9.44
25:	1:	1.0000	-8.85	8.85

Environmental Crack Growth Check for Sustained Stresses
(Kmax less than KIscc): NOT SET

AFT SKIRT VERTICAL WELD ANOMLY: PR PV4025190
MODEL: EC01

ANALYSIS RESULTS:

BLOCK	STEP	FINAL FLAW SIZE A	C	K MAX A-TIP	C-TIP
1		0.203047	0.203022	15.018041	14.987268
2		0.206193	0.206140	15.135390	15.103451
3		0.209442	0.209361	15.255821	15.222582
4		0.212802	0.212689	15.379496	15.344811
5		0.216278	0.216131	15.506592	15.470300
6		0.219877	0.219694	15.637302	15.599225
7		0.223607	0.223384	15.771837	15.731776
8		0.227477	0.227211	15.910428	15.868162
9		0.231495	0.231181	16.053328	16.008614
10		0.235671	0.235306	16.200820	16.153384
11		0.240018	0.239595	16.353214	16.302749
12		0.244547	0.244060	16.510858	16.457021
13		0.249272	0.248715	16.674142	16.616542
14		0.254209	0.253573	16.843502	16.781702
15		0.259377	0.258652	17.019436	16.952934
16		0.264794	0.263969	17.202509	17.130735
17		0.270485	0.269546	17.393369	17.315671
18		0.276476	0.275407	17.592770	17.508395
19		0.282799	0.281580	17.801590	17.709667
20		0.289490	0.288099	18.020866	17.920381

FINAL RESULTS:
Broke through, 1-d stress intensity exceeds critical value:
K max (TC01) = 28.17 K cr = 22.00
AT CYCLE NO. 1. OF LOAD STEP NO. 1 OF BLOCK NO. 21
CRACK SIZE A = 0.289490 , A/C = 1.00483

FATIGUE CRACK GROWTH ANALYSIS

(computed: NASA/FLAGRO, 1986 Aug version, 1987 Jul rev.)
U.S. customary units [inches, ksi, ksi sqrt(in)]

PROBLEM TITLE

AFT SKIRT VERTICAL WELD ANOMALY - PR-PV4025190

GEOMETRY

MODEL: SC01-Surface crack in finite width plate (2D)

Plate Thickness, t = 1.3750
" Width, W = 7.5000

FLAW SIZE:

a (init.) = 0.2000
c (init.) = 0.2000
a/c (init.) = 1.000

MATERIAL

MATL 1: 2219-T852 AL, FORGING [BK=0]

Material Properties:

Matl No.	YS	K1e	K1c	Ak	Bk	Thk	Kc	KIscc
1	30.5	22.0	22.0	0.75	0.00	1.375	22.0	

Matl No.	C	n	p	q	DKo	Co	d	DK1	Alpha	Smax/SIGo
	Crack Growth Eqn Constants (closure)									
1	0.158D-06	2.729	0.50	0.50	2.50	1.00	1.00	6.23	1.75	0.30

AFT SKIRT VERTICAL WELD ANOMALY - PR-PV4025'90
MODEL: SC01

FATIGUE SPECTRUM INPUT TABLE

MAXIMUM STRESS SPECTRUM

(Note: Stress = Input Value * Stress Factor)
Stress Factors SF0, SF1: 29.5 0.000E+00

S T E P	M A T L	NUMBER OF FATIGUE CYCLES	S0 t1	S0 t2	S1 t1	S1 t2
1:	1:	1.0000	-1.00	1.00	0.00	0.00
2:	1:	1.0000	-0.95	0.95	0.00	0.00
3:	1:	1.0000	-0.90	0.90	0.00	0.00
4:	1:	1.0000	-0.86	0.86	0.00	0.00
5:	1:	1.0000	-0.82	0.82	0.00	0.00
6:	1:	1.0000	-0.78	0.78	0.00	0.00
7:	1:	1.0000	-0.74	0.74	0.00	0.00
8:	1:	1.0000	-0.71	0.71	0.00	0.00
9:	1:	1.0000	-0.67	0.67	0.00	0.00
10:	1:	1.0000	-0.64	0.64	0.00	0.00
11:	1:	1.0000	-0.61	0.61	0.00	0.00
12:	1:	1.0000	-0.58	0.58	0.00	0.00
13:	1:	1.0000	-0.55	0.55	0.00	0.00
14:	1:	1.0000	-0.52	0.52	0.00	0.00
15:	1:	1.0000	-0.50	0.50	0.00	0.00
16:	1:	1.0000	-0.47	0.47	0.00	0.00
17:	1:	1.0000	-0.45	0.45	0.00	0.00
18:	1:	1.0000	-0.43	0.43	0.00	0.00
19:	1:	1.0000	-0.41	0.41	0.00	0.00
20:	1:	1.0000	-0.39	0.39	0.00	0.00
21:	1:	1.0000	-0.37	0.37	0.00	0.00
22:	1:	1.0000	-0.35	0.35	0.00	0.00
23:	1:	1.0000	-0.33	0.33	0.00	0.00
24:	1:	1.0000	-0.32	0.32	0.00	0.00
25:	1:	1.0000	-0.30	0.30	0.00	0.00

Environmental Crack Growth Check for Sustained Stresses
(Kmax less than KIscc): NOT SET

AFT SKIRT VERTICAL WELD ANOMALY - PR-PV4025190
MODEL: SC01

FATIGUE SPECTRUM STRESS TABLE

MAXIMUM STRESS SPECTRUM

S T E P	M A T L	NUMBER OF FATIGUE CYCLES	S0 (ksi) t1	S0 (ksi) t2	S1 (ksi) t1	S1 (ksi) t2
1	1	1.0000	-29.50	29.50	0.00	0.00
2	1	1.0000	-28.02	28.02	0.00	0.00
3	1	1.0000	-26.55	26.55	0.00	0.00
4	1	1.0000	-25.37	25.37	0.00	0.00
5	1	1.0000	-24.19	24.19	0.00	0.00
6	1	1.0000	-23.01	23.01	0.00	0.00
7	1	1.0000	-21.83	21.83	0.00	0.00
8	1	1.0000	-20.95	20.95	0.00	0.00
9	1	1.0000	-19.77	19.77	0.00	0.00
10	1	1.0000	-18.88	18.88	0.00	0.00
11	1	1.0000	-18.00	18.00	0.00	0.00
12	1	1.0000	-17.11	17.11	0.00	0.00
13	1	1.0000	-16.23	16.23	0.00	0.00
14	1	1.0000	-15.34	15.34	0.00	0.00
15	1	1.0000	-14.75	14.75	0.00	0.00
16	1	1.0000	-13.86	13.86	0.00	0.00
17	1	1.0000	-13.27	13.27	0.00	0.00
18	1	1.0000	-12.69	12.69	0.00	0.00
19	1	1.0000	-12.10	12.10	0.00	0.00
20	1	1.0000	-11.50	11.50	0.00	0.00
21	1	1.0000	-10.92	10.92	0.00	0.00
22	1	1.0000	-10.32	10.32	0.00	0.00
23	1	1.0000	-9.74	9.74	0.00	0.00
24	1	1.0000	-9.44	9.44	0.00	0.00
25	1	1.0000	-8.85	8.85	0.00	0.00

Environmental Crack Growth Check for Sustained Stresses
(Kmax less than KIscc): NOT SET

AFT SKIRT VERTICAL WELD ANOMALY - PR-PV4025190
MODEL: SC01

ANALYSIS RESULTS:

BLOCK	STEP	FINAL FLAW SIZE A	FINAL FLAW SIZE C	K MAX A-TIP	K MAX C-TIP
1		0.203562	0.203516	15.596960	17.273901
2		0.207259	0.207169	15.736645	17.434760
3		0.211099	0.210971	15.880740	17.600647
4		0.215094	0.214930	16.029515	17.771878
5		0.219253	0.219058	16.183274	17.948813
6		0.223588	0.223369	16.342353	18.131850
7		0.228115	0.227876	16.507128	18.321431
8		0.232846	0.232594	16.678020	18.518053
9		0.237801	0.237544	16.855503	18.722278
10		0.242998	0.242744	17.040113	18.934739
11		0.248460	0.248219	17.232453	19.156148

ADVISORY: ESTIMATED NET SECTION STRESS > YIELD STRENGTH.
AT CYCLE NO. 0. OF LOAD STEP NO. 1 OF BLOCK NO. 12
CRACK SIZE A = 0.248460 , A/C = 1.00097

BLOCK	STEP	FINAL FLAW SIZE A	FINAL FLAW SIZE C	K MAX A-TIP	K MAX C-TIP
12		0.254212	0.253996	17.433248	19.387363
13		0.260284	0.260106	17.643307	19.629341
14		0.266711	0.266587	17.863590	19.883217
15		0.273535	0.273484	18.093496	20.148328
16		0.280806	0.280852	18.333978	20.425811
17		0.288589	0.288759	18.589698	20.720937
18		0.296957	0.297288	18.859843	21.032948
19		0.306009	0.306546	19.147998	21.365975
20		0.315878	0.316680	19.457245	21.723593

FINAL RESULTS:
Unstable crack growth, max stress intensity exceeds critical value:
K max = 22.02 K cr = 22.00
AT CYCLE NO. 1. OF LOAD STEP NO. 1 OF BLOCK NO. 21
CRACK SIZE A = 0.315878 , A/C = 0.997467

REFERENCES

1. MSFC-HDBK-1453, Fracture Control Program Requirements, October 1987.

2. Failure Analysis Associates, NASCRAC NASA CRack Analysis Code, February 1989.

3. JSC-22267, NASA/FLAGRO Fatigue Crack Growth Program, August 1986.

4. Rockwell International, FLAGRO4 Fatigue Crack Growth Program.

5. MSFC-STD-1249, Standard Guidelines and Requirements for Fracture Control Programs, September 1985.

6. Forman, R.G., and Hu, T.: "Application of Fracture Mechanics on the Space Shuttle."

7. Broek, D.: Elementary Engineering Fracture Mechanics, Fourth Revised Edition. Martinus Nijhoff Publishers, Dordrecht, The Netherlands, 1986.

8. Tada, H., Paris, P.C., and Irwin, G.R.: The Stress Analysis of Cracks Handbook. Del Research Corporation, Hellertown, PA, 1973.

9. Rooke, D.P., and Cartwright, D.J.: Compendium of Stress Intensity Factors. Her Majesty Stationary Office by Hillingdon Press, Uxbridge, Middix, United Kingdom, 1976.

10. Knott,, J.F.: Fundamentals of Fracture Mechanics. Butterworth, London, United Kingdom, 1973.

11. Lee, H.: Space Shuttle Main Engine High Pressure Turbopump Turbine Blade Cracking. NASA TM-100327, May 1988.

12. NASA Memo ED24 (87-25) Ryan to Schuerer: Critical Stress Intensity Values (L1c) for MAR-M-246, September 1987.

13. MSFC Final Report, Failure Investigation Engine 0212 Test 904-044, Appendix J.

14. MSFC Memo ED24 (89-130), Wilson to Rowe: Fracture and Fatigue Crack Growth Properties of Waspaloy at 550 °F, 4,400 psi in Hydrogen.

15. MSFC Memo EP42 (83-042), Littles to Olivier: Main Ring Inspection Criteria for Cracks, April 1983.

16. MSFC Memo EE61/427-82, Olivier to Littles: Space Telescope Fracture Control Plan Life Loading Scenario, October 1982.

17. MSFC Memo ED22 (83-18), Holland to Faile: OTA Load Spectra, February 1983.

18. MSFC Memo ED22 (83-29), Holland to Faile: OTA Load Spectra Revised, February 1983.

19. MSFC-RQMT-691.2 Rev. A, Space Telescope On Orbit Maintenance Mission Space Support Equipment Design and Performance Requirement, March 1984.

20. MSFC-RPT-1481: Stress Analysis of Space Telescope (HST) On Orbit Maintenance Mission Space Support Equipment.

21. MSFC-RPT-1482: Fracture Mechanics Analysis of Space Telescope (HST) On Orbit Maintenance Mission Space Support Equipment.

22. MSFC-RPT-1535: Structural Analysis of the External Tank Attach Ring 270 Degree Configuration, February 1988.

23. MSFC-RPT-1545: Fracture Mechanics Analysis of the External Tank Attach Ring 270 Degree Configuration, April 1988.

24. SE-019-057-2H: SRB Loads Data Book One Fatigue and Fracture Data, June 1982.

25. MSFC Memo ED25 (87-73), Stallworth to McKannan: Fracture Mechanics Analysis Results of B-1 Stand LOX Inner Tank Leak Before Burst Analysis, December 1987.

26. Trimed, Inc., NASTRAN Model.

27. Ryan, R.S.: Fracture Mechanics Overview Presentation. ED01, Cultural Overview, June 1989.

APPROVAL

COMPENDIUM OF FRACTURE MECHANICS PROBLEMS

By R. Stallworth, C. Wilson, and C. Meyers

The information in this report has been reviewed for technical content. Review of any information concerning Department of Defense or nuclear energy activities or programs has been made by the MSFC Security Classification Officer. This report, in its entirety, has been determined to be unclassified.

for JAMES C. BLAIR
Director, Structures and Dynamics Laboratory